

NOTE TO USERS

This reproduction is the best copy available.

UMI[®]

EARLY DEVELOPMENT AND CHARACTERIZATION OF A DNA-BASED RADIATION
DOSIMETER

DÉVELOPPEMENT ET CARACTÉRISATION D'UN DOSIMÈTRE À ADN

A Thesis Submitted

to the Division of Graduate Studies of the Royal Military College of Canada

by

Kirsten A. Avarmaa, B.Sc.

In Partial Fulfillment of the Requirements for the Degree of
Master of Applied Science

November 2010

©This thesis may be used within the Department of National
Defense but copyright for open publication remains the property of the author.

ROYAL MILITARY COLLEGE OF CANADA



Library and Archives
Canada

Published Heritage
Branch

395 Wellington Street
Ottawa ON K1A 0N4
Canada

Bibliothèque et
Archives Canada

Direction du
Patrimoine de l'édition

395, rue Wellington
Ottawa ON K1A 0N4
Canada

Your file *Votre référence*
ISBN: 978-0-494-71870-4
Our file *Notre référence*
ISBN: 978-0-494-71870-4

NOTICE:

The author has granted a non-exclusive license allowing Library and Archives Canada to reproduce, publish, archive, preserve, conserve, communicate to the public by telecommunication or on the Internet, loan, distribute and sell theses worldwide, for commercial or non-commercial purposes, in microform, paper, electronic and/or any other formats.

The author retains copyright ownership and moral rights in this thesis. Neither the thesis nor substantial extracts from it may be printed or otherwise reproduced without the author's permission.

AVIS:

L'auteur a accordé une licence non exclusive permettant à la Bibliothèque et Archives Canada de reproduire, publier, archiver, sauvegarder, conserver, transmettre au public par télécommunication ou par l'Internet, prêter, distribuer et vendre des thèses partout dans le monde, à des fins commerciales ou autres, sur support microforme, papier, électronique et/ou autres formats.

L'auteur conserve la propriété du droit d'auteur et des droits moraux qui protègent cette thèse. Ni la thèse ni des extraits substantiels de celle-ci ne doivent être imprimés ou autrement reproduits sans son autorisation.

In compliance with the Canadian Privacy Act some supporting forms may have been removed from this thesis.

While these forms may be included in the document page count, their removal does not represent any loss of content from the thesis.

Conformément à la loi canadienne sur la protection de la vie privée, quelques formulaires secondaires ont été enlevés de cette thèse.

Bien que ces formulaires aient inclus dans la pagination, il n'y aura aucun contenu manquant.


Canada

For my mother, who will always be an inspiration.

Acknowledgements

I have had the privilege of working with many talented individuals and organizations in the course of my work at RMC and abroad. I would, first and foremost, like to thank my supervisors Dr. Lewis and Dr. Bennett for their guidance and enthusiastic commitment to my successes in study and experimentation.

It has been a great pleasure to work with the interdisciplinary, multi-organizational team on this CRTI project. I would like to acknowledge all of our partners with special recognition of Isabelle Charlebois at CRI-CHUQ in Quebec City, for assistance and guidance with the polymeric transducer portion of this project, and kindly assisting with the French language.

I am indebted to the expertise, assistance and kindness of Diana Wilkinson, Aimee Jones, Louise Prud'homme-Lalond, and Trevor Jones at DRDC-Ottawa.

I must express my gratitude to Markus Fuerstner at CERN for the invitation to participate in exposures at the CERF facility, and Patricia Coulero at the Geneva University research hospital for lending laboratory space to prepare samples for transport. I am grateful to Kobus Slabbert and iThemba for providing the opportunity to use their neutron beam and facilities.

I would like to recognize my collaborators at RMC: Kevin McDermott for his knowledge and skills and for sharing them, and Tara Wood for her patience and assistance.

Finally, I would like to thank my good friends and fellow students in the Nuclear Group at RMC.

Abstract

Kirsten A. Avarmaa, M.A.Sc. (Nuc.Eng.). Royal Military College of Canada. November 2010. Development and Characterization of a DNA-Based Radiation Dosimeter. Supervisors: Lewis, Brent J., *Ph.D.* (Nuc. Eng.), P. Eng., Bennett, Leslie G.I., *Ph.D.* (Nuc. Eng.).

It is the priority of first responders to minimize damage to persons and infrastructure in the case of a nuclear emergency due to an accident or deliberate terrorist attack – if this emergency includes a radioactive hazard, first responders require a simple-to-use, accurate and complete dosimeter for radiation protection purposes in order to minimize the health risk to these individuals and the general population at large.

This work consists of the early evaluation of the design and performance of a biologically relevant dosimeter which uses DNA material that can respond to the radiation of any particle type. The construct consists of fluorescently tagged strands of DNA. The signalling components of this dosimeter are also investigated for their sensitivity to radiation damage and light exposure.

The dual-labelled dosimeter that is evaluated in this work gave a measurable response to gamma radiation at dose levels of 10 Gy for the given detector design and experimental setup. Further testing outside of this work confirmed this finding and indicated a working range of 100 mGy to 10 Gy using a custom-built fluorimeter as part of a larger CRTI initiative.

Characterization of the chromatic components of the dosimeter showed that photobleaching is not expected to have an effect on dosimeter performance, but that radiation can damage the non-DNA signalling components at higher dose levels, although this damage is minimal at lower doses over the expected operating ranges. This work therefore describes the early steps in the

quantification of the behaviour of the DNA dosimeter as a potential biologically-based device to measure radiation dose.

Résumé

Kirsten A. Avarmaa, M. Sc. A. (Génie nucléaire). Collège Militaire Royal du Canada.

Novembre 2010. Développement et Caractérisation d'un Dosimètre à ADN. Superviseur: Lewis, Brent J., *Ph.D.* (Génie nucléaire), Bennett, Leslie G.I., *Ph.D.* (Génie nucléaire).

Lors d'une urgence nucléaire, accidentelle ou délibérée, la priorité des premiers répondants est de limiter les dommages causés aux personnes et aux infrastructures. Afin de faire face à une urgence incluant un risque d'exposition aux radiations, les premiers répondants ont besoin d'un équipement de dosimétrie permettant une mesure fiable des radiations afin d'assurer leur sécurité ainsi que de minimiser les risques pour la population en général. Le système idéal de dosimétrie doit pouvoir détecter tous les types de radiations en plus d'être facile d'utilisation et précis.

Ce travail consiste à faire une évaluation du design et de la performance d'un dosimètre, basé sur l'ADN, pouvant mesurer les dommages biologiques causés par les radiations. Cette molécule, d'origine biologique, est sensible à tous les types de particules pouvant causer des torts biologiques. Le dosimètre est composé de brins d'ADN liés à des marqueurs fluorescents. Les différents composants de ce dosimètre seront aussi évalués pour mesurer leur sensibilité aux dommages causés par les radiations ou par l'exposition à la lumière.

Le dosimètre à double marquage, évalué dans ce travail, a permis, avec le premier design expérimental et un détecteur commercial, de mesurer des radiations gamma à une dose de 10 Gy. D'autres expérimentations, réalisées lors d'études subséquentes, ont permis de confirmer ces résultats et indiquent la possibilité de détecter les radiations de 100 mGy à 10Gy en utilisant un fluorimètre fait sur mesure dans le cadre d'un projet subventionné par l'IRTC.

La caractérisation des composants chromatiques du dosimètre a démontré que la photodécoloration ne devrait pas avoir d'effet sur la performance du dosimètre. Cette caractérisation a aussi démontré que, à fortes doses, les radiations peuvent endommager ces composants. Par contre, les dommages sont minimes à doses plus faibles, doses au dessus de l'éventail attendu. Ce travail décrit les premières étapes de développement et de caractérisation d'un dosimètre à ADN pouvant être utilisé pour mesurer les doses de radiation à l'aide d'un système basée sur la biologie.

Table of Contents

Abstract.....	v
Résumé	vii
List of Figures.....	xi
List of Tables	xii
List of Abbreviations	xi
Chapter 1 Introduction	1
Chapter 2 Goals of this Thesis.....	5
Chapter 3 Background	7
3.1 Ionizing Radiation	7
3.2 Deoxyribonucleic Acid.....	9
3.3 Biological Consequences of Radiation.....	11
3.3.1 Relative Biological Effectiveness	12
3.3.2 Effects of Radiation on DNA	12
3.4 State-of-the-Art Methods for Radiation Detection	14
3.4.1 Radiation Dosimetry	14
3.4.2 DNA Dosimeter Design Requirements.....	18
3.4.3 Förster's Resonance Energy Transfer.....	20
3.4.4 DNA as a Break Signalling Biomarker.....	22
3.5 New Method: Fluorescence Chain Reaction.....	27
3.6 New Method: Dual-Labelled Oligonucleotide Sensor	29
Chapter 4 Experimental Description.....	32
4.1 Polymeric Transducer Dosimeter.....	33
4.1.1 Materials	33
4.1.2 Pre-Irradiation Treatment and Irradiation	35
4.1.3 Post-Irradiation Treatment and Analysis.....	36
4.1.4 Polymeric Transducer Irradiation PCR Results.....	37
4.2 Dual-Labelled Oligonucleotide Dosimeter	39
4.2.1 Dosimeter Preparation	39
4.2.2 Detector Performance	41
4.2.2.1 Quenching Efficiency	42
4.2.2.2 Irradiation	43
4.2.2.3 Reporter Robustness.....	44
4.2.2.4 Measurement of Irradiation with the Dual-Labelled Dosimeter	51
Chapter 5 Discussion.....	56

5.1	Polymeric Transducer Dosimeter.....	56
5.2	Dual-Labelled Quenching Dosimeter.....	58
5.2.1	Quenching Efficiency of the Dual-Labelled Dosimeter	58
5.2.2	Reporter Sensitivity of the Dual-Labelled Dosimeter	60
5.2.2.1	Temperature Regulation Effects on Reporter Sensitivity	61
5.2.3	Photobleaching Effect.....	62
5.2.4	The Dual-Labelled Dosimeter Response to Gamma Radiation	63
5.2.5	Background Signal Evaluation	64
5.3	Comparison with Other Work.....	65
5.3.1	Fluor and Quencher Response to Radiation.....	65
5.3.2	Custom Fluorimeter Developed for Dual-Labelled Construct.....	69
Chapter 6	Conclusions	81
Chapter 7	Recommendations	83
References.....		85
Appendix A: Calculations.....		90
Appendix B: Experimental Data.....		92
Appendix C: Quality Control		103
Appendix D: Supporting Data.....		110
Curriculum Vitae		114

List of Figures

Figure 3.1:	DNA composition and depiction in this work.....	10
Figure 3.2:	Common biodosimetry.....	17
Figure 3.3:	Förster's resonance energy transfer dependencies.....	20
Figure 3.4:	Förster's resonance energy transfer mechanism.....	22
Figure 3.5:	Polymerase chain reaction mechanism	23
Figure 3.6:	Double stranded break detection scheme	24
Figure 3.7:	Molecular machine break detection scheme	25
Figure 3.8:	Molecular beacon break detection scheme.....	26
Figure 3.9:	Simple surface-bound oligonucleotide break detection scheme.....	27
Figure 3.10:	Fluorescence chain reaction break detection scheme.....	29
Figure 3.11:	Black hole quencher break detection scheme.....	31
Figure 4.1:	Schematic of the polymeric transducer dosimeter	34
Figure 4.2:	High dose mixed-radiation experimental arrangement	36
Figure 4.3:	High dose mixed-radiation PCR results.....	38
Figure 4.4:	Gamma dose measurements performed by Health Canada.....	39
Figure 4.5:	Dual-labelled DNA dosimeter molecules and components.....	40
Figure 4.6:	Quenching efficiency for dosimeter s of different lengths.....	43
Figure 4.7:	Cobalt gamma irradiator at DRDC-O	44
Figure 4.8:	Reporter response to gamma irradiation for a) Day 1, and b) Day 2	46
Figure 4.9:	Slope of the response curve for the reporter molecule at a concentration of 1.0 uM for a) Day 1, and b) Day 2	47
Figure 4.10:	Difference in reporter response between unirradiated and irradiated samples for a) Day 1, and b) Day 2.....	48
Figure 4.11:	Reporter response to irradiation for the exposures on Day 1 and Day 2.....	49
Figure 4.12:	Reporter response to repeated analytical light exposure over two days.....	50
Figure 4.13:	Reporter response to repeated analytical light exposure for the 1.0 uM dosimeter for Day 1 and Day 2.....	51
Figure 4.14:	Performance of the dual-labelled DNA dosimeter at 1, 5, 10, and 100 Gy.....	52
Figure 4.15:	Performance of the dual-labelled DNA dosimeter and reporter at 0 and 100 Gy	53
Figure 4.16:	Performance of the dual-labelled DNA dosimeter between 0 and 10 Gy.....	54
Figure 4.17:	Performance of the dual-labelled DNA dosimeter between 0 and 10 Gy at 1.0 uM.....	55
Figure 5.1:	Dual-labelled oligonucleotide dosimeter molecule	59

Figure 5.2	Reporter response to high dose irradiation.....	66
Figure 5.3	Quencher response to high dose irradiation.....	67
Figure 5.4	Customized fluorimeter setup at COPL.....	71
Figure 5.5	Calibration curve of FAM reporter and aqueous FITC.....	72
Figure 5.6:	Dual-labelled DNA dosimeter dose response curve at 0.5 uM irradiated with 0.1 -10.0 Gy gamma rays (corrected).....	74
Figure 5.7:	Black hole quencher absorbance with dose	76
Figure 5.8:	FAM reporter fluorescence response with dose	77
Figure 5.9:	Dual-labelled DNA dosimeter's fluorescence response with dose	78

List of Tables

Table 3.1 Radiation Interaction With Matter.....	8
--	---

List of Abbreviations

Partners

CRTI	CBRNE Research and Technology Initiative
COPL	Center for Optics, Photonics and Lasers
CRI-CHUL	Centre de Recherche en Infectiologie – Centre Hospitalier de l'Université Laval
DGNS	Director General Nuclear Safety
DRDC-O	Defence Research & Development Canada – Ottawa
IMI-NRC	Industrial Materials Institute of the National Research Council
KGH	Kingston General Hospital
RMC	Royal Military College of Canada

General

BHQ, BHQ1	Black Hole Quencher, Black Hole Quencher 1
CBRNE	Chemical, Biological, Radiological-Nuclear and Explosives
CERF	CERN-EU Reference Field
CERN	European Organization for Nuclear Research
DNA	Deoxyribonucleic Acid
-dsDNA	double stranded DNA
-ssDNA	single stranded DNA
DSB	Double Stranded Break
EDC NHS	1-Ethyl-3-(3-dimethylaminopropyl)carbodiimide – N-hydroxysuccinimide
	binding chemistry
FAM	Fluorescein
FCR	Fluorescence Chain Reaction
FISH	Fluorescence In-Situ Hybridization
FITC	Fluorescein Isothiocyanate
FRET	Förster's Resonance Energy Transfer
LD ₅₀	Median Lethal Dose
LET	Linear Energy Transfer
LOD	Limit of Detection
MEMS	Micro-electro-mechanical System
MPD	Maximum Permissible Dose
OSL	Optically Stimulated Luminescence
PCR	Polymerase Chain Reaction
-qPCR	quantitative PCR
PIC	Precision Ion Counter
PMT	Photo Multiplier Tube
RBE	Relative Biological Effectiveness
SSB	Single Stranded Break
TEPC	Tissue Equivalent Proportional Counter
TLD	Thermoluminescent Dosimeter

1 Introduction

A Chemical, Biological, Radiological-Nuclear and Explosives (CBRNE) incident may be the result of an industrial accident or the result of malicious intent. An emergency radiological or nuclear event is significantly different in terms of radiation protection and dose assessment than normal situations involving the use of radioactive or nuclear sources. Sudden and widespread exposure must be controlled immediately. Failure to respond in a timely manner to a radiological/nuclear emergency risks compounding the damage and entertains unpredictable consequences, which may be difficult to control.^[1] Ionizing radiation is a serious threat to the health of persons in the vicinity of the event as well as the first responders who arrive to manage and contain an incident. These first responders may be national, provincial or municipal police; Canadian Forces personnel; paramedics; or fire fighters. They will have experience with managing dangerous situations, but may or may not be fully experienced with radiological/nuclear exposure.

In order to protect Canadian citizens and critical infrastructure (for instance, facilities that could escalate damages if unprotected, e.g. nuclear power plants), it is vital that first responders responding to an emergency be adequately prepared for any CBRNE. Some strategies to reduce radiation exposure include rotating workers to minimize time exposure, reducing distance from sources, employing shielding, preparing workers and conditions to reduce exposure, using equipment to reduce exposure to internal sources, and when appropriate using medication (which competes with, or sequesters radionuclides for waste removal, e.g., Prussian Blue) to reduce the risk of incorporating radioactive material into the metabolism.^[1] First, though, it is important for first responders to be aware of existing radiation exposure and the extent of this insult. For this

assessment, first responders need a simple-to-use dosimeter that is able to accurately report radiation exposure and inform emergency workers when they should withdraw for their own safety, without requiring any additional training. The risk to first responders and persons affected by a radiological/nuclear accident or attack is significant. Even when doses are not strong enough to cause immediate sickness, radiation exposure has been correlated with an increased incidence of cancer later in life.^[2] High doses, specifically those exceeding 1-3 Sv, risk the development of radiation sickness that may show typical symptoms within hours, which include: vomiting, diarrhea, fever, decreased immune response, internal bleeding, and death.^[3] The LD₅₀, the dose for which 50% of an exposed population is predicted to die, occurs between 3.2 and 4.5 Sv.^[4]

The dose limits for radiation protection purposes for the “General Public” or a “Nuclear Energy Worker” are regulated. For instance, the Canadian Nuclear Safety Commission (CNSC) has adopted the revised recommendations set forth by the International Commission on Radiological Protection in 1991.^[5] These limit the maximum permissible dose received by persons exposed to, or working with, radiation. These dose limits are intentionally set at very low doses, to establish healthy policy and avoid risk. For instance: within a year, a member of the public is limited to 1 mSv radiation exposure, not including exposure from medical procedures or natural background radiation.^[5] In comparison, it should be noted that the average total annual effective dose (largely from natural background and cosmic radiation) in Canada is 1.7 mSv,^[6] and when other sources are included, the annual dose is 3.6 mSv.^[7] However, a person classified as a “Nuclear Energy Worker” (who must be trained in radiation safety and wear a personal dosimeter for radiation protection purposes in the workplace) is limited to 20 mSv per year, or 100 mSv averaged over 5 years, such that in no given year does the dose exceed a maximum value of 50 mSv.^[5] In the case of single dose exposures, the CNSC provides further guidelines, i.e., in a routine situation, the maximum

permissible dose (MPD) is 0.5 mSv (half of the public annual MPD), and in an emergency situation, this limit increases to 250 mSv - a dose below the threat of radiation sickness, but above the threat of stochastic effects (cancer).^[8]

Radiation is not discernible to the human senses and it is important that first responders have access to a dosimeter that can accurately report danger to the user. This situation is complicated by the fact that radiation itself is not a simple concept, but can be a complex entity encompassing many different particle types (e.g., alpha, beta, x-ray, gamma, and neutron) and a wide range of energies that interact with matter in different ways.^[9] Since, radiation fields are more frequently composed of a mixture of different particles and waves, radiation dosimetry must be inclusive.^[10] Unfortunately, the International Atomic Energy Agency notes that “no dosimeter is water or tissue equivalent for all radiation beam qualities,”^[11] (in reference to X-ray, gamma, and neutron exposures). This requirement is due to the widely varying nature of the differing types of radiation, and the practical problems associated with mixed-field measurement. Due to this differing nature and energy of the potential radiation field, various equipment of differing sensitivities and physical and structural attributes is typically needed.^[10] This is a problem that challenges existing dosimetry for relevancy in reporting doses received to the human body of workers and first responders who may deal with complicated radiation hazards.

The aim of this project is to improve the art of dosimetry by combining the advantages of existing dosimeter models: the accuracy, precision and portability of inorganic dosimetry and the simple biological relevance of DNA as a target for measurement as used in biodosimetry. In particular, the current work is focused on the use of biological materials that may be most sensitive to radiation in the first place. Deoxyribonucleic acid, DNA, is selected as a candidate for this

application. Since the genetic code serves as a blueprint for most of the components of the cell, if those components become damaged, they can be replaced, as long as the DNA remains intact. Similarly, when a cell is destroyed as a result of radiation, it can be replaced by a healthy cell. The destruction of DNA, however, has consequences for the cell. This result has been demonstrated experimentally, where cytoplasmic components show little effect from radiation, while irradiation of the nucleus results in drastic changes to the cell.^[12] Thus, an investigation in this thesis was carried out in the use and design of a novel radiation dosimeter using DNA as a target for measuring mixed-field radiation. This work is part of an initiative for research on emergency response as part of a larger CBRNE Research and Technology Initiatives (CRTI) project.

The DNA used in this work is synthetic, in that it is artificially manufactured in a laboratory, so that it may be any sequence that is deemed appropriate and representative. This dosimeter is also ‘naked’, in that it is devoid of all of the molecules, structures and enzymes that are associated with living, cellular material. Consequently, the DNA material cannot repair itself as used in this dosimeter, which offers a capability for more sensitive radiation detection.

The CRTI initiative is specifically driving the development of a small wearable DNA dosimeter to be used by first responders in emergency scenarios where radiation exposure is a possibility. A multi-disciplinary research group at the Royal Military College (RMC), Defence Research and Development Canada – Ottawa, Université Laval, Director General Nuclear Safety and National Research Council has been assembled to cover the various aspects associated with designing and building a MEMS (micro-electro-mechanical-system) device. This thesis work specifically focuses on the initial development and testing of the prototype device, particularly, the radiation target itself.

2 Goals of this Thesis

As stated in Section 1, the goal of this project is to take advantage of the biological relevance of DNA in the design of a novel radiation dosimeter, benefitting from simplicity, accuracy and portability. The main objective of this work is to focus on the earliest stage of dosimeter development and characterization.

During the course of this work, two different dosimeter constructs, each conforming to the initial requirements of the project, were evaluated (see Sections 3.5 and 3.6). Both consist of short strands of DNA, designed to elicit a signal following a break in the DNA. A suitable dosimeter must meet specific requirements where it needs to be incorporable into a small wearable dosimeter. The device needs to have sufficient accuracy and precision. The intention of this work is to examine the strengths and weaknesses of the two different constructs through initial experimentation in order to characterize the device and assess its suitability for the proposed application.

The goal of this work was to therefore describe the performance of the chosen dosimeter construct in terms of radiation reporting, as well as examine the radiation-resistance of the other components of the device that make up the complete molecular complex. Damage to the reporter molecules of the device will affect its measurement accuracy since the dosimeter consists of not only DNA, but also this system that is used to detect any such damage in the DNA. It is therefore important to recognize and quantify any effects to the whole construct since the dosimeter that consists of the DNA material and signalling molecules can be affected by both radiation exposure as well as light exposure. Light exposure is specifically required for a reading of the dosimeter with a spectrometer.

Finally, this work will demonstrate the potential application of this device for radiation dosimetry. An improvement in the current technology is also suggested for continued and future development of the device as well as its calibration.

In summary, the work carried out under this thesis investigation provided an initial benchmarking and radiation testing of the DNA construct with experimentation at the CERN Reference Field (CERF) facility with a mixed-radiation field, as well as experiments with a successive molecular design at DRDC-O using a cobalt-60 source. This work entailed an original investigation on the various components of the dosimeter and its performance. This initial work was also compared to other work carried out later by a multidisciplinary team with specializations in the development of custom spectrometry as a means to improve the sensitivity of the device.

3 Background

The background theory of radiation effects on matter is discussed in Section 3.1. Sections 3.2 and 3.3 describe the composition of DNA material and the biological consequences of radiation damage to the DNA, respectively. Radiation dosimetry techniques employing conventional physical and biodosimetry methods, as well as more sophisticated state-of-the-art approaches are presented in detail in Section 3.4. Finally, the two methods proposed in this work for the development of the DNA dosimeter, i.e., a Fluorescence Chain Reaction (FCR) (and later a Polymerase Chain Reaction (PCR)) and dual-labelled approach, are described in Sections 3.5 and 3.6, respectively.

3.1 Ionizing Radiation

Ionizing radiation describes the capability of energetic subatomic particles to interact with matter to form positive or negative charges^[13] and encompasses a number of different types of ionizing radiation. Directly ionizing radiation includes, notably, alpha and beta particles, while indirectly ionizing radiation includes electromagnetic radiation, x- and gamma rays, and neutrons. These different types of radiation, hereafter to be referred to simply as radiation, differ greatly in terms of their size (mass) and means of interaction as shown in Table 3.1, and also in terms of their energies.

Table 3.1 Radiation Interaction with Matter

	Components	Mass relative to electrons ^[14]	Interactions ^[15]	Track Description ^[15]
Alpha	2 protons & 2 neutrons	7293.89	Collisions transferring energy to electrons in matter	Straight, short range, 0.007 cm in skin
Beta	Electron or positron	1	Bremsstrahlung emissions (electromagnetic) and inelastic collisions transferring energy to other electrons*	Angular scattering with a range dependent on energy and density, may reach internal living tissues
Gamma/ X-ray	Electro- magnetic radiation	massless	Absorption or scattering primarily in the form of photoelectric effect, compton scattering or pair production	Cross section and density determine how photons penetrate matter, but photons are not limited by a range
Neutron	neutron	1837.74	Nuclear reactions transferring energy to new gamma rays and ions, and elastic scattering	Neutron interactions only occur within 10^{-15} m of an atomic nucleus, so may pass through a significant amount of matter before this occurs

*Elastic collisions also occur, but do not change charges.

The particle track reflects the linear energy transfer (LET) of the radiation. LET is “a measure of the average energy deposited along the track of a particle per unit length and depends on the type of particle and its energy.”^[16] LET tends to increase as ion energy decreases.^[15] LET has a significant impact on biological tissue, and the DNA in particular, which will be described in Section 3.3.1.

The absorbed dose is a measurement of the energy deposited by radiation in matter, and is commonly measured in the SI units of Gray ($\text{J} \cdot \text{kg}^{-1}$).

3.2 Deoxyribonucleic Acid

Deoxyribonucleic acid (DNA) is the genetic blueprint for all living things. DNA directs the production of proteins and enzymes that serve as the building blocks and communication functions that organize and maintain life.

A strand of DNA is composed of a sugar-phosphate backbone where each deoxyribose (the sugar) is attached to one of four nucleotide bases. The four nucleotides are Cytosine, Guanine, Adenine and Thymine (C, G, A, T). In the cell, DNA is usually in the form of double-stranded DNA (dsDNA), which is composed of two single strands of DNA (ssDNA) material (Fig. 3.1). These separate strands are complementary to each other: cytosine pairs with guanine, and adenine pairs with thymine. Double-stranded DNA in the cell assumes a helical configuration, completing a helical rotation in 10 base pairs, in the naturally-occurring DNA helix.^[17]

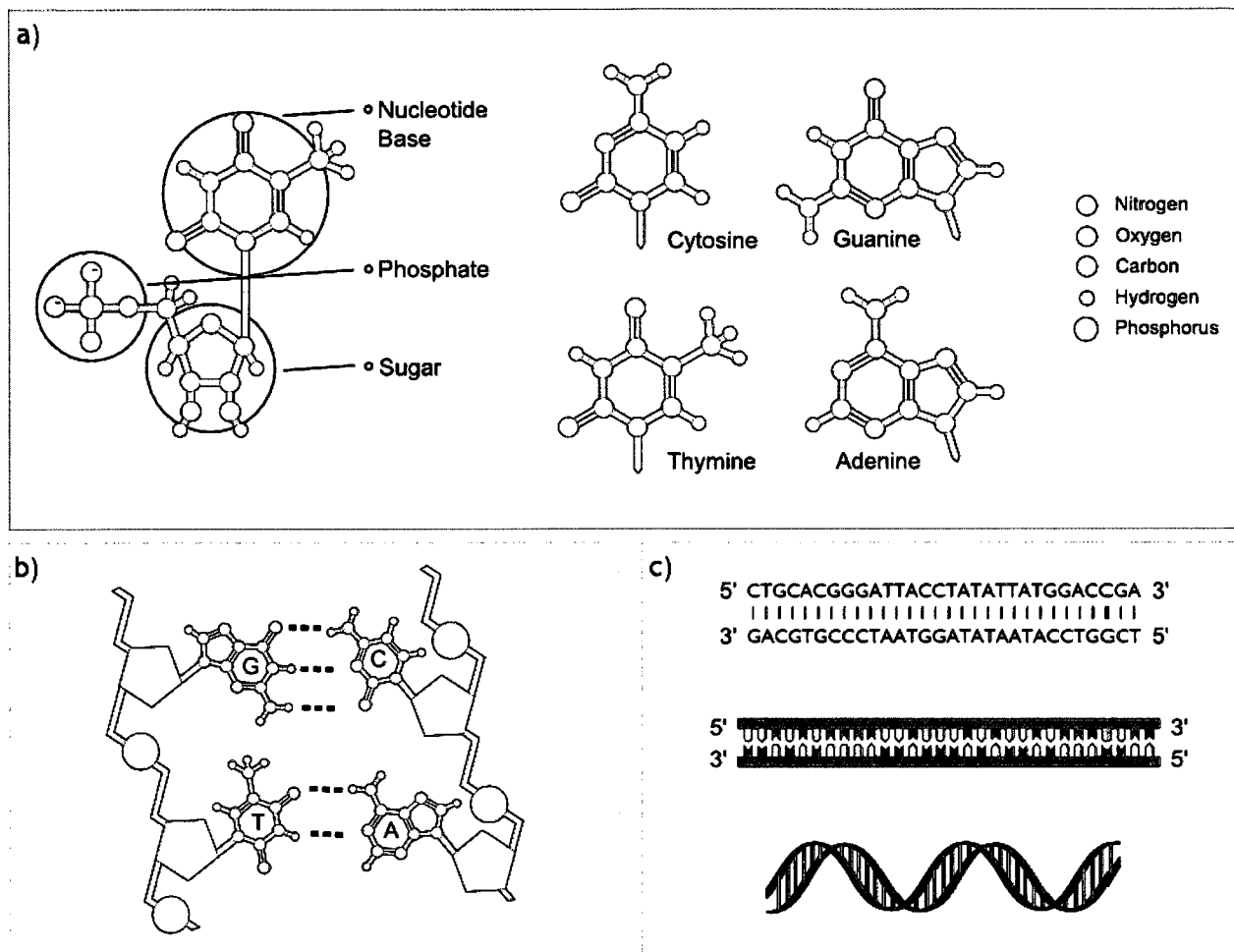


Figure 3.1: DNA composition and depiction in this work. a) A single deoxyribonucleic acid, its components, and the four nucleotide bases, b) base pairing via hydrogen bonding, c) pictorial depictions of DNA to be further used in this work.

DNA is organized in the cell into chromosomes spanning, in the human genome, up to 247 million base pairs in length (chromosome).^[18] Some chromosomes may contain thousands of genes responsible for all aspects of cellular and human life. A very short strand of DNA (under 500

nucleotide bases) is often referred to as an oligonucleotide (as used for the DNA constructs in this work).

During the growth cycle of a cell, new strands of DNA are replicated using each existing strand as a template, so that each new cell receives an identical complement of genetic information with which to continue building vital molecular units and producing new and healthy cells.

DNA has been selected in the current device development as the target material for the radiation energy for several reasons. DNA is not a material that is merely equivalent to biological material, but it is an important component of the biological cell itself, where changes to DNA may ultimately cause cell death (apoptosis) and stochastic effects (i.e., cancer).

3.3 Biological Consequences of Radiation

The immediately noticeable effects of radiation damage are not on the cellular level, but at the tissue and body level. With an acute exposure, radiation sickness is characterized by an evolution of distinct phases, for which the time between exposure and onset, and the duration are shorter as the dose becomes greater. The earliest symptoms are in the prodromal phase, which occurs within hours to days. An exposed individual may experience nausea and vomiting, and weakness and fatigue, with a decrease in the lymphocyte count.^[19] At higher dose levels, erythema (reddening of skin), fever, dizziness and diarrhea may be evident in the prodromal phase. This phase is followed by a latent phase where no new symptoms present themselves and the individual

appears to recover. This phase is followed by an overt systemic illness which may be characterized by infections, bleeding, gastrointestinal symptoms, and death.^[19]

3.3.1 Relative Biological Effectiveness

As discussed above, different types of radiation differ in terms of their LET, and thus affect living tissue in different ways. This situation gives rise to the concept of Relative Biological Effectiveness (RBE), which is the relationship between the effect of low LET X-rays to the effect of the dose of another type of radiation which causes the same quantitative biological effect (or end-point).^[15] This concept leads to the dose equivalent in sievert (Sv, which is also in units of $\text{J} \cdot \text{kg}^{-1}$). The RBE varies specifically with the type of radiation and energy. The cellular and genetic damage will depend on the track structure as the radiation interacts with the medium.^[16] Generally, RBE increases with LET^[16] to a maximum value at roughly $100 \text{ keV}/\mu\text{m}$. At this point, an energy transfer occurs once within every 2 nm, which is roughly the diameter of dsDNA, meaning that both strands are being broken by one track. The overall risk to the cell due to single stranded breaks (SSB) is generally less than that of double stranded breaks, where a DSB is the result of at least two SSB on opposing DNA strands within a distance of 10 base pairs and occurring close in time.^[15, 16, 20]

3.3.2 Effects of Radiation on DNA

At the cellular level, radiation can cause cytotoxicity and cell death, mutagenesis and carcinogenesis.^[16, 21] Ionizing radiation imparts energy in the living cell, which can break bonds and

weaken structures; however, the most sensitive material to radiation is the DNA, due to its role in cell replication and information propagation. The integrity of the genetic code is vital to the production of cellular components, and enzymes involved in cellular metabolism and intracellular communication. Furthermore, genetic integrity is important in the production of future generations of cells in the cases of tissue repair and rapidly reproducing cell types, such as in the bone marrow, skin, and the lining of the aero-digestive tracts (mouth, nose and throat).^[22]

As mentioned in Section 3.1, radiation can cause DNA damage either directly or indirectly. Indirect damage is caused by energy deposition in water molecules within a 4 nm diameter from the centre of the DNA strand.^[23, 16] This deposition creates highly energetic ions, $\cdot\text{OH}$ free radicals, $\cdot\text{H}$ ions and electrons.^[24] These energetic molecules can interact with and cause damage to the DNA. Free radicals formed outside this 4 nm diameter in a living cell are usually scavenged by other molecules and structures in the cell such that they cannot affect the DNA.^[25] Direct damage occurs when ionizing radiation deposits energy directly into the DNA strand itself.^[24]

Through these direct and indirect interactions, radiation can cause single-stranded breaks and double-stranded breaks, in addition to base lesions, sugar damage, apurinic/apyrimidinic sites (structural deformities in individual bases) and DNA-protein crosslinks.^[16, 20] A strand break is assumed to occur via direct action when absorbed energy exceeds 17.5 eV. With an indirect strand break, an $\text{OH}\cdot$ radical has a 13% probability of interaction if it diffuses within the vicinity of the DNA.^[16]

Single-stranded breaks and double-stranded breaks may have a significant effect on cell function and survival.^[26] As mentioned above, DSBs occur when two SSBs are created on opposing

DNA strands in proximity. DSBs are generally the result of clustered damage, which is generally caused by high LET radiation.^[20] Clustered damage is two or more lesions formed within 1-2 helical turns caused by a single radiation track.^[20] Clustered damage may occur without causing DSBs, but may still have a significant impact on genetic integrity and cell survival.^[20]

3.4 State-of-the-Art: Methods for Radiation Detection

3.4.1 Radiation Dosimetry

The most precise and accurate instruments for radiation dosimetry are generally heavy, bulky and prohibitively expensive, which are particularly unsuited for emergency response use. These are generally in the form of survey equipment, such as the Tissue Equivalent Proportional Counter (TEPC). The TEPC is composed of a tissue equivalent (TE) plastic case, either spherical or cylindrical, sealing in a low pressure TE gas. Together, these components satisfy the Bragg-Gray conditions, i.e., electronic equilibrium, where the wall thickness is greater than the charged particle range, and there is a compositional uniformity between the wall and gas.^[27] As with other types of proportional counters, the TEPC measures ionizations that avalanche to an anode within the detector volume, resulting in a dependable dose reading with calibration.^[27]

Personal dosimetry, however, may fall short of the standards of survey and stationary dosimetric equipment.^[10] The most common dosimeters in use around the world include: Radiographic Film Badges, Thermoluminescent Dosimeters and Silicon Diode Detectors.

Radiochromic film is a simple radiation detector where ionizations in the film initiate chemical processes and colour change.^[28] Film badges are easy to use, as they require no post-exposure processing and no amplification technique is required.^[28] Film dosimetry can distinguish between no dose and high doses (i.e., doses exceeding 1 Gy^[28]) but are not useful for low-dose use.

Thermoluminescent detectors (TLDs) also employ a simple principle, but require post-exposure treatment in order to assess the received dose. The TLD is a material which traps the ionizing effects of radiation in the form of electron-hole pairs in carefully induced impurities.^[29] The application of heat allows trapped electrons to return to the ground state with the release of a photon which can be measured for dose assessment.^[29] A TLD can also be reused. Similarly to TLDs, Optically Stimulated Dosimeters (OSL) have been developed that require light, and not heat, in order to release photons for dose determination. OSLs suffer the same limitation as TLDs in that they cannot function as an active dosimeter since the dose is assessed post-irradiation.

Silicon diode dosimeters utilize a silicon semiconductor which is defined by a depletion zone; the border between the p (positive) and n (negative) materials (in this case, doped silicon) forms an electric field consisting entirely of electron-hole pairs. Upon irradiation, the electrons are released into the circuit generating a current that can be measured, where the electron-hole pair is replaced.^[30] Variations of the silicon diode dosimeter geometry or materials allow it to measure either photons or neutrons,^[31] which must be taken into account for mixed-field measurement. Temperature can result in the production of 'dark current', which can lead to a false positive signal in the absence of any ionizing radiation.^[30]

On the other end of the spectrum of radiodosimetry are the “biodosimetry” methods, which in contrast consider the analysis of human tissues as a post-irradiation technique for radiation dose determination (Fig. 3.2). Biodosimetry does not rely on an inorganic material to approximate the response of a living system. With biodosimetry, the dose measurement comes directly from the subject's own biological system, usually in the form of the white blood cells that are particularly susceptible to radiation effects.

Common methods of biodosimetry utilize biomarkers to identify the state of the DNA damage. Dicentric chromosome assays consist of an analysis of lymphocyte DNA (white blood cells) for chromosomes with well-characterized aberrations, which have two centromeres unlike the single centromere of healthy chromosomes (or they may form a complete ring shape).^[32] The micronuclei assay involves an analysis of binucleate cells, arrested in late mitosis (when genetic material has been replicated, but not completely separated), for genetic material that has failed to be incorporated into a daughter nucleus.^[32] The comet assay visualizes DNA damage by applying a current to DNA suspended in a gel, drawing broken fragments into a comet-like tail that can be seen when the DNA is stained.^[33] Fluorescence in-Situ Hybridization (FISH) is a translocation frequency analysis technique, which involves tagging condensed DNA in metaphase with chromosome specific probes to examine DNA translocations with coloured chromosomes.^[34]

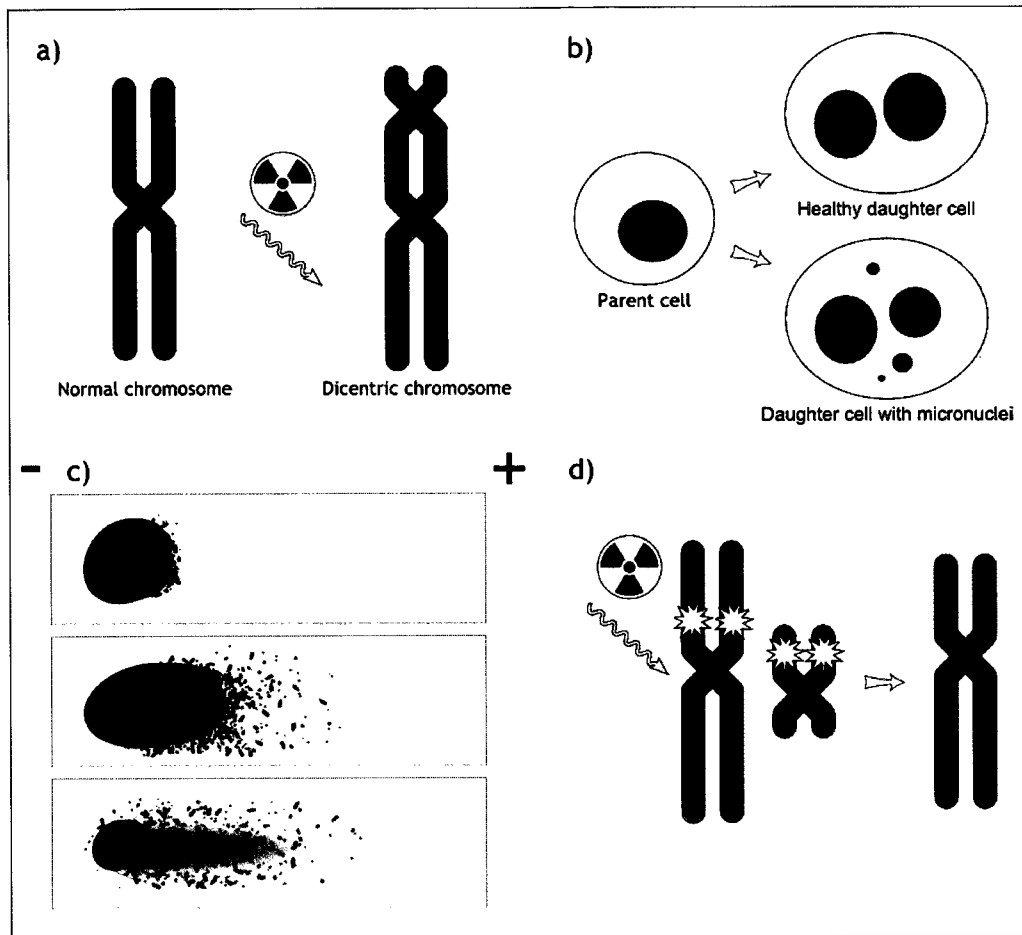


Figure 3.2 Common biodosimetry. a) Dicentric chromosomes, b) micronuclei, c) comet assay, d) FISH staining.

Unfortunately, biodosimetry has limitations. Biodosimetry cannot be used as an active dosimetry method, requiring a post-exposure analysis, which may include lengthy periods of incubation to ensure correct cell-cycle arrest. The dicentric test, for instance, may take more than 52 hours to complete. Biodosimetry also lacks the precision of inorganic methods, having high limits of detection (LOD), ranging from 0.1 to 10 Gy.^[23] This effect is due to the cell's innate ability to repair and excise damage caused to genes and cells by removing traces of damage.

DNA repair is orchestrated by a number of complementary pathways that identify and correct damage, whether caused by ionizing radiation or any other environmental insults.^[35] Simple SSBs can often be easily repaired due to the presence of a complementary strand.^[16, 36] DNA repair pathways may be responsible for managing the comparatively minimal radiation we are constantly exposed to in our environment, including cosmic radiation, terrestrial radiation, and from food and water sources.

Unfortunately, DNA repair pathways are not perfect and, in some cases, can compound the damage or orchestrate genetic rearrangements, allowing DNA damage to persevere.^[16, 20, 35] Damage in the form of SSBs or DSBs can cause the erroneous joining of broken ends of DNA, which can lead to the joining of strands that do not belong together, and can cause mutations and gene loss.^[16] This mechanism leads to the typical structures seen in the dicentric analysis and FISH. The intricacies of DNA repair complicate the ability of biodosimetry to accurately reflect the radiation dose. Hence, any radiation dosimetry should be able to take advantage of the biological relevance of DNA, yet avoid the problems associated with repair. It should also be developed with a sufficient accuracy and portability as that of an inorganic dosimeter (see Section 3.4.2).

3.4.2 DNA Dosimeter Design Requirements

Radiation can cause several types of genetic damage. For the development of the “DNA dosimeter,” it is important to target damage resulting in distinct breaks that split a DNA strand in two. Pragmatically, it is easier to detect breaks that separate two pieces of DNA than to detect non-specific and non-breaking damage. Secondly, as mentioned in Section 3.3.2, radiation damage which

results in breaks in DNA is considered to have an impact on the cell function and survival, although the correlation of the number of DNA breaks to the tissue-level risk (i.e., cancer) is not well known.

While double-stranded DNA more faithfully represents the conditions in the human cell, the choice of a single-stranded DNA sequence as a target for DNA damage serves several purposes. First, single-stranded breaks (SSBs) in a double-stranded model would be obscured by complementary strand binding. Both single- and double-stranded breaks (DSBs) have significant consequences for the survival of the cell. Although it is recognized that DSBs may be the greater cause of chromosome translocations or loss of genetic material resulting in impaired cellular functioning or cell death,^[26] the SSBs that contribute to DSBs are far easier to record in their unpaired form. In addition, it is important that this device uses “naked” DNA as a radiation target to avoid the molecular processes that serve to repair such damage to optimize the sensitivity of the device.

It is possible both to measure DNA damage in the laboratory and also to predict this damage with mathematical models. For instance, Moiseenko et al. used an atomistic model of hydrated DNA to examine radiation damage pathways and were able to calculate single stranded breaks for photons and tritium at approximately 2.6×10^{-7} SSB/Gy/bp.^[25] Here, bp refers to a ‘base pair,’ which corresponds to the configuration where two DNA strands are paired – it is used in this work in reference to single nucleotides (as is common practice). In previous experiments, DNA was irradiated and run through a sequencing gel electrophoresis in order to quantify the damage, which was found to be 1×10^{-6} SSB/Gy/bp.^[21] The number of breaks in DNA with irradiation are proportional to the dose, but not to the dose rate.^[37] It is noted that the strand break frequency can be affected by other variables such as temperature, and the components of the DNA solution,

including: the buffer solution, DNA concentration, oxygenation, etc.^[21] These theoretical and experimental results provide a baseline against which the efficiency of the DNA dosimeter can be benchmarked. Finally, it should be noted that direct strand damage is not sequence dependent, which allows for some flexibility in the specific design of the device.^[21]

3.4.3 Förster's Resonance Energy Transfer

Förster's resonance energy transfer (FRET) is a method of visualizing and quantifying the proximity and interaction of molecules by altering their fluorescence output with the use of a fluorophore (or fluor). FRET refers to the quantum mechanical transfer of excited state energy from a donor fluorophore to an acceptor chromophore (which is a light absorbing molecule).^[38] The quantum mechanical nature of this energy-transfer process occurs via dipole-dipole coupling instead of by photon release from the donor fluorophore.^[38] The efficiency of this process depends on three factors (Fig. 3.3): (i) spectral overlap between the donor emission and acceptor excitation, (ii) the distance between donor and acceptor (generally limited to within 10 nm/100 Å), and (iii) also the relative orientation of the donor and acceptor.^[39]

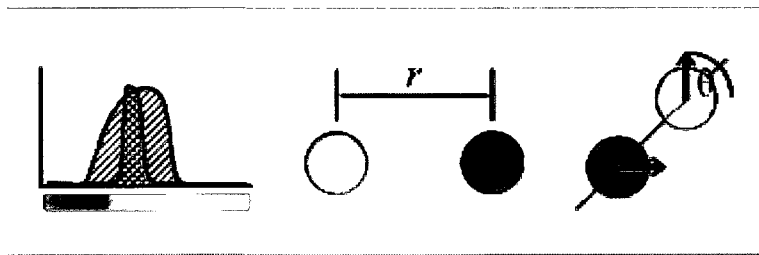


Figure 3.3: Forster resonance energy transfer dependencies. From left to right: the effect of spectral overlap, the distance between the molecules and their relative orientation.

The rate of energy transfer from the donor to the acceptor molecule is governed by the relation:

$$k_T = \frac{1}{\tau_d} \left(\frac{R_0}{r} \right)^6 \quad [3.1]$$

where τ_d is the radiative lifetime of the donor for the given donor-acceptor interaction, R_0 is known as the “Förster parameter,” the distance at which transfer of energy occurs at 50% (a consequence of the strength of the dipole-dipole contributions to energy transfer, characteristic of the specific donor and acceptor pair), and r is the intermolecular separation distance between the two molecules. As a result, the rate of energy transfer is proportional to r^{-6} , which strongly limits the interaction distance. Considering the model introduced in Section 3.6, strand breakage by radiation separates the two molecules so that fluorescence will occur.

The nature of the acceptor gives rise to a variety of applications of the FRET process (Fig. 3.4). For instance, the acceptor may be a fluorophore like the donor, emitting fluorescence on the stimulation of the donor.^[39] However, the acceptor can be a molecule that does not release energy in the form of light as it returns to a non-excited state (which is known as a dark acceptor, or a quencher).^[39] Also, the acceptor may even be the same as the donor, as long as the emission and excitation spectra have an appropriate overlap. A quencher is specifically utilized in this work, so that DNA strand breakage can be quantified with a fluorescent signal.

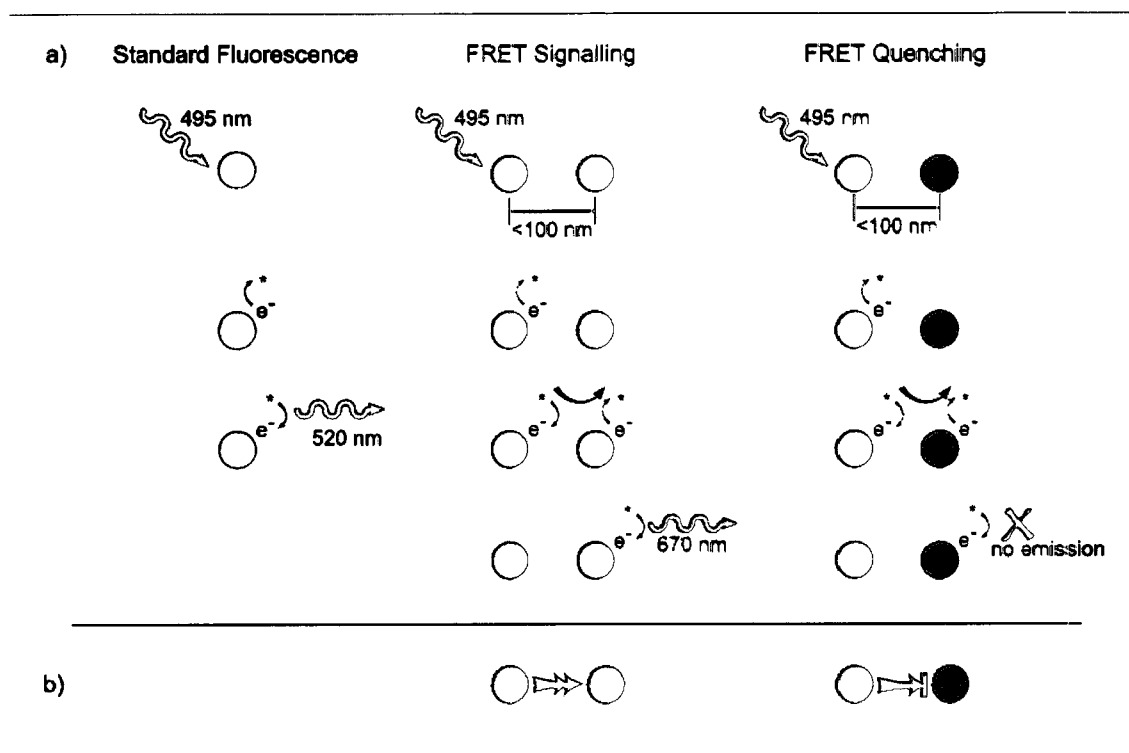


Figure 3.4: Forster's resonance energy transfer mechanisms. a) The processes of excitation and emission, b) depiction used in this work.

3.4.4 DNA as a Break Signalling Biomarker

The versatility of DNA as a potential signalling biomolecule has been reported in the literature. With four distinct bases, and nearly unlimited options in sequence and strand length, researchers have a great deal of design flexibility for various DNA applications. Combined with existing molecular methods and tools, DNA can be employed in a wide array of analytical systems, not the least of which is radiation dosimetry.

The most common use of DNA as a detection tool simply involves cyclical, exponential replication of a small quantity of DNA followed by the binding of small oligonucleotide probes in

order to register the presence of specific sequences. This is known as polymerase chain reaction (PCR) and, by regulating the number of PCR cycles, the initial quantity of DNA can be determined. This approach is known as quantitative PCR (qPCR). PCR duplicates the natural process of DNA replication in the living cell, which requires the following components: unlinked nucleotides, DNA polymerase, a pair of oligonucleotide primers which bracket the region to be amplified on opposing strands, and the sample DNA to be amplified. The number of copies of identical strands of DNA can be measured by analyzing the fluorescence of a dye (SYBR green) that binds to the new copies. The replication process is depicted in Fig. 3.5.^[40]

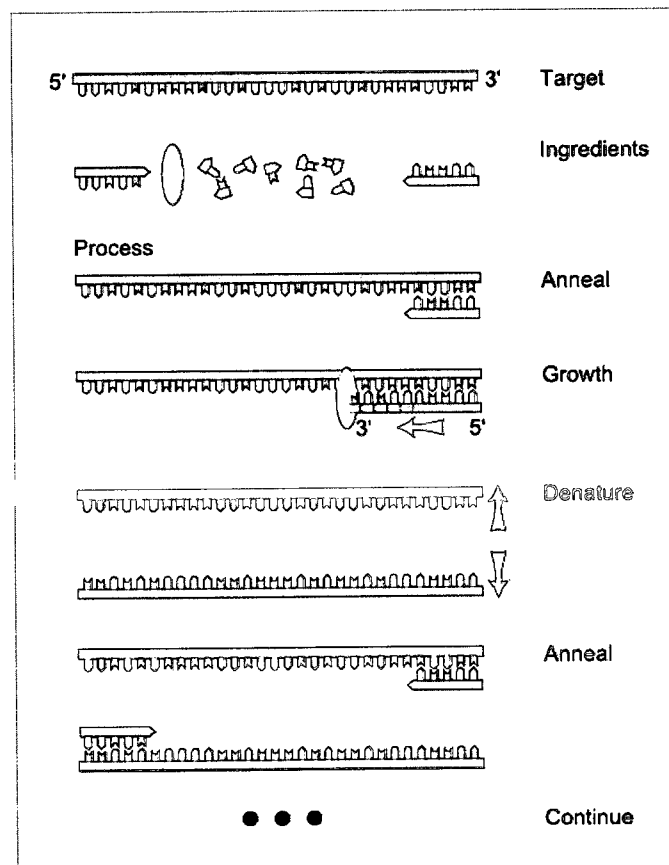


Figure 3.5: The polymerase chain reaction mechanism.

One of the least complicated methods for the use of DNA as a radiation dosimeter is by simple visual analysis (Fig. 3.6). For instance, in a study by Matsunaga et al., DNA was deposited on glass slides in solution, and then physically elongated and fixed with a cover slip.^[37] Dried samples were exposed to gamma radiation from 0 to 30 Gy, stained, and photographed through a fluorescence microscope by a cooled CCD camera for visual and computational analysis. Double-stranded breaks were easily identifiable as gaps in the elongated DNA strands.^[37] As expected, the DSBs counted in this method were proportional to the dose of irradiation, but this method did not have the same sensitivity as traditional inorganic methods.^[37] Also, this method is difficult to scale to a flexible portable system, since it requires precise optical scanning of a two-dimensional surface.

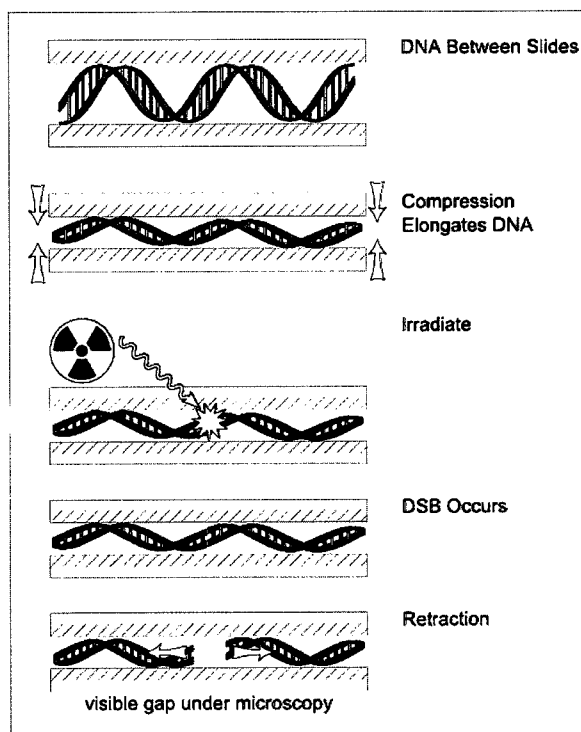


Figure 3.6: Elastic double-stranded break detection scheme.

Recent developments in break detection take advantage of the cell's naturally-occurring hardware to construct molecular machines that move and process information and energy.^[41] For example, molecular machines have been designed to detect dsDNA breaks using two fluorophores in order to label a single strand of self-binding DNA (Fig. 3.7). The single stranded DNA contains complementary binding regions to allow it to behave like double stranded DNA. In this case, the *vaccinia* virus topoisomerase has been used to split the molecule opposite the loose strand ends. These paired biosensors bind to two different kinds of DSBs selectively, thereby localizing the break.^[41] Although this method has proved useful for DSB localization (which may lead to cell death), it requires a significant amount of incubation time combined with sensitive temperature regulation.

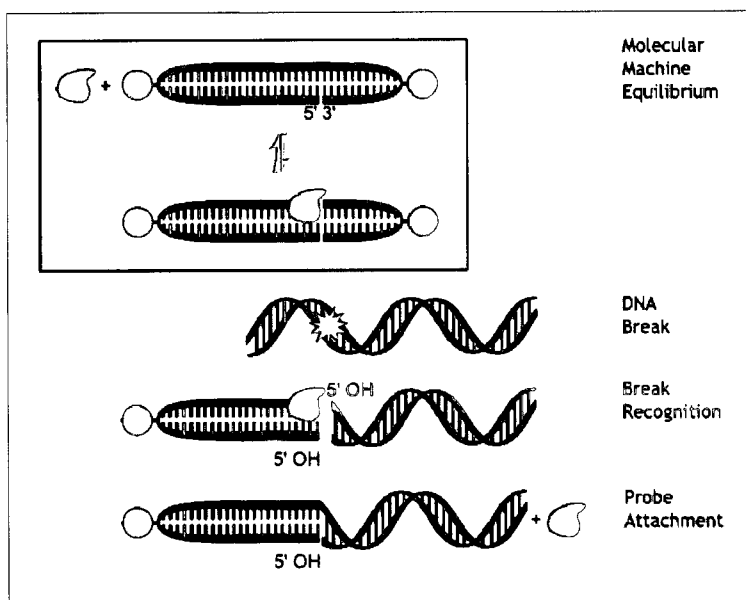


Figure 3.7: Molecular machine break detection scheme.

A much more elegant method for the detection of DNA breaks comes from the field of molecular beacon design. These beacons are a type of biosensor designed with a fluorophore and a quencher at each end of a short strand of ssDNA with complementary regions adjacent to the

chromophores and a probe sequence in the middle. These constructs form a stem and loop configuration in the absence of a target sequence. The presence of a target induces beacon binding to the target, so that the stem portion of the structure is pulled apart, resulting in a signal with a separation of the fluorophore from the quencher.

“DNA Break Lights” take advantage of this configuration, but turn it into a scission beacon, relying on a site specific cleavage to break DNA in the stem section of the beacon, causing weakening of the complementary binding, with a release of the fluorophore from the quencher (Fig. 3.8).^[42]

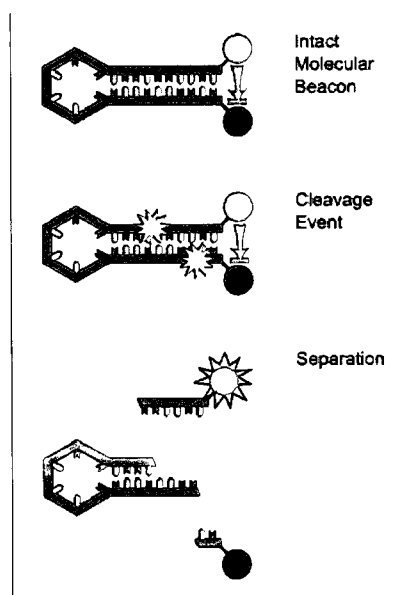


Figure 3.8: Molecular beacon break detection scheme.

This method benefits from a 99% quenching efficiency in its pre-sensing state and demonstrable limit of detection in the picomolar range (as of 2000).^[42] Unfortunately, the break light method requires both site specific cleavage and temperature regulation to guarantee a reasonable separation of the fluorophore from the quencher.

A recent study has yielded the developments of a simple oligonucleotide chip assay which detects SSBs that are cleaved along their length from a solid support (Fig. 3.9). A 20-base single stranded oligonucleotide with a fluorescein fluorophore bound to its 5' end was secured to a silicon oxide wafer via an avidin-biotin link.^[43] A breakage in the strand causes it to separate from the solid surface and into the supernatant, which is subsequently collected and measured by laser stimulation.^[43] However, this method has a limit of detection in the nanomolar range, and requires mechanical separation from the exposure volume for analysis.

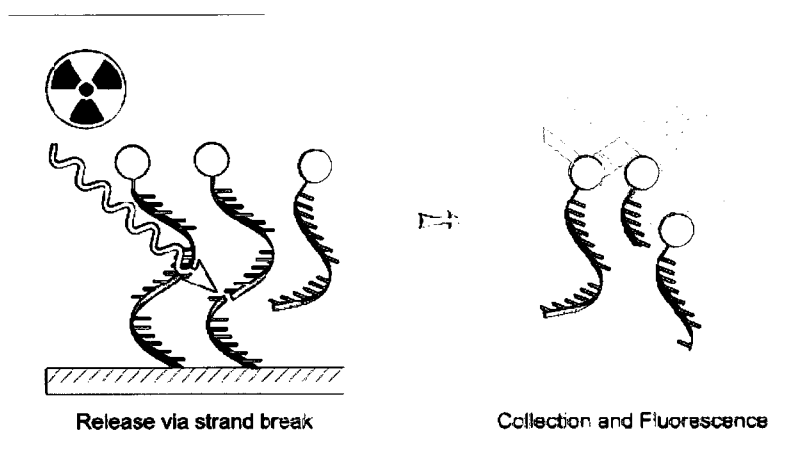


Figure 3.9: Simple surface-bound oligonucleotide break detection scheme.

3.5 New Method: Fluorescence Chain Reaction

The first method explored for the development of the DNA dosimeter (as part of a CRTI project) was the use of signal amplification to report individual strand breaks (Fig. 3.10). This method, referred to as Fluorescence Chain Reaction (FCR), was designed to detect trace copies of DNA in a solution.^[43]

FCR DNA detection begins with a molecular duplex: a cationic polythiophene and a DNA probe. The probe is a traditional DNA probe, consisting of the complementary strand to the DNA sequence of interest, the detection target, and a reporter molecule: Alexa Fluor 546 with an excitation peak at 554 nm and emission at 570 nm.

The polythiophene has a number of unique properties that are well suited for this application. First, it has configuration-dependent spectral properties. When in solution, the polythiophene assumes a loose configuration with an excitation of 425 nm and a maximum of emission at 525 nm that appears yellow. Secondly, when mixed with a DNA sequence of similar length, the polythiophene assumes a rigid, planar conformation, and is spectrally quenched, appearing red with an absorbent peak at 527 nm. Finally, when a strand of DNA complementary to the duplex DNA is combined with the duplex, the strands bind, and the cationic polythiophene is twisted back into a loose conformation around the dsDNA to form a triplex unit.^[45]

The polythiophene combined with the DNA probe exhibit another property in solution that greatly improves the signal-to-noise ratio of this method. It forms an aggregate with other duplexes, and takes advantage of the Alexa Fluors' close emission /excitation wavelengths and overlap with the polythiophene excitation. When a target-binding event occurs, it can be detected via FRET. The solution is illuminated with an LED (light emitting diode) at the polythiophene's excitation maximum. The stimulated polythiophene fluoresces at a wavelength of 525 nm corresponding to the Alexa Fluor 546 nm excitation maximum, which overlaps its emission spectrum so that this signal cascades to nearby Alexa Fluors, inducing the whole unit to emit a signal.^[46]

FCR detection may be able to detect unique target sequences at the femtomolar range, making it an incredibly powerful tool for diagnostics, molecular identification, and research analysis.^[21] However, the same property that makes it so useful for these applications, may also hinder it as a tool for DNA dosimetry. The polyelectrolyte aggregates form with a variable number of duplex units,^[45] which may have implications since the DNA dosimeter needs to be a quantitative tool.

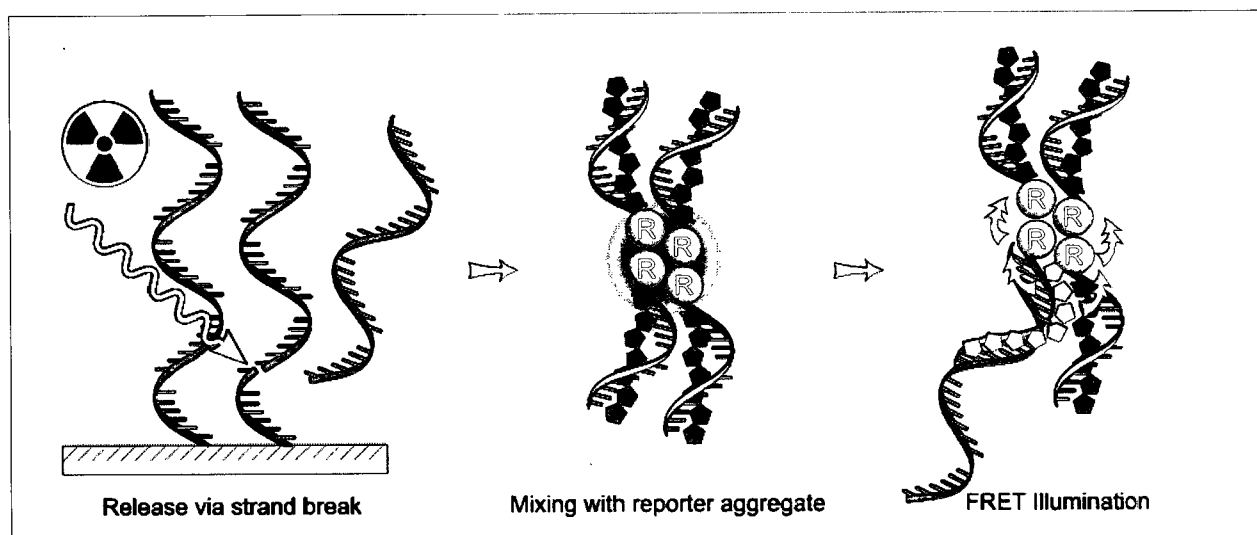


Figure 3.10: Fluorescence chain reaction break detection scheme.

In the current dosimeter development, qPCR was eventually used in the place of the FCR method since the PCR materials and equipment are more easily manufactured (see discussion in Section 4.1).

3.6 New Method: Dual-Labelled Oligonucleotide Sensor

The second DNA dosimeter method that was explored instead at RMC (and that is investigated specifically in this work) takes advantage of the same kind of simplicity in design and

use as the DNA break lights already discussed. The important improvement over the previously described FCR/PCR method is that the dosimeter no longer has to be bound to a surface (which gives rise to background contamination issues as discussed in Section 4, which significantly affect the signal-to-noise ratio).

The major difference between this method and “break lights” is the abolishment of the self-binding stem – removing the need for site specificity in terms of break location, and allowing the device to work over a broad range of temperatures, unrestricted by a need to disanneal. Unfortunately, as a drawback, this configuration limits the length of DNA that can be used for the biosensor, so that they are within the 100 Å of the FRET range. The chromophores used in this design are Fluorescein (FAM), a fluorophore with an excitation wavelength of 495 nm and an emission wavelength of 520 nm (green). The FAM is paired to a Black Hole Quencher (BHQ-1) that quenches in the range of 480-580 nm.

Just as in “break lights,” a signal can be detected as soon as a break occurs (Fig. 3.11), with a separation of the quencher and fluorophore. The signal will therefore increase with an increasing number of DNA breaks between the chromophores.

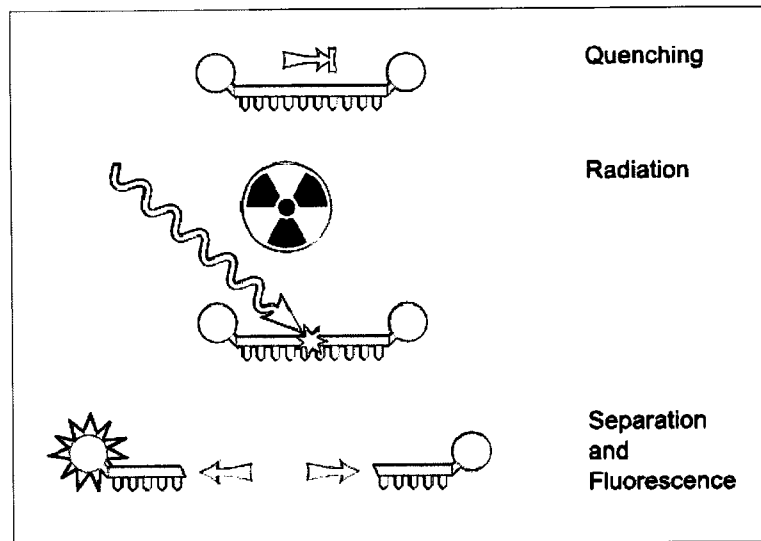


Figure 3.11: Black hole quencher break detection scheme.

4 Experimental Description

As discussed in Chapter 3, two different models of the DNA dosimeter were developed as prototype devices for radiation measurement. In the original development, the Centre de Recherche en Infectiologie de l'Université Laval (CRI) developed a novel concept based on a polymeric transducer, which was supported by a PCR technique. As part of this research initiative, and encompassed in this work, the Royal Military College (RMC) was tasked to carry out radiation testing at domestic and international facilities (see Section 4.1). An opportunity arose where RMC was invited to perform experiments at the CERN-EU high energy reference field (CERF) and at the Geneva University research hospital. This facility provides an integral mixed radiation field for dosimeter calibration. The CERF facility is specifically able to provide a stimulant (high-energy) neutron spectrum as experienced at jet aircraft altitudes and in space.^[47, 48] Additional testing of this prototype device was also carried out in domestic experiments in a well-defined gamma radiation field at Health Canada. These experiments, however, revealed a limited signal-to-noise capability for the device, particularly at the lower radiation levels where this device was expected to operate.^[49]

Consequently, a new device was developed instead by an RMC researcher (K. McDermott), which employed a dual-labelled oligonucleotide approach (see Section 4.2). For this thesis investigation, additional experimentation was carried out at the Defence Research and Development Canada – Ottawa (DRDC-O) facilities in order to characterize and quantify the improved device. In particular, this testing focused on an assessment of the device to respond to DNA breakage at various absorbed dose levels. In addition, the performance of the components of the black hole quencher (BHQ) dosimeter was also evaluated in this work, which included the efficiency of the

quenching function of the dosimeter and the possible destruction of the fluorescent reporter (FAM) molecule.

The procedures and results of this experimentation are documented in this chapter.

4.1 Polymeric Transducer Dosimeter

In order to test and develop the optimal configuration of the DNA dosimeter system developed by CRI, which was based on a polymeric transducer concept, quantitative Polymerase Chain Reaction was used in the place of the Fluorescence Chain Reaction (FCR). This change was considered since PCR materials and equipment are commonly manufactured and easier to use. A description of these experiments is detailed in the following sections, including: (i) a description of the development of the device (Section 4.1.1), (ii) the preparation of the device for irradiation testing (Section 4.1.2), and (iii) the post-irradiation treatment and analysis (Section 4.1.3). The results of this experimentation are presented in Section 4.1.4.

4.1.1 Materials

As mentioned, single-strand DNA oligonucleotides were developed by CRI for qPCR analysis. As shown in Figure 4.1, the oligonucleotide itself is 70 bases long consisting of a 50-base 'target' region and a 20-base 'tag' region. This construct is analogous to the 70-base FCR oligonucleotide that was originally conceived. The PCR methodology measures the amount of 'tag'

released by any DNA breakage occurring in the target area. Any number of 70-base oligonucleotides that remain unbound to the support following preparation are detectable via the 70-base qPCR and represent a background contributor in this method (see discussion in Section 4.1.4)

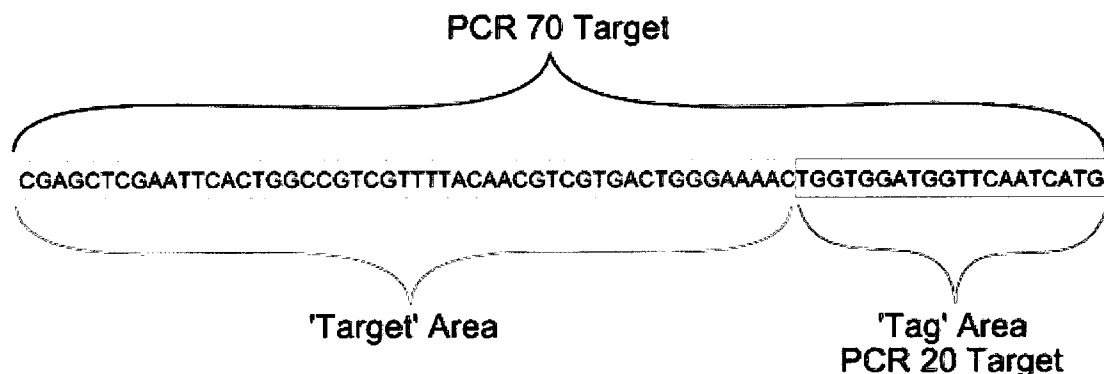


Figure 4.1: Schematic of the Polymeric Transducer Dosimeter.

The 70-base sequence is subsequently bound to a solid surface by a short spacer. The 70-base oligonucleotides were fixed on a solid support (glass and plastic slides) at the Industrial Materials Institute of the National Research Council (IMI-NRC). Plastic slides were printed using EDC NHS coupling.^[50] The aldehyde-coated glass slides were printed using an Omnigrid Accent microarrayer manufactured by GeneMachines, San Carlos, CA. These slides were washed to remove loose or unattached DNA oligonucleotides from their surfaces, and then vacuum sealed for transportation. In conjunction with the slide preparation process, 20 uL hybridization chambers (HybriWells, Invitrogen, Carlsbad, CA) were used to protect the DNA during handling and irradiation.

4.1.2 Pre-irradiation Treatment and Irradiation

For the irradiation of the slides, microfluidic or hybridization chambers were applied to the slides with a sterile smoothing tool. The dosimeter slides were further arranged on a sheet of Plexiglas and the unit was secured with metal clips.

Irradiations in a mixed-field (containing neutrons, photons, electrons, muons, pions, and protons) were subsequently performed at CERF as part of this thesis work. This facility is set up at one of the secondary beams from the Super Proton Synchrotron at CERN. Particles (i.e., protons and pions) from a charged hadron beam hit a copper target, which is 50 cm long and 7 cm in diameter (Fig. 4.2). The secondary particles resulting from this interaction are then filtered by an 80-cm thick concrete shielding placed above the copper target. Normally, dosimeters are placed on top of the concrete shielding (as in Fig. 4.2) for typical low-dose testing. As mentioned, the resultant neutron field is due to primary particle interactions with the copper target and secondary particle interactions in the concrete. This resultant field is a reasonable simulant of the integral neutron spectrum experienced at jet altitudes and in space, where a so-called “evaporation” and “spallation” peak at 1 and 100 MeV, respectively, are observed. Real-time physical dosimetry at the facility is provided in the form of an in-house precision ion chamber (PIC). For this investigation, higher dose irradiations were required, necessitating a relocation of the dosimeter samples inside the shielding enclosure closer to the copper target (Fig. 4.2). Here, samples were removed from their Plexiglas support to an in-house plastic exposure tray. Although there was no precise physical dosimetry performed at this specific location, the dose was estimated to be ~ 5 Gy by CERN

research personnel based on past research experience and field calibration.

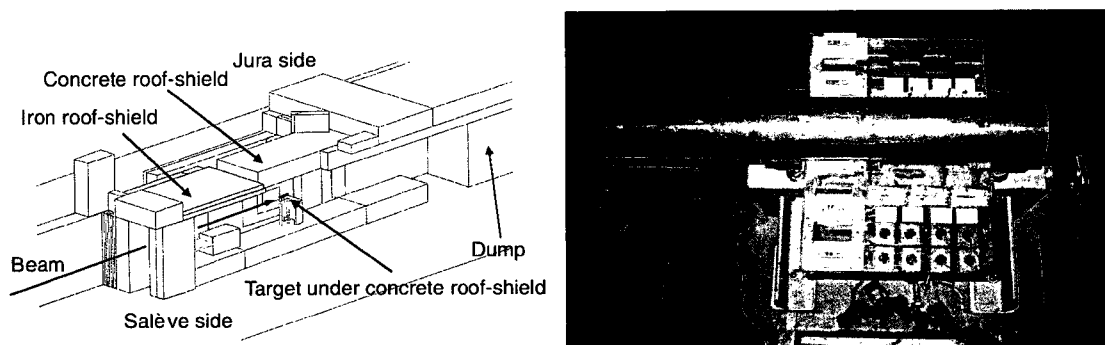


Figure 4.2: High dose mixed-field radiation experimental arrangement. (Drawing courtesy of CERF.^[51])

4.1.3 Post-Irradiation Treatment and Analysis

Following irradiation, DNA fragments were collected from the slides using a washing procedure. Any unattached DNA was transferred in this process to microtubes for transport and analysis. Here, the volume of water used for the washing is twice that of the chamber volume (20 uL as hybriwell chambers have a 10 uL capacity). In this process, the slides had two volumes of wash applied and collected. After transfer to microtubes, these samples were stored on dry ice for transport back to Canada.

Analysis of the transported samples was performed at the Centre de Recherche en Infectiologie – Centre Hospitalier de l'Université Laval (CRI-CHUL) where real-time quantitative qPCR was employed. A Rotor-Gene 3000 Thermocycler (Corbett Research, Sydney Australia), and SYBR green probes were used for this procedure. For the samples collected from slides, a short 20-base qPCR (complementary to the probe region) was run to measure the tag on the fragmented

DNA material. A full 70-base qPCR was also run for comparison to assess any background material not attached to the slides.

4.1.4 Polymeric Transducer Irradiation PCR Results

The unirradiated 20-base and 70-base PCR represents the background of loose DNA that was incompletely bound to the slide surface. The irradiated 20-base PCR is the specific quantity of interest, which indicates strands of DNA that have been fragmented due to the radiation.

As shown in Figure 4.3, there is a significant difference between the unirradiated (control) and irradiated samples for the 20-base (tag) and 70-base PCR analysis due to the separation of the values and their standard deviations. The background can be derived from the unirradiated control samples: 70-base PCR (8.7×10^8 ($\pm 1.5 \times 10^8$) copies) measures the number of complete strands not bound to the slide and released during the washing process, and 20-base PCR (9.4×10^8 ($\pm 1.9 \times 10^8$) copies) measures this as well as ends cleaved from bound oligonucleotides due to ubiquitous background radiation. The 70-base PCR measures the average amount of background minus strands that have been cleaved between the two ends, (1.1×10^9 ($\pm 1.3 \times 10^8$) copies). Copies of 20-base PCR (3.7×10^9 ($\pm 5.9 \times 10^8$)) were detected for DNA release by radiation at an estimated dose of 5 Gy. The error bars in the figure are for 1 standard deviation. This observation indicated a significant influence of the 5 Gy radiation field for DNA breakage where the observed tag signal (for the 20-base oligonucleotide) can be seen well above the background 70-base nucleotide signal by a factor of about four.

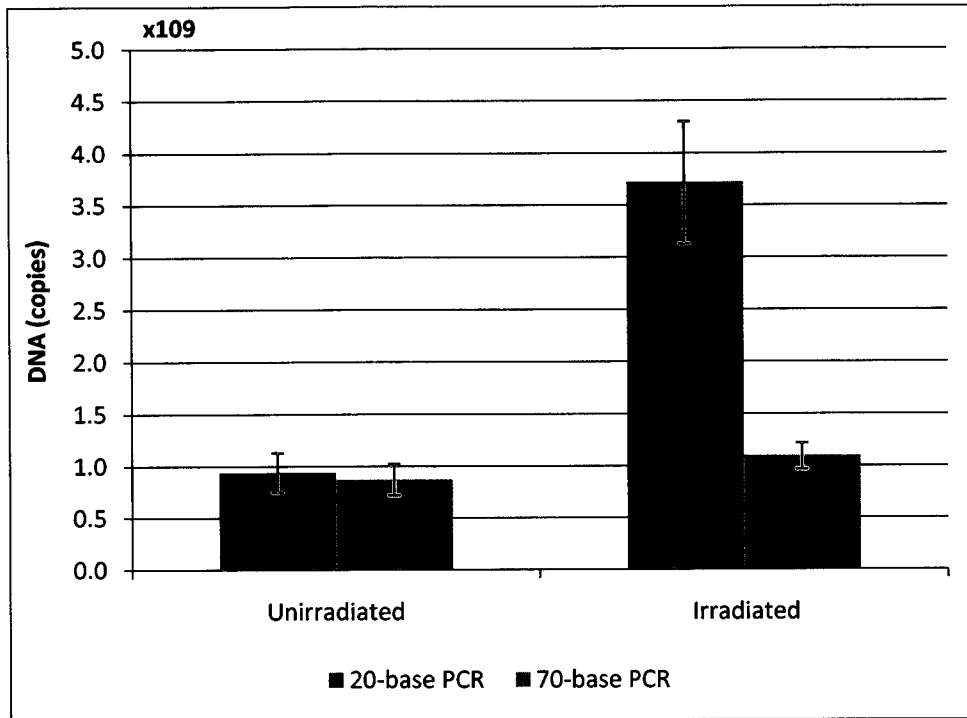


Figure 4.3: High dose mixed-radiation PCR results. Error bars one standard deviation.

As discussed in Chapter 3, neutrons have a radiation quality which is an order of magnitude greater than that of gamma radiation. Hence, the corresponding dose equivalent is ~50 Sv, which corresponds to an extremely high radiation field that would be lethal to humans.

Similar gamma-field testing of the dosimeter construct (outside of this study) was also conducted by CRI research personnel using a Cs-137 Gamma Cell 40 (Atomic Energy of Canada Ltd, Ottawa, Canada) with a dose rate of 0.9 Gy/min located at Health Canada, used for radiobiological investigation. In this latter study, a response for the polymeric transducer dosimeter above background could not be successfully obtained over the absorbed dose range of 250 mGy to 1 Gy (Fig. 4.4). A further analysis by CRI research personnel revealed that there were large amounts of unattached DNA (i.e., 10^9 to 10^{11} copies/ μ L) which contributed to the very large background

signal. Consequently, RMC moved forward instead with a new design of dosimeter utilizing the dual-labelled oligonucleotide approach. This new dosimeter concept was further tested in this thesis work at dose levels up to 10 Gy in a gamma field at DRDC-O (Section 4.2).

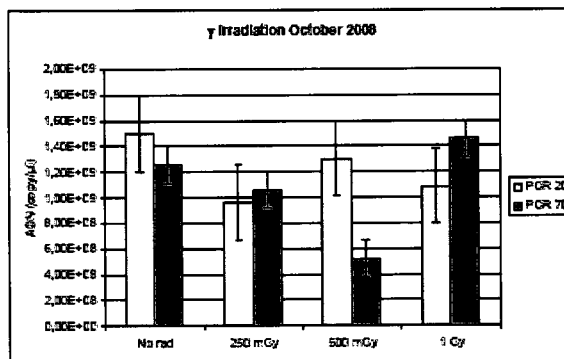


Figure 4.4: Gamma dose measurements performed by Health Canada.

4.2 Dual-Labelled Oligonucleotide Dosimeter

A description of the irradiation testing is detailed in the following sections, including: (i) the dosimeter preparation (Section 4.2.1), (ii) the performance of the black hole quencher and reporter molecule (Section 4.2.2), and (iii) irradiation results (Section 4.2.3).

4.2.1 Dosimeter Preparation

All single-strand oligonucleotides were manufactured at BioSearch (Novato, CA). Three molecules were considered as candidates for the DNA dosimeter: FAM-dT(10)-BHQ1, FAM-dT(20)-BHQ1, FAM-dT(30)-BHQ1. In this nomenclature, “dT(10)” is a 10-base Thymine. The following molecules: dT(10), dT(20), dT(30), and FAMdT(10), FAMdT(20), and FAMdT(30), were

used in order to assess different dosimeter designs and performance, i.e., the response of the detector as a function of the distance between the reporter fluor molecule and the black hole quencher (BHQ). Figure 4.5 shows the different construct molecules and components of the dual-labelled oligonucleotide dosimeter that was considered for testing and detector optimization.

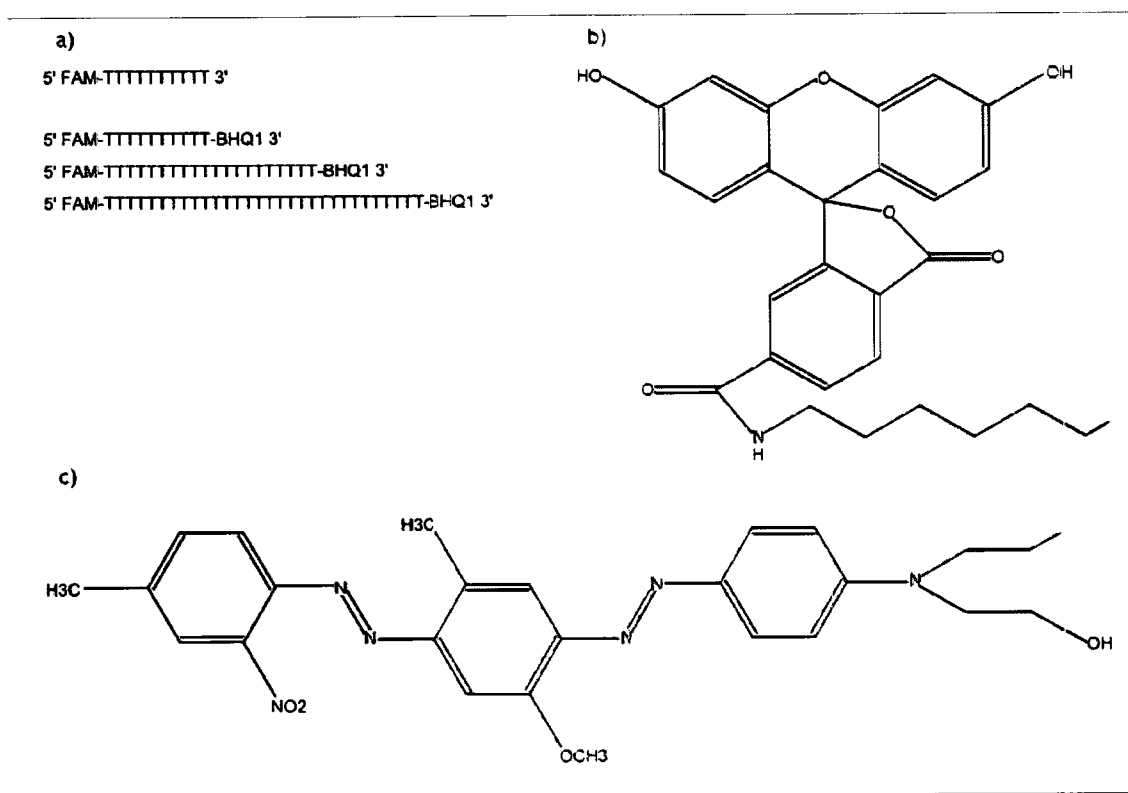


Figure 4.5: Dual-labelled DNA dosimeter molecules and components. a) Different configurations of the DNA dosimeter b) The structure of the FAM component of the dosimeter, c) The structure of the BHQ1 component of the dosimeter.

Samples of the dosimeter molecules were suspended in high-purity water that was diluted to the desired concentrations and distributed in 96-well microplates. The microplates had a volume of 150 μL /well. The polystyrene microplate surfaces were prepared with a “polyethylene oxide-like”

non-binding treatment, proprietary to Corning®, so that the DNA material did not bind to the plate surface. The wells were sealed with an adhesive polyester film in order to protect them during irradiation and handling. The results were analyzed at DRDC-O on a Synergy HT Microplate Reader (BioTek, Winooski, VT), with Photomultiplier Tube (PMT) sensitivities of 75 and 85. The goal of this project is to measure breakages in oligonucleotide dosimeters. It is therefore important to quantify the signal as reported by the analytical equipment, in terms of the reporting of the individual fluors. A conversion factor was therefore derived from the empirical measurements of the standard curve of the FAM-dT(10) at each photomultiplier tube (PMT) sensitivity. The reported fluorescence intensity is thus multiplied by an appropriate conversion factor in order to determine the number of individual reporter molecules or single stranded breaks (The calculation is presented in Appendix A).

4.2.2 Detector Performance

Radiation can deposit energy in the black hole quencher or the reporter fluor (FAM) molecule, causing damage to these molecules, besides any DNA breakages to the oligonucleotide. Thus, it is important to assess the effect of radiation on the complete construct. A baseline efficiency experiment without irradiation was therefore performed to determine the quenching efficiency of the BHQ as a function of the number of bases (Section 4.2.2.1). The impact of radiation on the fluor is detailed in Section 4.2.2.3.

The raw data for the various experimental runs are summarized in Appendix B. An analysis of the quality of these data is also presented in Appendix C. Finally, an assessment of the DNA

fluorescence and the calibration of the BioTek Synergy HT spectrometer instrument used at DRDC-O are documented in Appendix D.

4.2.2.1 Quenching Efficiency

Three different lengths of dosimeter molecules were examined to investigate and maximize the performance of the dosimeter, i.e., 10, 20 and 30 bases of irradiation target between the fluor and quencher. These lengths were chosen based on the length of a double stranded helical DNA. Thus, three candidate dosimeters (FAM-dT(10)-BHQ1, FAM-dT(20)-BHQ1, FAM-dT(30)-BHQ1) were analyzed prior to irradiation in order to obtain baseline data for the evaluation of the quenching efficiency of the BHQ1 quencher at various concentrations from 0 (control) to 1 μ M.

As mentioned, these three lengths were analyzed first without exposure to radiation. The results are shown in Figure 4.6, where the error bars are one standard deviation. These results are compared to the projected strength of the unimpeded reporter fluor at the same concentration value. As shown in the figure, at a concentration of 1.0 μ M, the FAM-dT(30)-BHQ1 has a signal that is the least quenched at 21.69% of the strength of the reporter, compared to 15.24% for the FAM-dT(20)-BHQ1 and 0.06% for the FAM-dT(10)-BHQ1 construct, which is the most strongly quenched. For the dosimeter design, a strongly quenched dosimeter is necessary in order to improve the signal above the background.

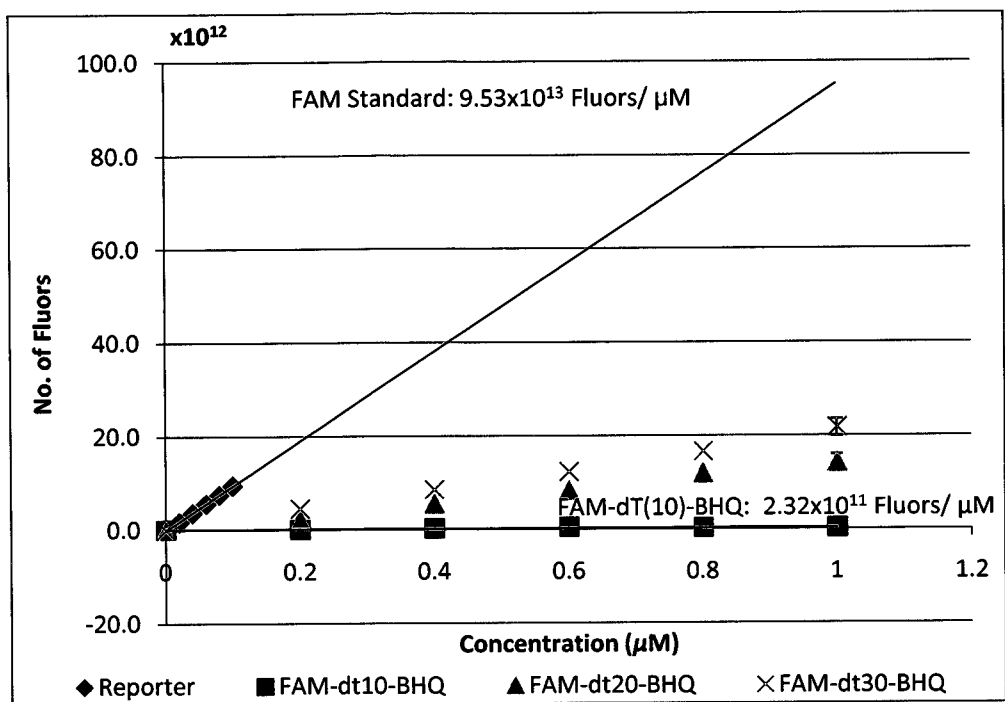


Figure 4.6: Quenching efficiency for dosimeters of different lengths. Error bars of one standard deviation for 1 μM only.

4.2.2.2 Irradiation

Irradiations were performed at DRDC-O using a Cobalt-60 source (Fig. 4.7) with a dose rate of 12.28 Sv/h at a distance of 1 m. This dose rate was based on the given source strength (accounting for decay) and confirmed by DRDC-O research personnel with physical dosimetry. Dual-labelled dosimeters with concentrations of 0.0 (i.e., a water control) to 1.0 μM were exposed to the gamma source over an irradiation dose range of 0 to 10 Gy.

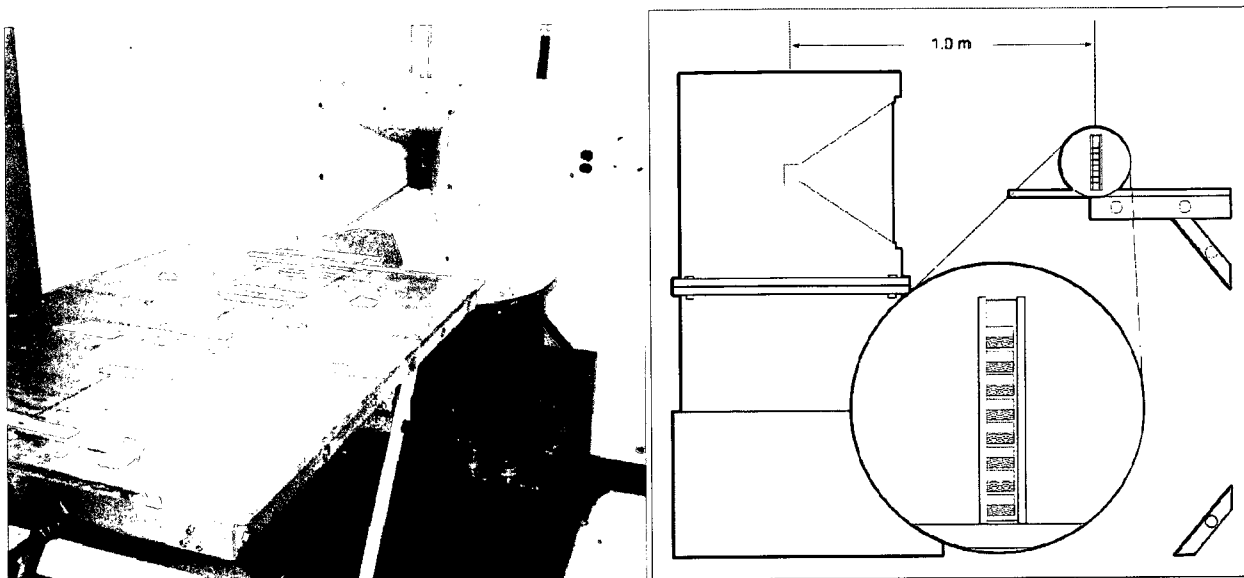


Figure 4.7: Cobalt gamma irradiator at DRDC-O. (Drawing depicts experimental setup)

4.2.2.3 Reporter Robustness

The FAM-dT(10) was selected as the dosimeter of choice since it was most effective with the selected BHQ (see Section 4.2.2.1), leading to the lowest background signal. As mentioned, this construct consists of a reporter molecule and a 10-base thymidine DNA sequence, which was exposed to a range of doses of radiation (0.1 to 10 Gy). A range of concentrations (0.0 to 0.1 μM) was used to evaluate the degradation of the FAM due to irradiation.

The FAM-dT(10) construct, which contains an unquenched reporter molecule, was analyzed to determine the impact of radiation on the reporter molecule alone. All radiations were single irradiations with no cumulative exposure because of the possibility of photobleaching (a deterioration of fluorescence described later in this section). The dosimeter was originally stored in a cool environment and unpacked for testing. Following warming to room temperature, water

beading on the adhesive surface was observed. As such, plates that showed beading were set aside for a second day of testing and left overnight at room temperature.

Since data were collected on successive days, the data sets have been treated separately. Figure 4.8 (a) and (b) show the effect of the absorbed dose on fluorescence on the two separate days, where different doses were explored to attempt to narrow the limit of detection. Figures 4.9 (a) and (b) also show the calculated slope for the given regression line for the “free” observed reporters for the reporter molecule at a concentration of 1.0 μM . Here, slopes of -7.72×10^{10} and -5.62×10^{11} reporters/Gy are observed. In particular, the slope increases from Day 1 to Day 2 indicating that some kind of effect is occurring between the two days of experiments. Figures 4.10 (a) and (b) also show the difference in response between the un-irradiated and irradiated FAM-dt(10) samples for the two days at various radiation levels at 1.0 μM

It is important that the reporter molecule remains undamaged by radiation since this will impact the ability of the dosimeter to register DNA breakage. Hence, this effect must be corrected for in the final analysis. Figure 4.8 (a) and (b) show the effect of radiation on the decreasing response of the fluorescence signal with increasing radiation levels for the reporter molecule, i.e., the decrease in response is more affected at higher dose levels as expected. In addition, as previously mentioned, the second day of irradiation shows the greatest effect of fluor degradation as further depicted in Figure 4.11.

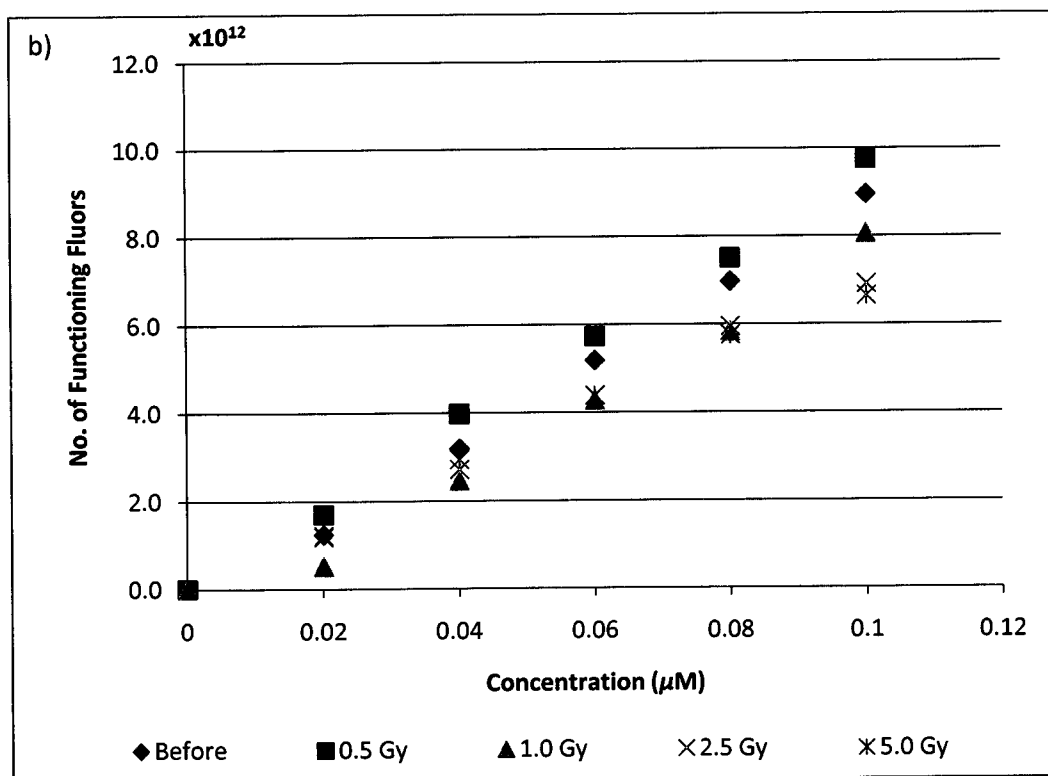
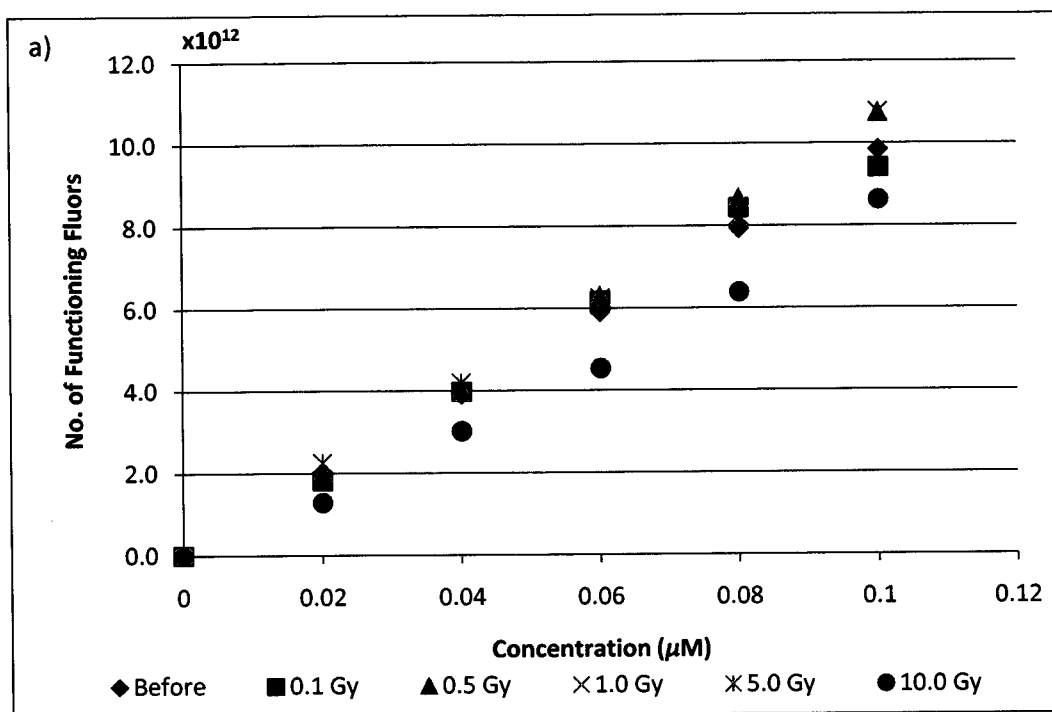


Figure 4.8: Reporter response to gamma radiation for a) Day 1 and b) Day 2.

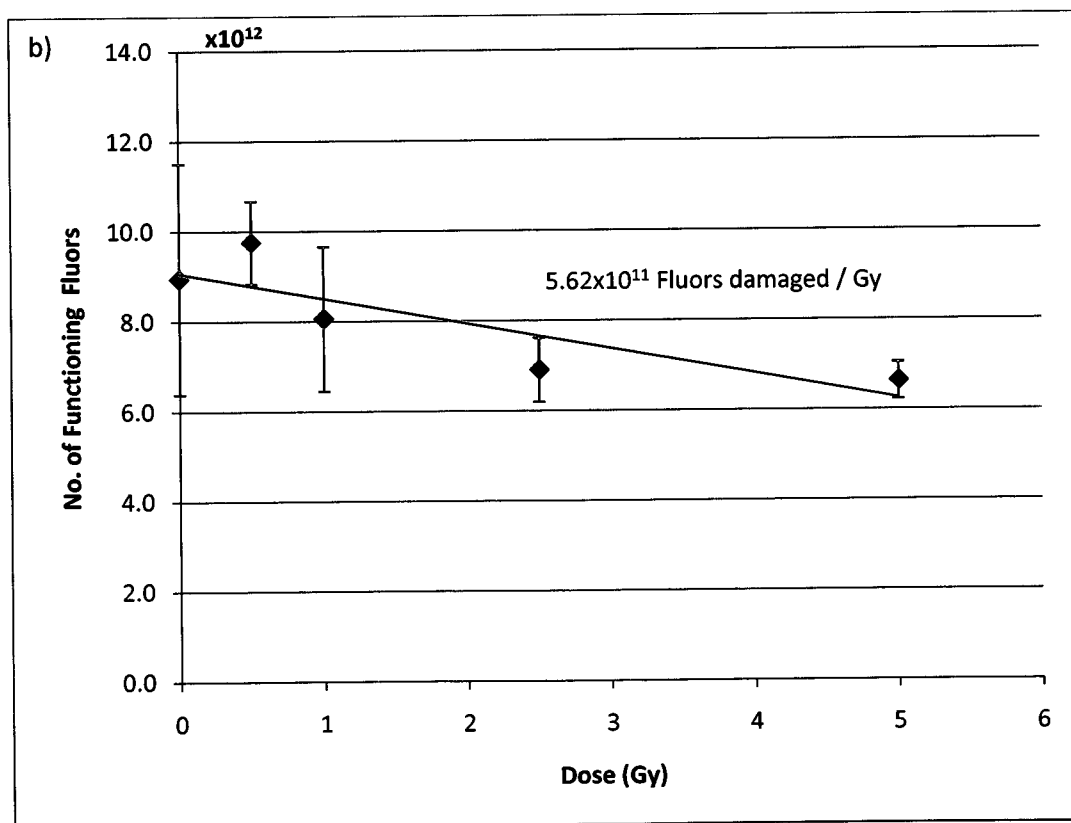
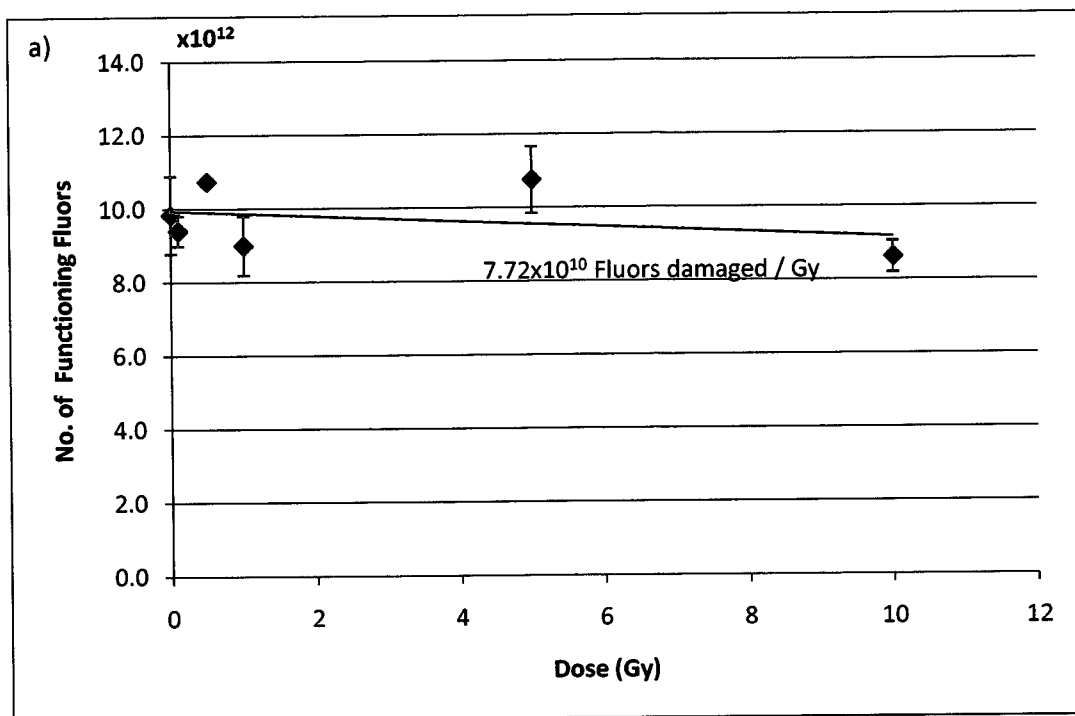


Figure 4.9: Slope in the response curve for the reporter molecule at a concentration of $1.0 \mu\text{m}$ for a) Day 1 and b) Day 2. Error bars one standard deviation.

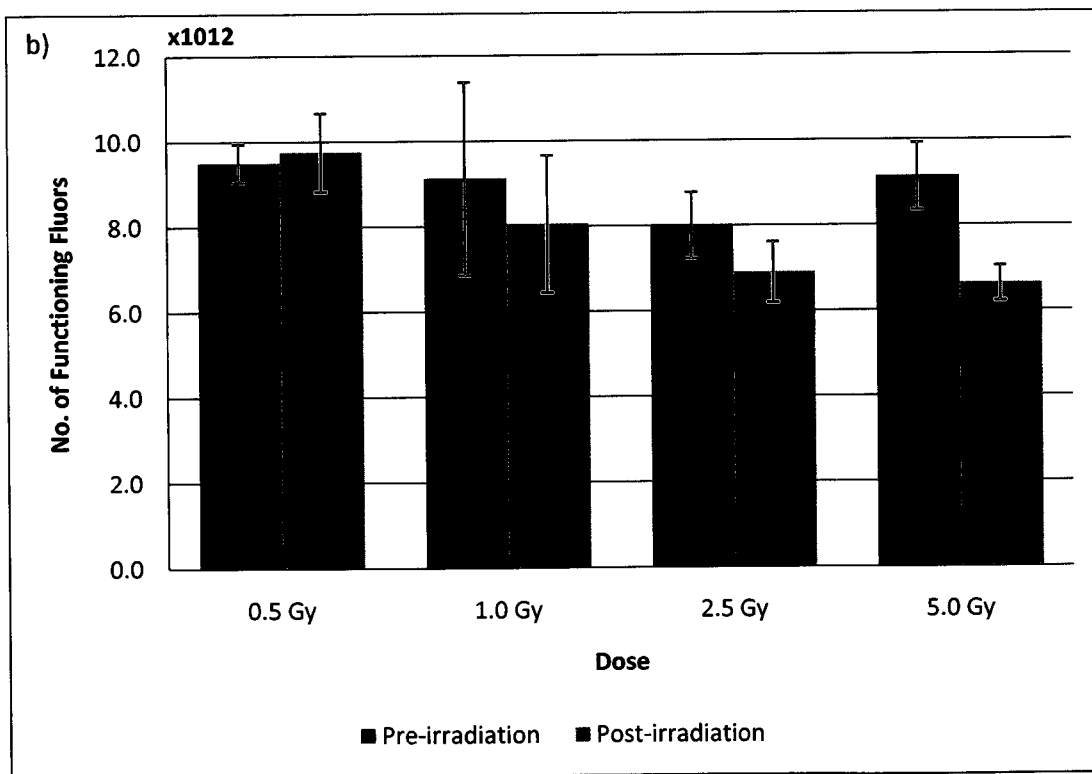
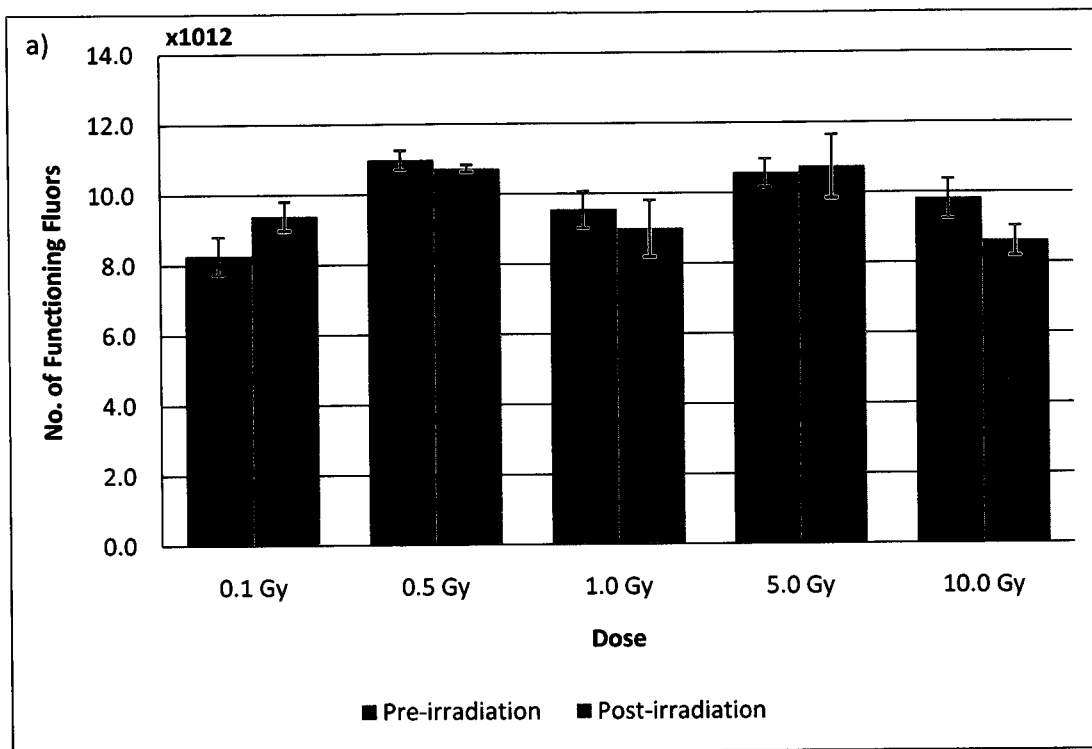


Figure 4.10: Reporter response to irradiation between unirradiated and irradiated samples for a) Day 1 and b) Day 2. Error bars one standard deviation.

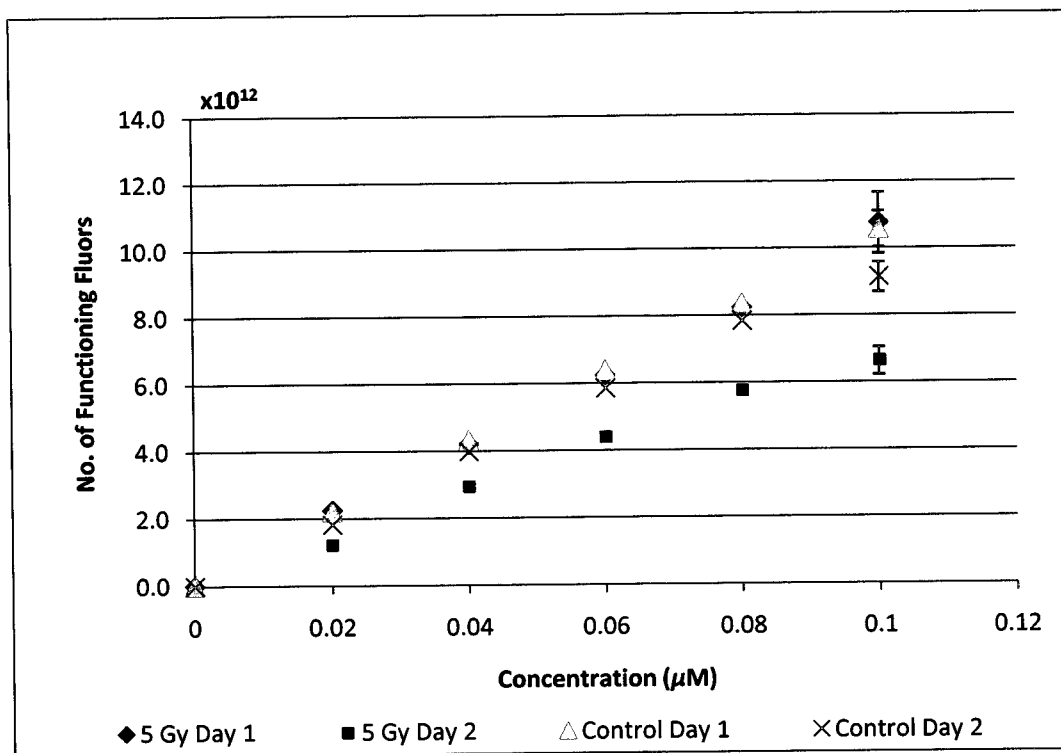


Figure 4.11: Reporter response to irradiation for the experiments on Day 1 and Day 2. Error bars one standard deviation, shown for 1.0 μM only.

One of the concerns with using fluorophores is the effect of photobleaching. Repeated exposure of fluors to light, stimulating the fluorescent effect, leads to the eventual destruction of the fluor. Photobleaching effects may become important if the dosimeter is continually read (since it is required to be used as an active device) in order to assess the cumulative exposure in nuclear emergency response applications. Hence, to assess this latter effect, the reporter fluor was exposed repeatedly with the BioTek Synergy HT spectrometer. Here, the reporter fluor was subjected to multiple sequential readings to assess the potential of the incoming laser beam which may damage the dosimeter molecule. Figure 4.12 indicates some effect of photobleaching over the two days. Analyses were performed between 10:48 and 11:38 am on Day 1 and 9:53 and 10:04 am on Day 2. However, on further analysis of these data, it can be seen in Figure 4.13 that the repeated reads on

Day 1, with a slope of 2.94×10^9 fluors damaged per exposure, are somewhat different than those on Day 2 with a slope of 4.96×10^{10} fluors damaged per exposure.

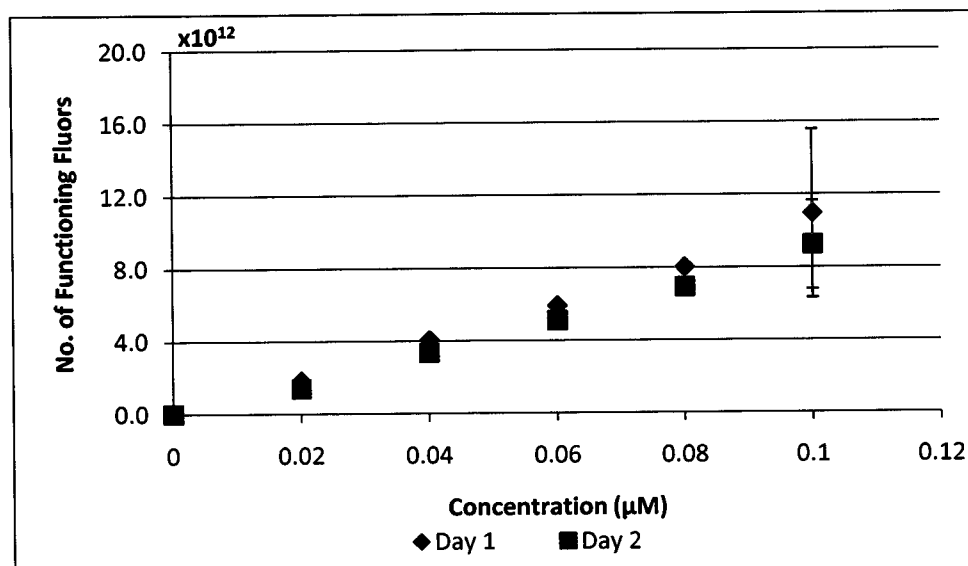


Figure 4.12: Average reporter response to repeated analytical light exposure between 2 days.
Error bars of 1 standard deviation for 0.1 μM only.

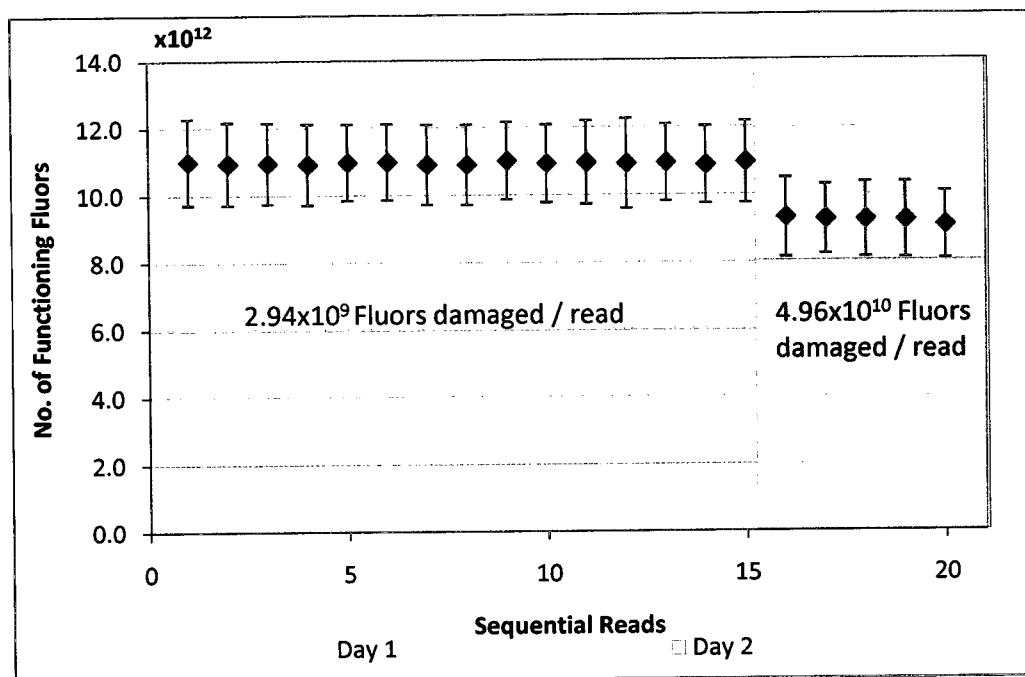


Figure 4.13: Reporter response to repeated analytical light exposure for the 1.0 μm dosimeter for Day 1 and Day 2. Error bars of one standard deviation.

4.2.2.4 Measurement of Irradiation with the Dual-Labelled Dosimeter

The performance of the dual-labelled FAM-dt(10)-BHQ1 dosimeter was assessed in irradiations from 1 to 100 Gy to first establish a possible link between the absorbed dose and the fluorescence signal strength as depicted in Figure 4.14. Figure 4.15 also shows the high dose response (100 Gy) for the FAM-dT(10)-BHQ1 molecule compared to the reporter fluor for various concentrations. The photomultiplier tube sensitivity was 85 for this investigation. The number of DNA breaks given in these figures reflects the number of fluors measured by the fluorimeter, and thus is the same quantity as measured previously. The error bars are for one standard deviation in these figures.

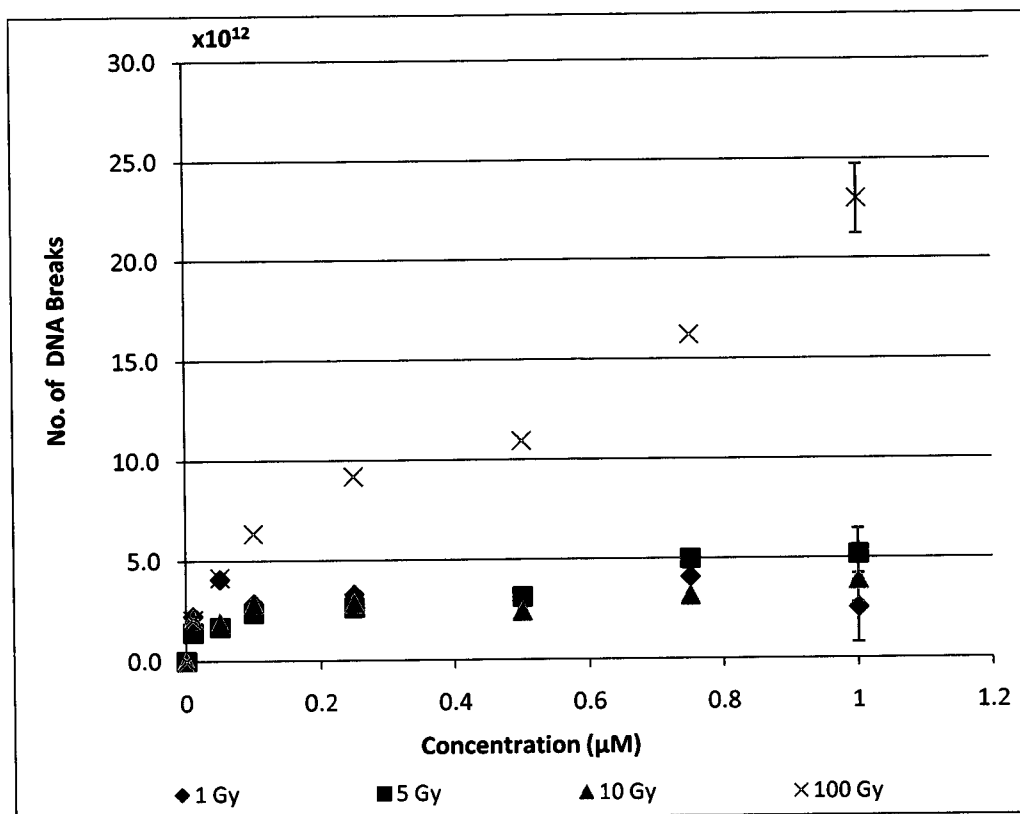


Figure 4.14: Performance of the dual-labelled DNA dosimeter at 1, 5, 10, and 100 Gy. Error bars one standard deviation.

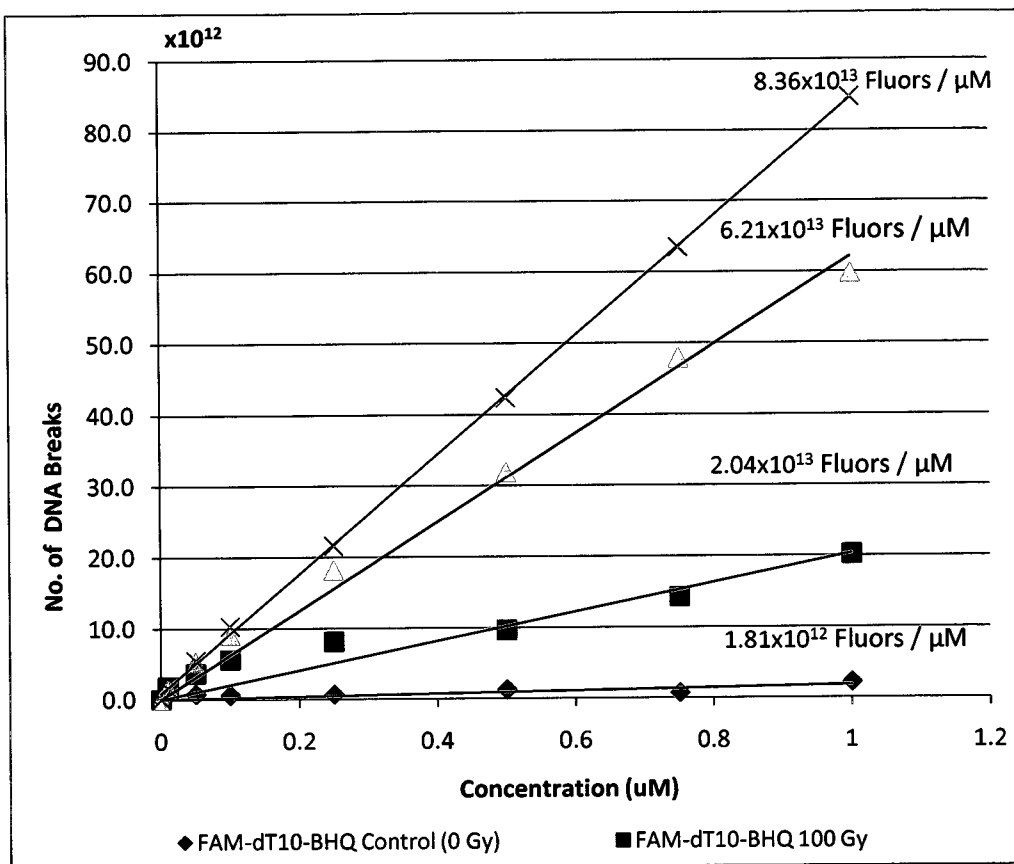


Figure 4.15: Performance of the dual-labelled DNA dosimeter and reporter at 0 Gy and 100 Gy.

The overall performance of the dosimeter molecule in Figure 4.14 as a function of the various dose levels of 1, 5, 10 and 100 Gy indicates that only at the very high dose level of 100 Gy is there a statistical significance in the observation of more fluorescent reporter molecules, no longer being suppressed by BHQ-1 quenchers. In particular, as shown in Figure 4.15, there is a distinct increase in fluorescence signal due to DNA breakage by over a factor of ~ 9 at 100 Gy from the reporter fluor molecule (reporter molecule FAM-dT(10)). There is a notable decrease in fluorescence at this level of irradiation of the reporter with a decrease of 30%. The irradiated

reporter fluor clearly has a significantly higher signal strength than the irradiated dosimeter molecule at 100 Gy.

Further analysis of the data on Day 1 was conducted to investigate the reponse capability of the FAM-dT(10)-BHQ1 dosimeter at lower dose levels. Figure 4.16 shows a clear delineation between the response at a dose level of 10.0 Gy compared with the remaining lower dose levels, providing a clearer distinction than that shown in Figure 4.14. Figure 4.17 also shows that for the 1.0 μM dosimeter there is a dose increase with a slope of 2.23×10^{11} DNA breaks/Gy.

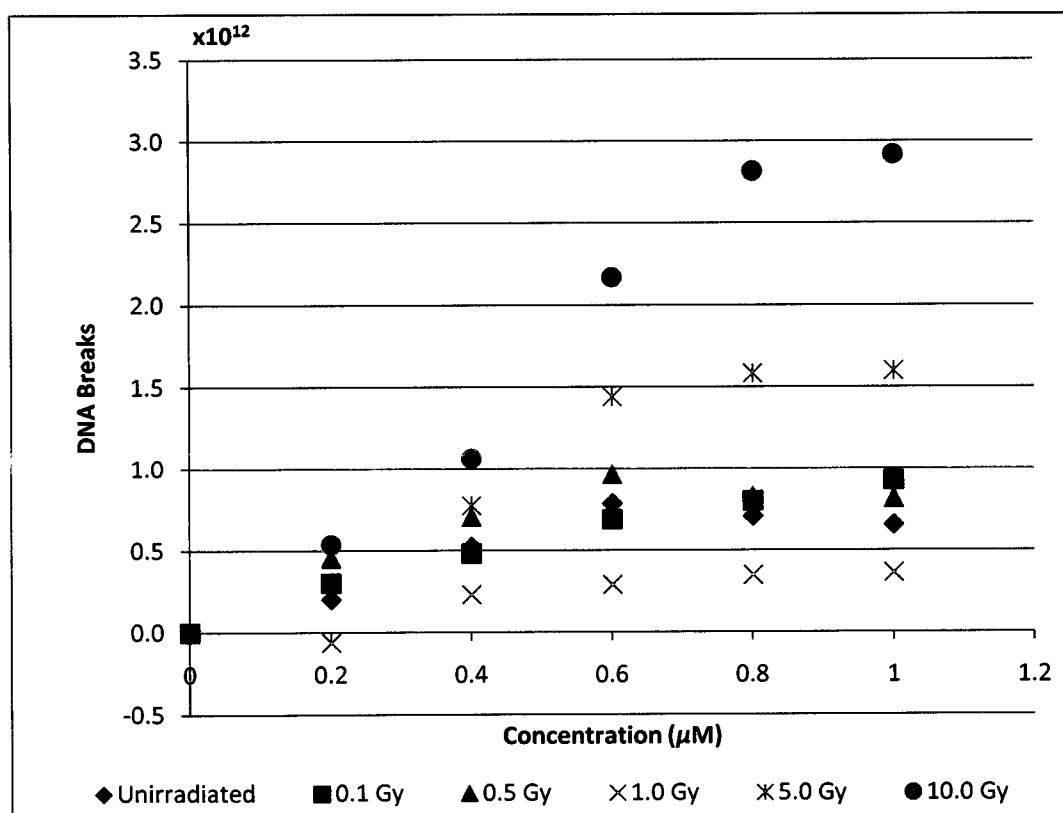


Figure 4.16: Performance of the dual-labelled DNA dosimeter between 0 and 10 Gy.

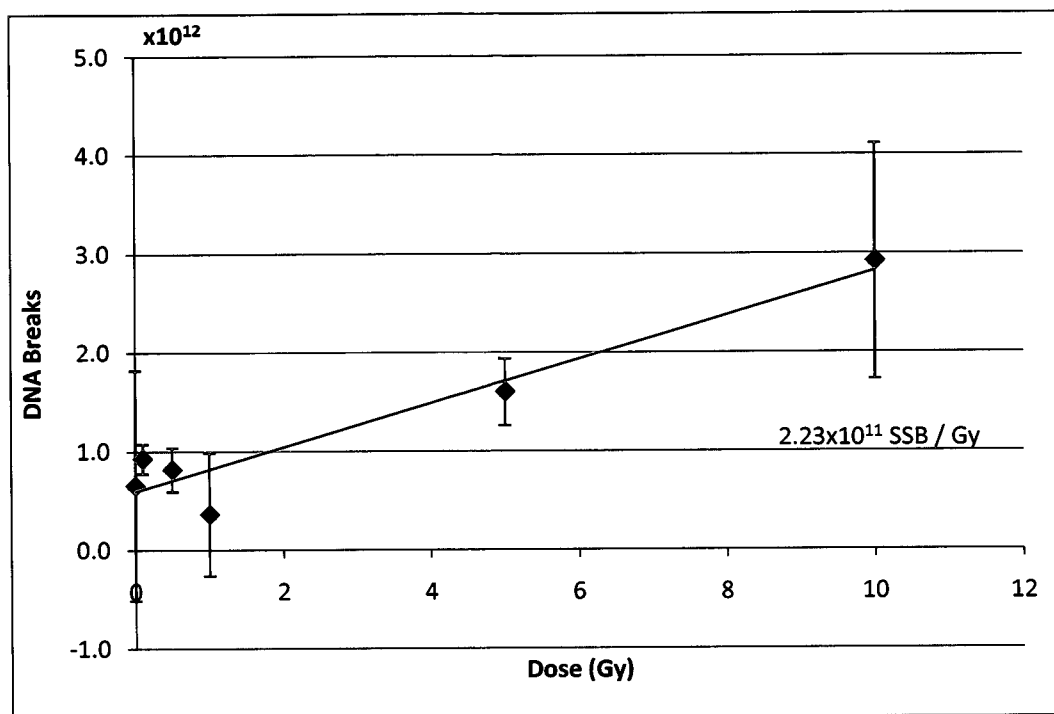


Figure 4.17: Performance of dual-labelled DNA dosimeter between 0 and 10 Gy at 1.0 μ M.
Error bars are for one standard deviation.

5 Discussion

Experimentation concentrated on both the polymeric transducer and the dual-labelled approach for the DNA dosimeter, examining the science, as well as some of the key characteristics and challenges of this type of biosensor. These approaches were originally developed for other applications.^[44, 42] As such, they required characterization for the current application, with radiation testing in order to determine their performance and suitability for the given application as a DNA dosimeter. The following sections detail the interpretation of the experimentation as carried out with the two different constructs. Sections 5.1 and 5.2 will deal specifically with the experiments described in Chapter 4 on the polymeric transducer and dual-labelled quenching dosimeter, respectively. Section 5.3 discusses related work by other researchers in the RMC group with further testing and detector/experimental setup optimization in order to achieve a lower limit of detection.

5.1 Polymeric Transducer Dosimeter

Irradiations using CERN's high energy reference field (CERF) were conducted to assess the performance of the Fluorescence Chain Reaction model of dosimeter. Doses obtained on top of the well-characterized shielding at the CERF facility, which is used as a reference platform for dosimeter characterization for aircrew and space crew applications, failed to provide any meaningful data for the given construct. Subsequently, slides were exposed directly beneath the copper target within the target enclosure to obtain a much higher dose level, estimated to be 5 Gy (and somewhere between 5 and 50 Sv for the mixed radiation field). Quantitative PCR was performed on these samples, revealing that irradiated samples released 3.8 times more of the 20-base target region

than the 70-base full region (which represents the system's background). This is statistically significant above these background measurements. These results validated the capability of the dosimeter, based on the FCR approach to measure radiation with the release of a measurable amount of the terminal tag region of the DNA oligonucleotide. Despite the sufficient difference in signal to noise at this high dose, a high background measurement of 0.9×10^9 unattached DNA base pairs was consistently present as measured at CRI, which significantly affects the limit of detection of the given device for lower-dose measurement. The cause of this high background level was determined to be largely due to the printing processes used to attach DNA to the solid surface. Attempts to optimize the surface binding proved unsuccessful to improve the signal-to-noise ratio. As such, the dual-labelled approach was proposed and investigated as an alternative technique (see Section 5.2).

In terms of design constraints, the polymeric transducer construct requires mechanical processes for proper signalling to occur. Cleaved DNA strands must be transported unidirectionally in a volume in order to mix with reporting complexes so as to avoid false positives. This result can be achieved using a microfluidic system including mixing channels, bead arrays and microfluidic pumps. The lifetime of the working dosimeter is reliant on the prepared fluid volume in the dosimeter reservoir, which must be minimal since the dosimeter has to be wearable. Further complications can arise with the complexity of a needed mechanical system for reading.

5.2 Dual-Labelled Quenching Dosimeter

The dual-labelled oligonucleotide dosimeter was designed as a simpler alternative to the polymeric transducer. Implementation of this construct in a wearable device requires only a compact liquid volume in addition to the micro-optics for reading. No complex mechanical parts are required as long as the dosimeter remains above water's freezing temperature.

Several steps were taken to characterize the functionality of this dosimeter and its components including: an investigation of the quenching efficiency, i.e. the ability of the quencher to successfully inhibit fluorescence in an undamaged state (Section 5.2.1), testing of the reporter sensitivity to various conditions of handling and radiation exposure (Section 5.2.2), and an investigation of the response of the dosimeter to gamma radiation, including an assessment of the limit of detection (Section 5.2.3).

5.2.1 Quenching Efficiency of the Dual-Labelled Dosimeter

All three BHQ dosimeter configurations were heavily quenched compared to the extrapolated standard curve for the uninhibited fluor (Fig. 4.6). Extrapolation is required because full concentrations would saturate the spectrometer at this sensitivity. The dosimeter molecules with DNA lengths of 20 and 30 bases, however, emitted a fluorescent signal at 15.2 and 21.7% of the predicted fluor level which may have implications for robustness and for the use of the dosimeter at low dose-levels (see Section 5.3). The 10-base dosimeter molecule has near-complete quenching at 0.06% of the extrapolated reporter level, making it an ideal candidate for the DNA dosimeter.

The maximum length of ssDNA is not limited by the same constraints as natural (B form) dsDNA. The length of the dual-labelled dosimeter was approximated using Maestro (Schrödinger, New York, NY) molecular modelling software (Fig. 5.1). The length of the entire dT(10) dosimeter molecule (which also contains the fluor and quencher as depicted in Figure 5.1) is roughly 100 Å from end to end, with the dT(10) nucleotide portion with a separation distance (r) of about 60 Å in this stretched-out configuration. This length agrees with the premise that the working range for FRET is within 100 Å. The stretched-out configuration is a maximum distance since the DNA strand is flexible and may not always be stretched out. dT(20) and dT(30) would be estimated at a length of approximately 160 and 220 Å, respectively, exceeding the practical length for this application. From Eq. 3.1, the r^6 term is the reason that FRET is dubbed a “spectroscopic ruler”, i.e., when two FRET chromophores double their separation distance, the FRET efficiency drops to $1/64^{\text{th}}$ of the initial state. Hence, the detector configuration needs to be considered when testing the experimental efficiency of the system so that optimization of the donor-acceptor pair, as well as the distance between them, will help lower the limit of detection. An optimization is required since the use of more bases will result in a larger target for any radiation interaction, but a greater separation distance. The current investigation suggests that dT(10) is a reasonable length for this dual-labelled construct.

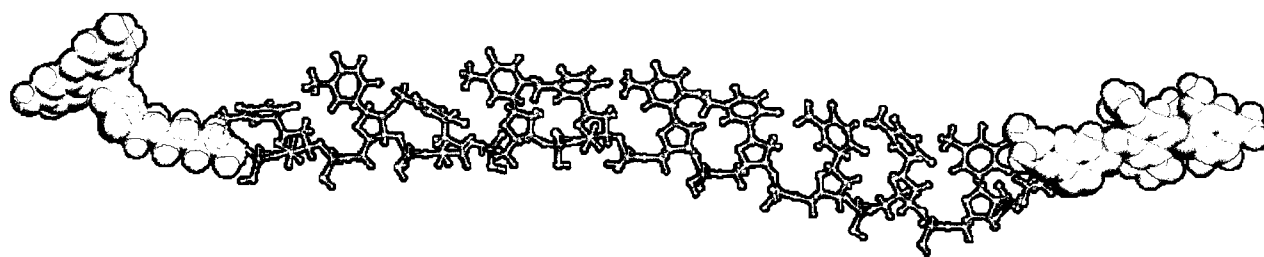


Figure 5.1: Dual-labelled oligonucleotide dosimeter molecule. FAM at left, BHQ at right.

It may be prudent to examine the sizes of the various components since both the FAM and BHQ components are comparatively-sized molecules that would be susceptible to radiation interaction. The molecular weight of 6-FAM is 1176.35 amu and the molecular weight of the BHQ-1 is 554.49 amu. The molecular weight of dT10 (10 monophosphate thymine molecules) is 3222 amu. Since damage to the thymine bases may not affect the DNA sugar-phosphate backbone, it is necessary to restrict the focus of this region. Considering only the atoms in the sugar-phosphate chain and those immediately connected to them, the mass of this target is 1630.5 amu, which is greater than each of the chromophores, comparable to the added molecular weights of these latter components.

5.2.2 Reporter Sensitivity of the Dual-Labelled Dosimeter

Over the course of two days, the reporter molecule (FAM-dt(10)) was tested for any degradation to radiation.

On the first day, there was an observed decrease in the fluor signal with increased dose. Bond breaking in the reporter molecule was expected with energy deposition and it was necessary to quantify this effect for the working range of the dosimeter (i.e., up to 2-3 Gy, at LD₅₀). At a concentration of 0.1 μ M, the decrease in the fluor signal from pre-exposure levels was $\sim 7.8\%$ at 10 Gy with an overall decrease of 7.72×10^{10} fluors destroyed per Gy. This level of destruction is not significant for the functionality of the dosimeter.

A plate-by-plate analysis supports this finding (Fig. 4.10 (a)), but reveals a slightly greater degradation of 12.2% at a 10 Gy dose level. The remaining data, for dose levels at 5.0, 1.0, 0.5 and 0.1 Gy show no statistical deviation in the FAM performance.

5.2.2.1 Temperature Regulation Effects on Reporter Sensitivity

As discussed briefly in Chapter 4, experimentation to assess the performance of the dual-labelled oligonucleotide dosimeter on successive days provided some unexpected results. The response was not consistent over the two days. At a concentration of 1.0 μM , the signal decrease from the unirradiated samples through increasing dose was 31.3% at just 5 Gy (which can be extrapolated to 62.5% at 10 Gy).

It should be noted that not only was the fluor more sensitive to radiation damage on the second day, but that photosensitivity was increased (Figure 4.13) and the un-irradiated reporter molecules were also affected. The standard deviation for all 1.0 μM un-irradiated samples on the first day was 1.06×10^{12} fluors, while the standard deviation for all 1.0 μM un-irradiated samples on the second day was 2.56×10^{12} fluors (i.e., a 2.4 fold increase).

Since storage conditions were controlled (samples were stored in a styrofoam box and wrapped in aluminum foil to prevent light exposure), only a few variables could have contributed to this change in sensitivity. It is speculated that this observation may be attributed to possible condensation effects, where sensitive DNA could deposit on the adhesive film prior to testing. This

result could also be attributed to temperature control effects. Following sample preparation, i.e., when the DNA dosimeter molecules were hydrated, diluted, and pipetted into the 96-well-plates, the samples were kept between 0 to 4° C in storage for three days prior to the experiment, at which time the samples were allowed to warm to room temperature. At this point, some of the plates displayed droplets of condensation on the film surface. The samples were sorted at this point for the second day of experimentation. In contrast, the second set of samples was kept at temperature for 24 hours prior to experimentation in order to allow any condensation to dissipate. The protocol change may have rendered the results for the second day of experimentation suspect.

Thus, this observed variability in results suggests that sample preparation and temperature control is an important consideration in the design of the dosimeter.

5.2.3 Photobleaching Effect

FAM (fluorescein) is a reporter dye that, like other such fluorescing dyes, is susceptible to photobleaching effects with a loss of fluorescence following exposure to light. It was hypothesized that photobleaching might play a role in the performance of the BHQ DNA dosimeter following the degraded performance where incremental doses were applied to the same sample as part of the proof-of-concept trial (as opposed to just individual irradiations on a given sample).

In particular, a single 96-well-plate with increasing concentrations of the reporter molecule (FAM-dt(10)) was exposed to multiple reads on both the first (15 reads) and second day (5 reads). The reporter exhibited no discernable decrease in fluorescence in response to the 15 sequential reads

performed on the first day with a measured slope of 2.94×10^9 fluors damaged per exposure, which is 4 orders of magnitude smaller than that due to radiation effects alone. Similar results were observed on the second day with a slope of 4.96×10^{10} fluors damaged per exposure for the five exposures which may indicate some decreased stability in the fluorophore.

It can be concluded that repeated sampling of the DNA dosimeter should not result in any significant destruction of the FAM fluor. This portion of the experimentation describes the procedures necessary to characterize the function of the dosimeter.

5.2.4 The Dual-Labelled Dosimeter Response to Gamma Radiation

Preliminary trials confirmed that the dual-labelled oligonucleotide dosimeter was responsive to high gamma-ray dose levels. Here the energetic gamma radiation would disrupt the molecule so that the fluorescence could be detected with the BioTek Synergy HT Spectrometer. This increase in fluorescence is assumed to be due to the cleaving of the DNA strand that tethers the FRET pair together; however, as mentioned in Section 5.2.2, damage to both the fluor and quencher can occur when exposed to irradiation, which must be quantified (see Section 5.2.5).

The early trials clearly showed that the construct responds at very high dose levels up to 100 Gy, but there is difficulty measuring in the lower dose range of 0 to 10 Gy (Fig. 4.14). Further experimentation indicated that the dosimeter was able to distinguish down to 10 Gy (Fig. 4.16).

In the lower dose range of 0 to 10 Gy, the number of breaks ranged from 5.3×10^{10} to 6.5×10^{12} breaks (in 150 μL), spanning similar ranges across the different trials. These resulted in measured damage rates of 2.3×10^{-4} and 2.51×10^{-4} SSB $\cdot\text{Gy}^{-1}\cdot\text{bp}^{-1}$. Thus, there was some repeatability in the experiments which enforced the suitability of this construct as a robust tool for radiation measurement.

5.2.5 Background Signal Evaluation

The polymeric transducer complex was abandoned in favour of the dual-labelled oligonucleotide due to the high background noise issues. Previous work on the project concluded that, in the polymeric transducer construct, 10^{14} 70-base oligonucleotides were bound to the solid substrate. However, 10^{10} oligonucleotides were detected, unbound, in the un-irradiated samples, 0.01% of the applied material.^[52] By comparison, in the dual-labelled system, 6.5×10^{11} fluorophores are detected in an un-irradiated solution containing 9.0×10^{13} dosimeter molecules, which is 0.7% of the dosimeter molecules (improved to 0.3% in related work (Section 5.3)). It is important to note, however, that the background estimation for the polymeric transducer is a lower-bound value. In particular, the polymeric transducer is washed approximately 16 times where each wash contains a significant number of unbound DNA thereby artificially reducing the actual background levels.

Preparation conditions (e.g., non-sterile handling or physical damage) and ubiquitous background radiation may contribute to the background measurement in either case. It has been noted before that suspending DNA constructs in water may make it susceptible to free radical attack which is a possible liability with storage. It is possible that the use of buffer solutions (e.g., a

solution containing radiation scavengers) may be able to restrict this damage, but their effect on the dual-labelled dosimeter, particularly in radiation conditions, has not been characterized as yet.

5.3 Comparison with Other Work

Further studies have provided data and results complimentary to this work. Preliminary analyses performed at DRDC-Ottawa provided the data required for an in-depth look at the contributions of fluor and quencher damage to the fluorescent signal obtained by dosimetric testing (Section 5.3.1). Studies using a custom-built fluorimeter in response to the low sensitivity of the BioTek Synergy HT spectrometer are detail in Section 5.3.2.

5.3.1 Fluor and Quencher Response to Radiation

Ionizing radiation deposits damaging energy either directly or indirectly into the molecule structure of the dosimeter, altering its spectral properties. The dosimeter does not discriminate between direct and indirect effects, similar to natural DNA. This device is in fact designed to allow for enhanced free radical interaction (since there is an absence of damage-scavenging structures and the presence of anti-oxidants).

Energy deposited in the dual-labelled dosimeter can have a number of effects. Radiation can damage and cause breaks in the DNA backbone (as intended in the current application). Any radiation damage that causes restructuring or breaking of the thymine bases will not alter the spectral properties of the dosimeter. However, energy deposition may also cause damage to either chromophore at the opposite ends of the thymine chain, which could alter their spectral properties. Such changes must be taken into account for appropriate dose measurement. These chromophores were therefore tested with exposure up to 100 Gy in order to quantify such effects.

The FAM standard (FAM-dT(10)) was analyzed at 1.0 μM without any irradiation as a baseline and following irradiation at several doses (1, 5, 10, 100 Gy) at a photomultiplier tube sensitivity of 85 (Fig. 5.2). From this study, it can be seen that fluor degradation is linear with the gamma radiation dose.

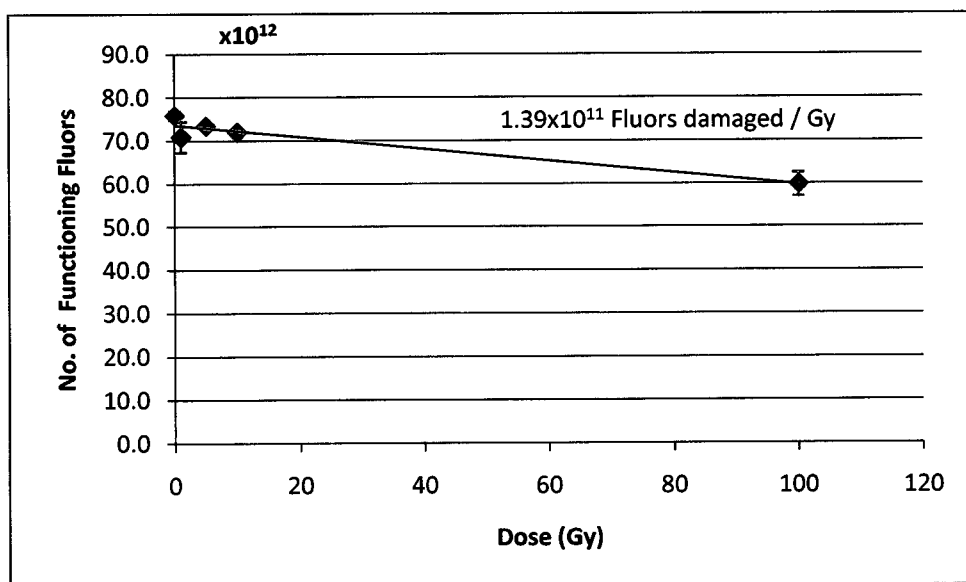


Figure 5.2: Reporter response to high dose irradiation.

A similar process was performed at DRDC-O in order to determine the impact of radiation on the quencher chromophore. Absorbance of 1.0 μM FAM-dT(10)-BHQ molecule was measured at 534 nm, the maximum wavelength for BHQ absorbance, in a clear 96-well plate in volumes of 200 μL . The absorbance was measured at 0, 10, 50 and 100 Gy doses (Fig. 5.3) and a linear trend was also observed. The DRDC-O results were scaled for a 150 μL volume (See the calculation in Appendix A for derivation of the correction factor for this scaling).

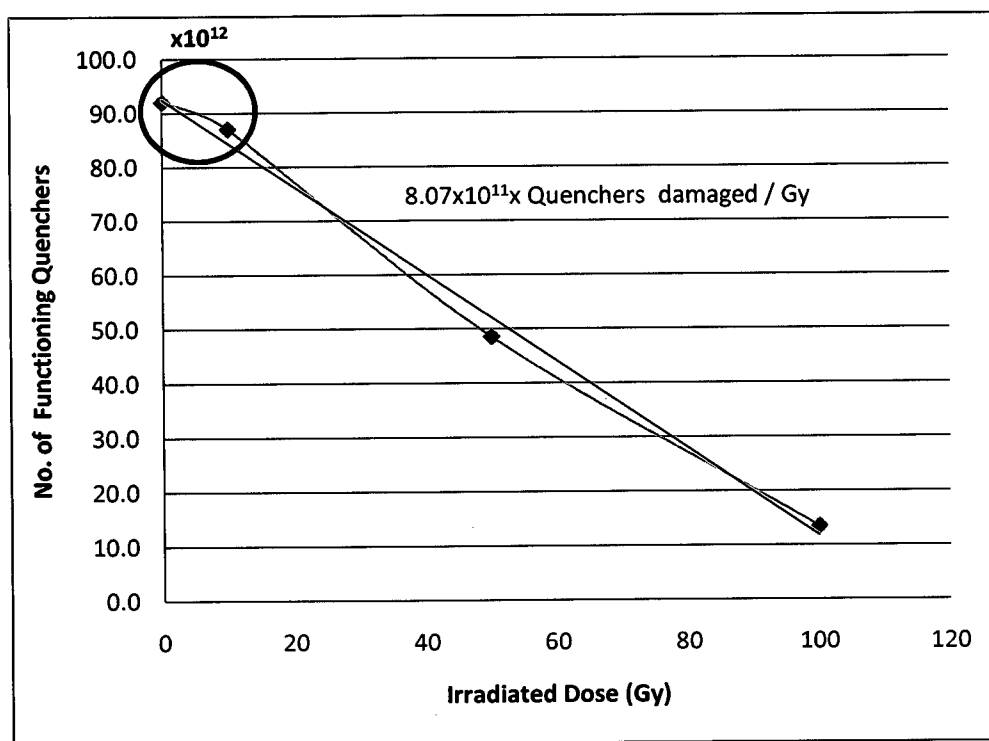


Figure 5.3: Quencher response to high dose irradiation.

From these tests, it can be determined that, for a volume of 150 μL for a 1 μM solution of dosimeter, 8.07×10^{11} BHQ components and 1.39×10^{11} FAM components are damaged per Gy of gamma irradiation which affect the spectral properties of the dosimeter. Since damage to the BHQ component will compromise its ability to quench the fluor, this will result in an increase in the

reported signal. Similarly, damage to the FAM component will compromise its ability to fluoresce, and decrease the reported signal. The overall effect can be expressed as a single figure of $\sim 6.0 \times 10^{11}$ fluors damaged per Gray. However, most of this effect is due to damage of the BHQ. This combined chromophore damage appears as 6.68×10^{-4} SSB \cdot Gy $^{-1}$ \cdot bp $^{-1}$, but is not caused by damage to the oligonucleotide chain. Since the dual-labelled oligonucleotide dosimeter reports $\sim 2.4 \times 10^{-4}$ SSB \cdot Gy $^{-1}$ \cdot bp $^{-1}$, it appears that the BHQ component of the dosimeter is particularly sensitive to radiation damage. This sensitivity, when compared with SSBs, may be in part due to the fact that both cleaving and non-cleaving damage can affect the spectral properties of the BHQ, but only cleaving damage to DNA will increase the dosimeter signal. At this level, the signal due to DNA SSBs would be statistically insignificant.

The consequence of BHQ damage in the current set of experiments at the high dose level is therefore an important consideration, but this effect decreases at lower dose levels. This result may explain the appearance of a different slope of damage for the low doses in this trial (Fig. 5.3, highlight), and is expanded upon in Section 5.3. In particular, the need to further investigate the degradation of both the FAM and BHQ at lower dose levels was realized as a result of the current investigation.

Lower dose experiments were also performed in Section 5.3 by other investigators in order to provide additional experimental data for the dual-labelled construct so that these results could be more accurately compared to the value of 2.7×10^{-7} SSB \cdot Gy $^{-1}$ \cdot bp $^{-1}$ determined by Moiseenko et al., based on a theoretical analysis of DNA single-strand breakage by irradiation^[25]. As mentioned, the current investigation has yielded a much higher value for breakage (6.7×10^{-4} SSB \cdot Gy $^{-1}$ \cdot bp $^{-1}$).

5.3.2 Custom Fluorimeter Developed for Dual-Labelled Construct

As shown in Chapter 4, the dosimeter is only sensitive at higher dose levels (i.e., greater than 5 Gy as depicted in Fig. 4.15). This result occurs in the current investigation at least in part because of the limited sensitivity of the fluorescence instrumentation discovered in this investigation (i.e., the BioTek Synergy HT Spectrometer as used at DRDC-Ottawa). This has been investigated in studies following this work by the research group using a more sensitive fluorescence spectrometer that was custom built at the Centre d'Optique, Photonique et Laser (COPL) at Laval University.^[51] This enhanced fluorimeter was developed and built as part of the larger CRTI project for further experimentation in order to detect smaller changes in fluorescence for increased dosimeter sensitivity (which was beyond the scope of the current work in this thesis). This development proved to be significant for such lower dose-detection capability. The custom-built FAM-fluorimeter was configured for the detection of FAM-labelled oligonucleotides in microvolumes using disposable, plastic cuvettes (see Figure 5.4). The fluorimeter was initially calibrated with aqueous FITC (a FAM derivative) and FAM-dT(10) solutions contained into these low-cost plastic cuvettes (Eppendorf Uvettes). Figure 5.5 shows that the calculated limit of detection (LOD) is 13 pM (1.3×10^{-11} M) for aqueous FITC solutions and 23 pM (2.3×10^{-11} M) for FAM-labelled oligos. The latter is at least 3 orders of magnitude more sensitive than the commercial BioTek Synergy HT Spectrometer used in this thesis investigation.

In particular, the detection platform developed by COPL provides: (i) a better mechanical stability of the system allowing for a lower measurement variability from sample-to-sample and over

several hours of operation; and (ii) a redesigned user interface (written in LabView[®]) which allows the user to be more efficient and accurate with respect to instrumental parameter control and data collection/archiving. For instance, this software permits improvements in the pre-defined data sampling time, automatic calculation and storage of mean, standard deviation on the measured signal, excitation laser power setting/control, automated fluorescence filter selection, and experimental parameters settings as logged in a separate data file for traceability.

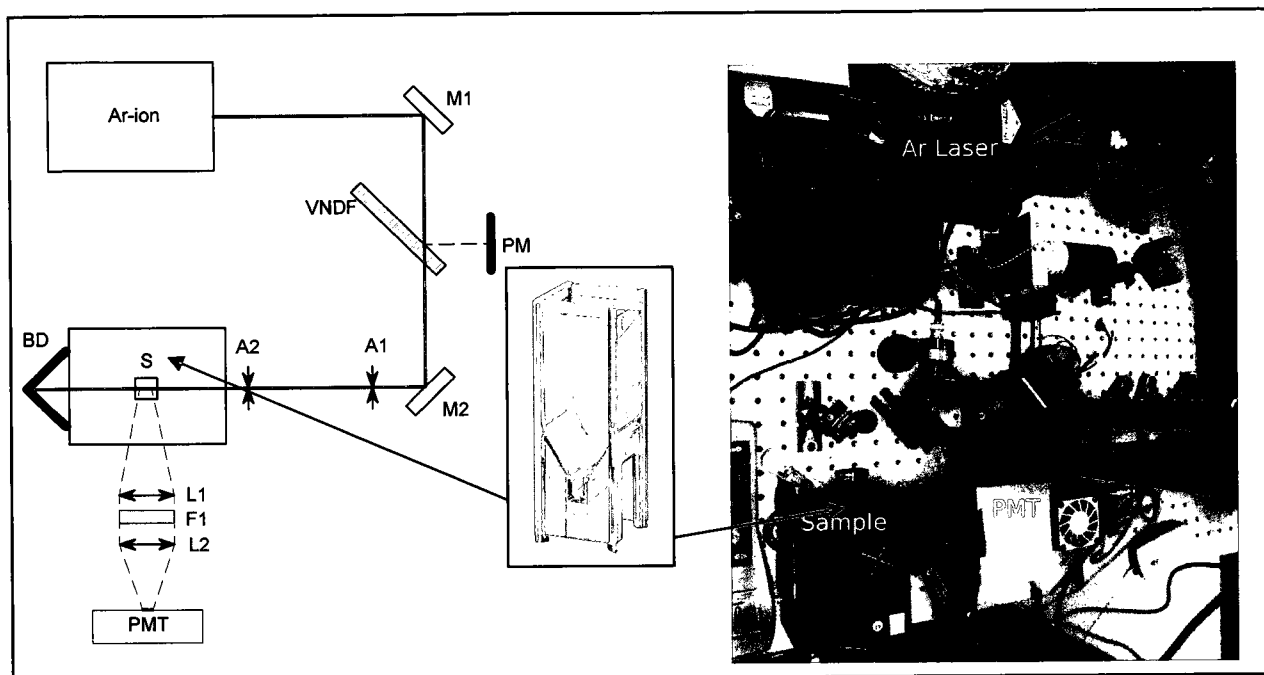


Figure 5.4: A customized fluorimeter setup at COPL. Built to measure FAM fluorescence of the dual-labelled oligos in 50 μL solution using disposable eppendorf uvette® sample cuvettes. Excitation : Ar+ CW Laser, 488 nm (typical excitation power = 30 uW); $M_{1,2}$ = turning mirrors, PM = power monitor; VNDF = variable neutral density filter; $A_{1,2}$ = apertures; BD = beam dump; S = sample holder, 1 cm pathlength; $L_{1,2}$ = lenses; F_1 = bandpass filter, Semrock FF01-528/38; PMT = Photon-counting PMT, Hamamatsu H7421-40.

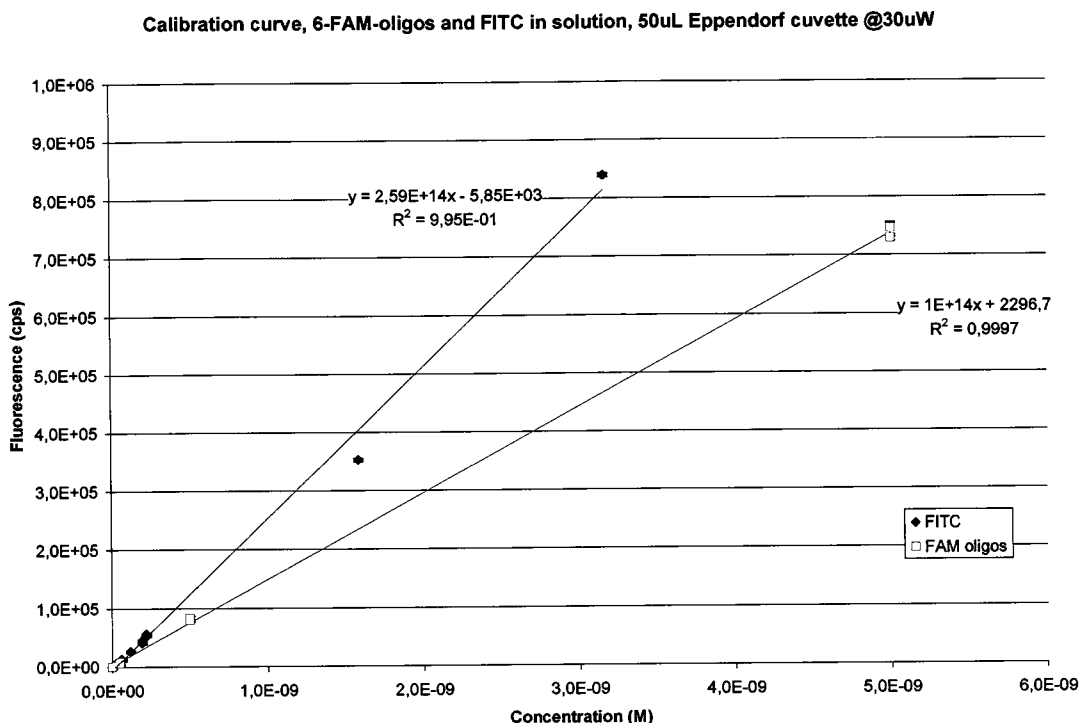


Figure 5.5: Calibration curve of FAM reporter and aqueous FITC. Fluors in 50 μ L Eppendorf Cuvettes

Moreover, with this new fluorimeter design, further testing by other investigators at RMC, shows that for the irradiation of samples of 0.5 μ M FAM-dT(10)-BHQ1, an improvement down to 1 Gy is now detectable with this configuration.^[51] Additional testing at a higher DNA concentration of 1 μ M of FAM-dT(10)-BHQ1 showed that the fluorescence signal is at the top end of the dynamic fluorescence range of the COPL FAM-Fluorimeter.^[51] However, although higher concentrations of DNA would provide an increased target size for the radiation, this increased concentration also leads to higher background noise levels.

Additional testing was therefore carried out by the RMC group (outside the scope of this thesis investigation) as part of the CRTI project with three replica aliquots of the DNA molecule

FAM-dT(10)-BHQ1 at a concentration of 0.5 μ M in ddH₂O. These DNA samples were independently exposed to a ⁶⁰Co source (the same source as described in section 4.2.2.2) of 100 mGy to 10 Gy and assayed for fluorescence using 50 μ L samples in the FAM fluorimeter. With the new added capability for detection, a distinct linear increase in fluorescence is now observed when the dual-labelled DNA was exposed over this radiation range (Fig. 5.6). The detection response was further corrected for a loss of absorbance of the Black Hole Quencher (BHQ) and fluorescence of the FAM reporter molecules as discussed in Section 4.2.2. Several additional experiments were specifically conducted to better quantify the breakdown of the BHQ and FAM with the newly-designed fluorimeter as shown in Figures 5.7 and 5.8, respectively. The BHQ absorbance (measured at 535 nm) supports earlier conclusions that low levels of radiation do not degrade the quencher with the same rate as higher levels of radiation (Figure 5.3 versus Figure 5.7). Interestingly, a similar result is observed where lower dose levels of radiation do not degrade the reporter FAM molecule as seen on comparison of Figures 5.2 and 5.8.

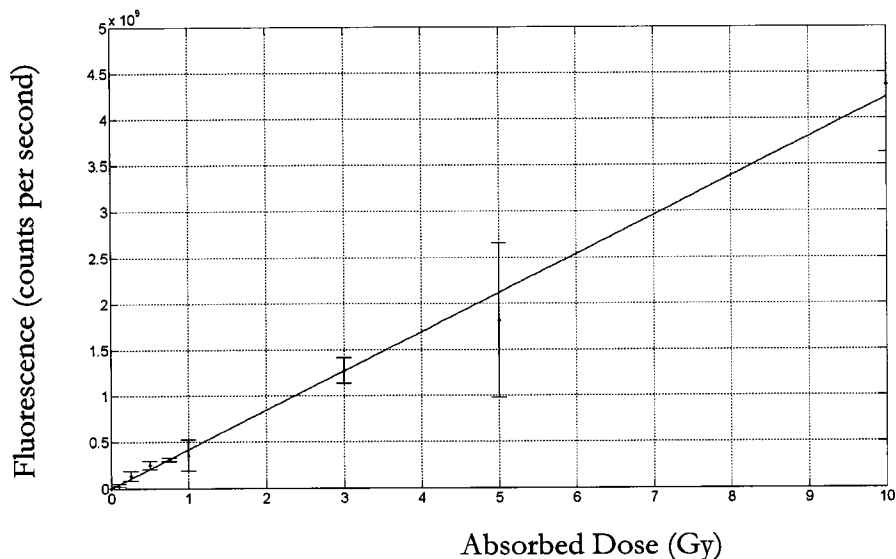


Figure 5.6: Dual-labelled oligo dose response curve at 0.5 μ M irradiated with 0.1 – 10.0 Gy gamma-rays. (corrected)

Hence, the sensitivity of the device is directly related to the limit of detection for the fluorescent signal (compare Figs. 4.15 and 5.6). In particular, with the increased sensitivity of the fluorimeter, the dosimeter response in Figure 5.6 yields a slightly higher detectability of $\sim 1.2 \times 10^{-3}$ SSB \cdot Gy⁻¹ \cdot bp⁻¹ (which is comparable with 2.4×10^{-4} obtained in the current thesis work in Section 5.2.5). This value describes a corrected detection limit (accounting for both FAM and BHQ destruction via radiation) for the DNA dosimeter. As such, 1 SSB can be detected in ~ 800 DNA molecules for 1 Gy of radiation. As mentioned, this linear relationship of fluorescence with dose is consistent with that also seen in Figure 4.15.

Additional experiments for the CRTI project were further carried out with X-rays using a 6 MV linear accelerator (linac) at the Kingston General Hospital (KGH), under the care of Dr. John Schreiner. These experiments were carried out as a further reproducibility check and to investigate the lower dose range and limit of detection of the dosimeter. In the accelerator, the electrons bombard a tungsten target creating a spectrum of X-ray photons through bremsstrahlung radiation (with maximum photon energy of 6 MeV). Dose levels for these additional irradiations (done in triplicate) ranged from 0.01 to 1.0 Gy.

The results from the two CRTI experiments at DRDC-Ottawa and KGH are compared in Figure 5.9. Both sets of results again confirm the linear relationship between fluorescence signal and dose, i.e., the least-squares slopes from the experiments were comparable (2.6×10^3 versus 3.0×10^3 photons·s⁻¹·mGy⁻¹). However, the intercepts are significantly different from each other, which represent the amount of background noise present in the system. The noise is due to the portion of molecules not undergoing FRET, where photons scatter off of the containment system and include other background interferences (see discussion in Chapter 3). COPL was able to reduce the background noise from scatter between the two experiments as is evident in Figure 5.9. Thus, Figure 5.9 explains the limited detection capability of the DNA construct used in this thesis in Chapter 3 because of the lower sensitivity of the fluorimeter reader employed. Hence, an improved fluorimeter will therefore help in the future to minimize the lower limit of detection of the DNA dosimeter within the 1 – 10 mGy range (which is currently observed at ~100 mGy as indicated in Fig. 5.9).

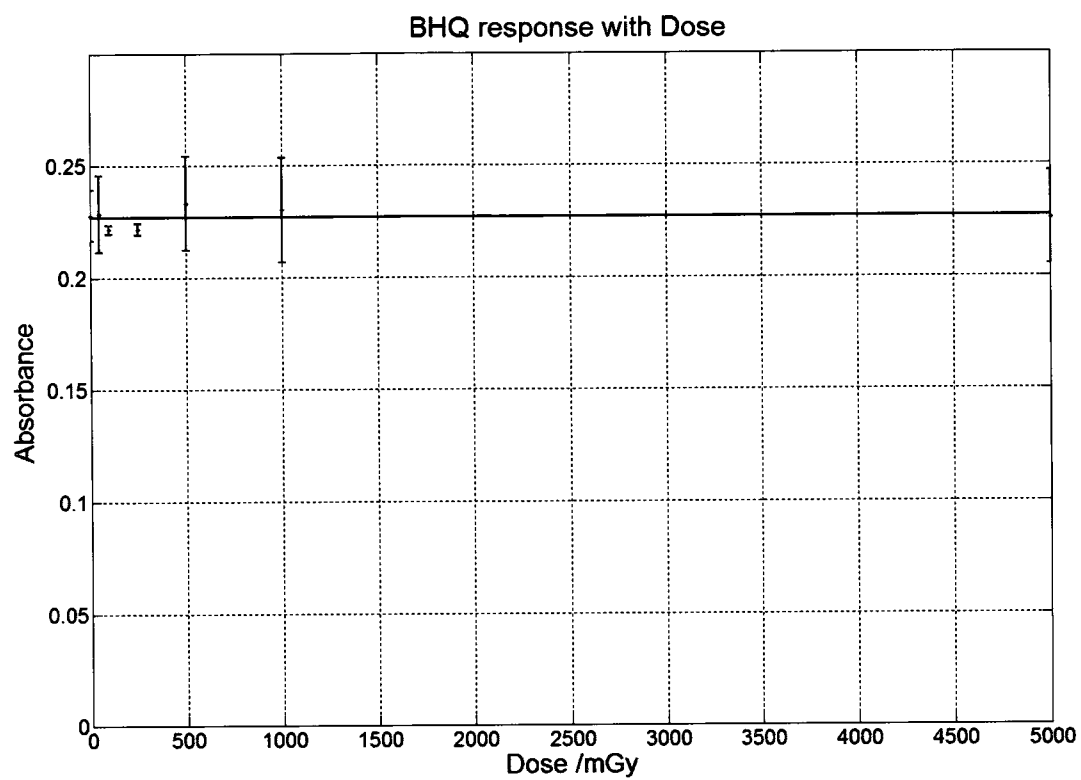


Figure 5.7: Black Hole Quencher Absorbance with Dose.

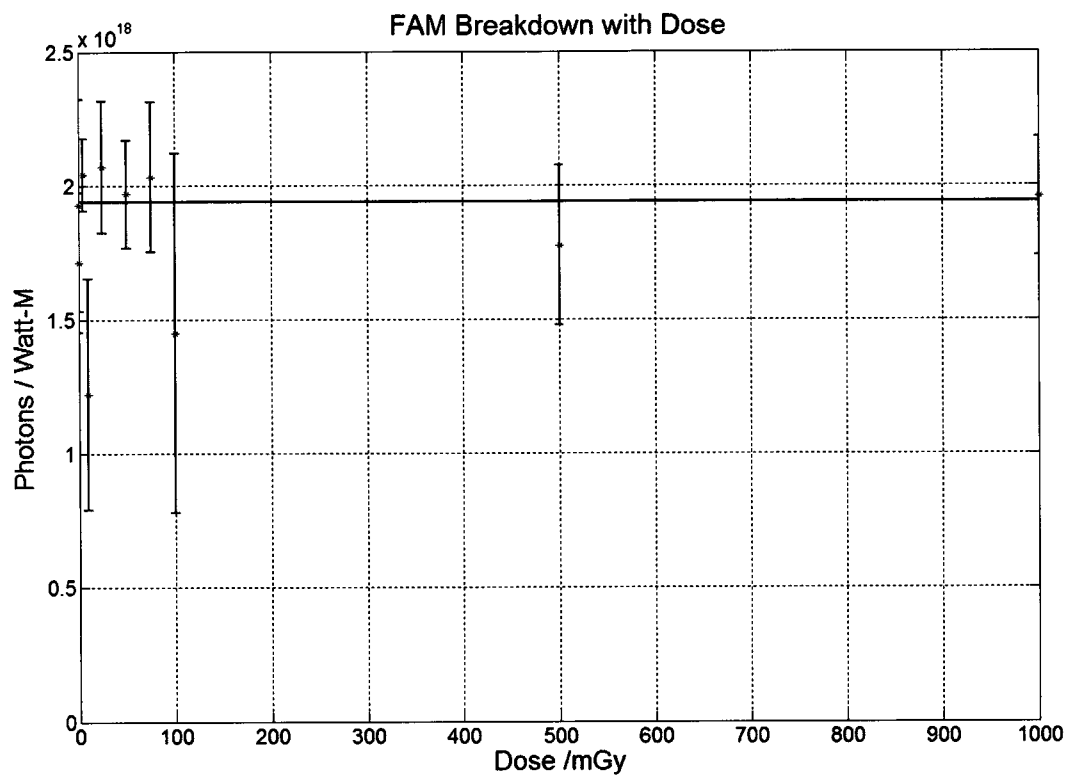


Figure 5.8: FAM reporter fluorescence response with dose.

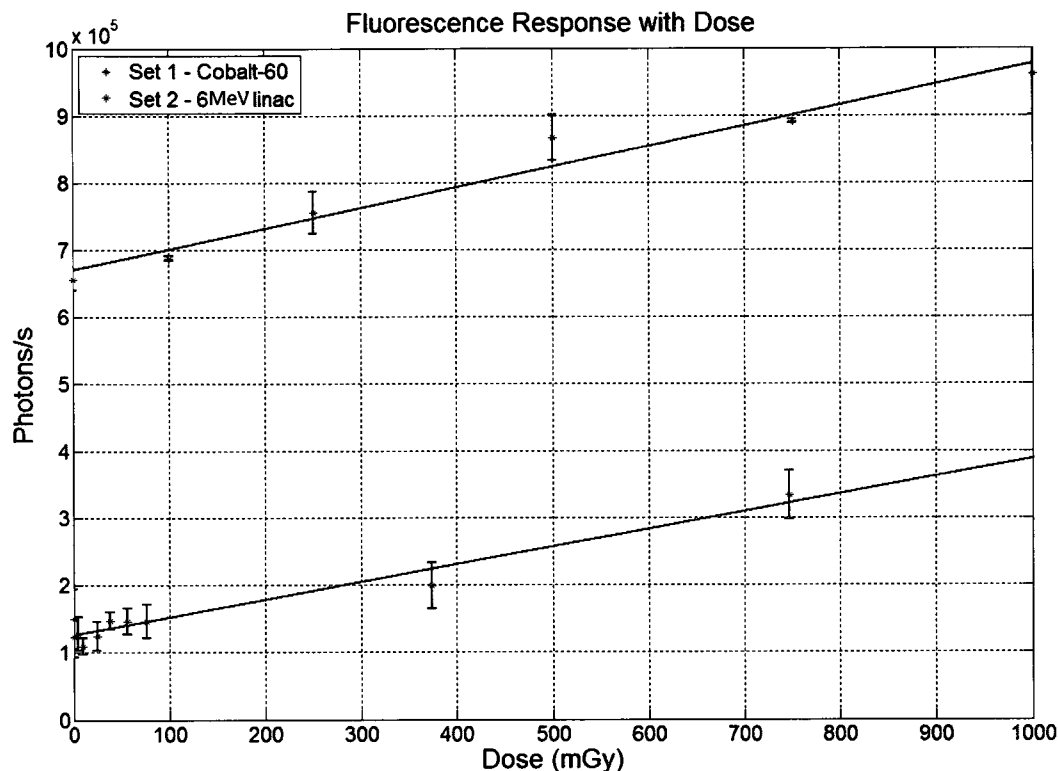


Figure 5.9: Dual-labelled DNA dosimeter's fluorescence response with dose.

In summary, the results suggest that this very simple reporter-target-quencher DNA molecule FAM-dT(X)-BHQ1 (where $X \sim \leq 10$) has great potential for being an accurate and quantitative means of measuring radiation dose via single-stranded DNA breaks. Radiation-induced single strand breaks within the DNA result in a quantifiable fluorescent signal. Proof of concept has been achieved with the early results of this thesis work and confirmed in later experiments for the CRTI project over a large range of radiation dose from 100 mGy to 100 Gy using a Cobalt-60 gamma-ray source and linac accelerator. Further refinements to both the molecule and the exposure/detection platform may lead in fact to even lower limits of detection for possible mixed-field applications. In particular, the dosimeter design needs to be optimized. As discussed in Chapter 3 and Section 5.2.1, the FRET signal falls off as the distance r between the BHQ and FAM

as r^6 in the DNA construct. An increased DNA concentration improves the lower detection limit since there are simply more targets. However, a greater target length with an increase in the number of oligos between the BHQ and FAM, results in a greater separation distance. Thus, there must be an optimum design for the dosimeter to maximize the fluorescent signal above the background noise levels, which can be determined through additional testing and perhaps theoretical Monte Carlo simulations.

A “DNA Dosimeter” is valuable because it responds to ionizing radiation in much the same way that natural DNA does in human cells and is also responsive to any type of ionizing radiation, except alpha particles, which do not normally have the penetrative power to reach cellular material in the first place. Ionizing radiation deposits energy in the DNA strand, causing molecular rearrangements and the breaking of bonds and strands. The dosimeter must only yield a response to just the DNA damage. Early concerns that the chromophore components of the dual-labelled dosimeter would be significantly affected by radiation damage has been allayed at lower-dose levels based on further investigation by others with the COPL custom-built fluorimeter. The results of this study show that there is a linear relationship between the radiation dose and measurable damage to the dosimeter. The effect of photobleaching does not affect the performance of the detector, which is key to its intended use as an active dosimeter.

Finally, the success of this work may have broad implications for other fields and industries. A simple means of measuring non-specific DNA damage may be a useful tool to determine the effects of chemicals which may potentially be damaging to genetic material. This work provides a very simple biosensor which could also potentially be adapted to a variety of other applications such as UV monitoring, which is important for water purification applications and skin protection to

prevent melanoma cancers. Moreover, the dosimeter may provide a capability for the testing of radio-protectors since the construct is more sensitive to radiation damage and has no repair mechanism to confound any testing results. It also provides a simple and direct structure for the testing of theoretical models of DNA damage.

6 Conclusions

A proof of concept has been carried out in this work to demonstrate the ability of a dual-labelled oligonucleotide approach. The construct consists of a Black Hole Quencher and Fluorescein reporter molecule on a deoxyribonucleic acid (DNA) strand, which is used as a biological (naked) DNA dosimeter. This dosimeter design was investigated in comparison to a previous design, using a polymeric transducer construct, which suffers from high complexity and excessive background complications. The dual-labelled dosimeter is pioneering since it tests damage in biological material (at the nano-scale level) instead of changes in inorganic matter as measured in current dosimetry techniques. Moreover, in comparison, other radiological detection devices only focus on a single radiation quality measurement; whereas the DNA dosimeter has the potential that it can provide cumulative dosimetry information for radiation of any linear energy transfer and for an unknown field. Multiple conventional dosimeters would generally be required for such mixed-field dosimetry, requiring financing, training, and analyses in excess of that which is proposed here.

Preliminary experiments conducted at DRDC-Ottawa over a dose range of 0 to 10 Gy have demonstrated a linear response of the fluorescence signal versus absorbed dose, with a specific sensitive response above about 5 Gy. This limitation is related to the inherent sensitivity of the Bio-Tek Synergy HT Spectrometer used at DRDC-Ottawa for the current experimentation. A custom-built fluorimeter at the Centre d'Optique, Photonique et Laser (COPL) has provided a three-order of magnitude increase in the measured fluorescence signal as determined in further experiments conducted by other members of the RMC group for this CRTI project. As such, this increased fluorimeter sensitivity has enabled the use of the DNA dosimeter construct over a very large range of absorbed dose from 100 mGy to 10 Gy.

This lower level of detection sensitivity makes this assay in fact comparable to detection levels currently obtained with standard biodosimetry techniques, with the possibility of increased improvement. Moreover, the fluorescence-based detection approach can be performed with low-cost, disposable microvolume sample containers. This is an important aspect when considering the potential of this approach for commercial product development.

This thesis work validated the original concept and formed important initial work in the overall CRTI project. A provisional patent has in fact also been filed to protect this state-of-the-art technology. This investigation has therefore laid the foundations for the further development of a personal and wearable DNA-based dosimeter.

7 Recommendations

1. Further testing is needed to investigate the lower level of detection of the device.

This testing should involve an investigation for the optimization of the signal-to-noise ratio by studying the device response as a function of: (i) the length of the DNA strand (between the fluor and quencher); (ii) the DNA concentration level (both in a wet and dry state if possible), and different candidate molecules for the fluor and quencher (that are more resistant to radiation breakdown and have an enhanced fluorescent signal). The custom-built fluorimeter at COPL should be used for such future testing and optimized in order to improve the signal-to-noise ratio. Techniques could be further developed to bind the DNA material to magnetic beads that could be read separately in order to improve the detector signal. Moreover, this optimization could include an investigation of the fluorescence background signal that can arise due to limitations of the FRET efficiency, and the distinguishing of the fluorescent signal due to the presence of any stray BHQ material liberated when other DNA dual-labelled oligonucleotides are broken. The design of the device could also be optimized with Monte Carlo modelling.

2. The detector response needs to be further investigated as a function of aging, photobleaching (i.e., light exposure) and temperature particularly for the given liquid construct. An investigation into alternative fluid solvents (e.g., with radiation scavengers, different oxygenation levels) would be beneficial.

3. Mixed-field radiation testing needs to be conducted in addition to low-LET gamma testing. For instance, experiments in collaboration with the iThemba Laboratories in South Africa could be carried out with quasi-monoenergetic neutron beams. Integral testing could also be done

behind the beam dump at the CERN Reference Field (CERF) that has been used previously for detector calibration for aircrew and spacecrew radiation instrument applications. In addition, polyenergetic neutron, gamma and alpha sources (neutrons: ^{252}Cf , ^{241}Am - ^9Be ; Gamma: ^{137}Cs ; Alpha: ^{244}Cm) could be further used for integral field testing at the DRDC-O laboratory for instance. Refined experiments could also be carried out at the Linac accelerator at Kingston General Hospital for low dose assessment.

4. There remains a significant interest to understand the nature of DNA damage and a theoretical description of this process. The rate of damage depends on a number of factors, including solution oxygenation, buffer components, etc. Quantification of these effects would assist in optimizing the performance of the device.

REFERENCES

1. S.V. Musolino, J. DeFranco, R. Schlueck. The ALARA Principle in the Context of a Radiological or Nuclear Emergency. *Health Phys.* 94(2), 109-111 (2008)
2. D. Pierce, D. Preston. Radiation-Related Cancer Risks at Low Doses among Atomic Bomb Survivors. *Rad. Res.* 154, 178-186 (2000)
3. F.A. Mettler, A.K. Gus'kova, I. Gusev. Health effects in those with acute radiation sickness from the Chernobyl accident. *Health physics.* 93(5), 462-9 (2007)
4. NCRP Report No. 98 "Guidance on Radiation Received in Space Activities?" *National Council on Radiation Protection & Measurements.* (1989)
5. Summary of Recommendations, Annals of the ICRP (ICRP 60), 21(1-3), 66-67 (1991)
6. R.L. Grasty, J.R. LaMarre. The Annual Effective Dose from Natural Sources of Ionising Radiation in Canada. *Radiation Protection Dosimetry.* 108(3), 215-226 (2004)
7. NCRP Report No. 93 "Ionizing Radiation Exposure of the Population of the United States." *National Council on Radiation Protection & Measurements.* (1987)
8. http://www.nuclearsafety.gc.ca/pubs_catalogue/uploads/0754_5.pdf Working in a Radiation Environment: produced by the Canadian Nuclear Safety Commission for First Responders (INFO – 0754 – 5)
9. J.E. Turner. Interaction of Ionizing Radiation with Matter. *Health Phys.* 88(6), 520-544 (2005)
10. A. Delgado. Mixed Field Dosimetry. *IRPA-10 (10th International Congress of the International Radiation Protection Association)* (2000)
11. International Atomic Energy Agency. Radiation Oncology Physics Handbook. (Austria) [Internet] Vienna, IAEA, 2005. STI/PUB/1196 Available from: <http://www-naweb.iaea.org/nahu/dmrp/syllabus.shtm>
12. H.S. Kaplan. Cellular effects of Ionizing Radiation. *Bulletin of the New York Academy of Medicine.* 36(10), 649-661 (1960)

13. M.F. Yudin, FM Karavaev. Terminology in the Field of Ionizing Radiation. *Measurement Techniques*. 19(8), 1228-1231 (1976)
14. National Institute of Standards and Technology. (2006) *Fundamental Physical Constants --- Complete Listing*. Retrieved March 5, 2010, from <http://physics.nist.gov/cuu/Constants/Table/allascii.txt>
15. J.E. Turner. Interaction of Ionizing Radiation with Matter. *Health Phys.* 88(6), 520-544 (2005)
16. M.A. Hill. Radiation Damage to DNA: The Importance of Track Structure. *Radiation Measurements*. 31, 15-23 (1999)
17. M. Mandelkern. The Dimensions of DNA in Solution. *J. Mol. Biol.* 152, 153-161 (1981)
18. U.S. National Library of Medicine: Genetics Home Reference. (2009) *Chromosome 1*. Retrieved March 24, 2010, from <http://ghr.nlm.nih.gov/chromosome=1>
19. I. Turai, K. Veress, B. Günlap, G. Souchkevitch. Medical Response to Radiation Incidents and Radionuclear Threats. *BMJ*. 328, 568-572 (2004)
20. N. Shikazono, M. Noguchi, K. Fujii, A. Urushibara, A. Yokoya. The Yield, Processing, and Biological Consequences of Clustered DNA Damage Induced by Ionizing Radiation. *J. Radiat. Res.* 50, 27-36 (2009)
21. W.D. Henner, S.M. Grunberg, W.A. Haseltine. Sites and Structure of γ Radiation-induced DNA Strand Breaks. *Journ. Bio. Chem.* 257(19), 11750-11754 (1982)
22. E.M. Rosen, S. Fan, S. Rockwell, I.D. Goldberg. The Molecular and Cellular Basis of Radiosensitivity: Implications for Understanding How Normal Tissues and Tumors Respond to Therapeutic Radiation. *Cancer Investigation*. 17(1) 56-72 (1999)
23. D. Wilkinson. "The Need for Radiation Biology!" Defense R&D Canada
24. A. Chatterjee, WR Holley. A General Theory of DNA Strand Break Production by Direct and Indirect Effects. *Radiation Protection Dosimetry*. 31(1/4), 241-247 (1990)
25. V. Moiseenko, A.J. Waker, W.V. Prestwich. Modeling Early Physical and Chemical Events for DNA Damaged Induced by Photons and Tritium Beta Particles. (Canada) AECL Internal Report. Chalk River (ON): Atomic Energy Canada Ltd., 1998. AECL-11850

26. D. van Gent, J. Hoeijmakers, R. Kanaar. Chromosomal Stability and the DNA Double Stranded Break Connection. *Nat. Gen.* 2, 196-206, (2001)
27. L.W. Brackenbush, J.C. McDonald, G.W.R. Endres, W. Quam. Mixed field Dose Equivalent Measuring Instruments. *Radiation Protection Dosimetry.* 10(1-4), 307-318 (1985)
28. M.J. Butson, P.K.N. Yu, T. Cheung, P. Metcalfe. Radiochromic Film for Medical Radiation Dosimetry. *Materials Science and Engineering R.* 41, 61-120 (2003)
29. J.H. Schulman, F.H. Attix, E.J. West, R.J. Ginther. New Thermoluminescent Dosimeter. *The Review of Scientific Instruments.* 31(12), 1263-1269 (1960)
30. R.L. Dixon, K.E. Ekstrand. Silicon diode dosimetry. *Int. J. Appl. Radiat. Isot.* 33, 1171-1176 (1982)
31. F. d'Errico, M. Luszik-Bhadra, T Lahaye. State of the Art of Electronic Personal Dosimeters for Neutrons. *Nuclear Instruments and Methods in Physics Research A.* 505, 411-414 (2003)
32. J. Zoetelief, J.J. Broerse. Dosimetry for Radiation Accidents: Present Status and Prospects for Biological Dosemeters. *Int. Journ. of Radiat. Bio.* 57(4), 737-750 (1990)
33. B. Columbia. The Comet Assay: A Comprehensive review. *Mutation Research.* 339, 37-59 (1995)
34. W.A. Hsieh, J.N. Lucas, J.J. Hwang, C.C. Chan, W.P. Chang. Biodosimetry using chromosomal translocations measured by FISH in a population chronically exposed to low dose-rate 60-Co gamma-irradiation. *Int. Journ. of Radiat. Bio.* 77(7), 797-804 (2001)
35. R. Hakem. DNA-Damage Repair; the Good, the Bad, and the Ugly. *The EMBO Journal.* 27, 589-605 (2008)
36. J.F. Ward. Biochemistry Of DNA Lesions. *Radiation Research.* 104 S-103-S111 (1985)
37. S. Matsunaga, K. Ohshio, E. Harada, S. Fujiwara, S. Uchiyama, K. Fukui. Development of New Dosimetry Using Extended DNA Fibers. *Journal of Bioscience and Bioengineering.* 98(5), 384-386 (2004)
38. Lakowicz, J.R. (1983). Principles of fluorescence spectroscopy (Chapter 10: Energy Transfer). New York, NY: Plenum Press.

39. Ganten, D., & Ruckpaul, K. (Eds.). (2006). *Encyclopedic Reference of Genomics and Proteomics in Molecular Medicine*. Germany: Springer Berlin Heidelberg.
40. R.K. Daiki, D.H. Gelfand, S. Stoffel, S.J. Scharf, R. Higuchi, G.T. Horn, K.B. Mullis, H.A. Erlich. Primer-Directed Enzymatic Amplification of DNA with a Thermostable DNA Polymerase. *Science*. 239(4839), 487-491 (1988)
41. V.V. Didenko, C.L. Minchew, S. Shuman, D.S. Baskin. Semi-Artificial Fluorescent Molecular Machine for DNA Damage Detection. *Nano Letters*. 4(12), 2461-2466 (2004)
42. J.B. Biggins, J.R. Prudent, D.J. Marshall, M. Ruppen, J.S. Thorson. A Continuous Assay for DNA Cleavage: The Application of “Break Lights” to Enediynes, Iron-Dependent Agents, and Nucleases. *PNAS*. 97(25), 13537-13542 (2000)
43. H.A. Ki, M.J. Kim, S. Pal, J.M. Song. Oligonucleotide Chip Assay for Quantification of Gamma-Ray Induced Single Strand Breaks. *J. of Pharmaceutical and Biomedical Analysis*. 49, 562-566 (2009)
44. S. Dubus, J. Gravel, B. Le Droff. PCR-free DNA detection using a magnetic bead-supported polymeric transducer and microelectromagnetic traps. *Anal. Chem*. 78(13), 4457-4464 (2006)
45. H. Ho, A. Najari, M. Leclerc. Optical detection of DNA and proteins with cationic polythiophenes. *Acc. Chem. Res.* 41(2), 168-178 (2008)
46. K. Doré, S. Dubus, H. Ho. Fluorescent polymeric transducer for the rapid, simple, and specific detection of nucleic acids at the zeptomole level. *Journ. Am. Chem. Soc.* 126(13), 4240-4244 (2004)
47. C. Birattari, T. Rancati, A. Ferrari, M. Hofert, T. Otto, and M. Silari, “Recent Results at the CERN-EC High Energy Reference Field Facility,” In: *Proc. Third Specialists Meeting on Shielding Aspects of Accelerators, Targets and Irradiation Facilities*, Tohoku University, Sendai, Japan, 219–234, (12–13 May 1997)
48. B.J. Lewis, M.J. McCall, A.R. Green, L.G.I. Bennett, M. Pierre, U.J. Schrewe, K. O’Brien, E. Felsberger, “Aircrew Exposure from Cosmic Radiation on Commercial Airline Routes,” *Radiation Protection Dosimetry*. Vol. 93, No. 4 (2001) 293-314.

49. I. Charlebois, A. Jones. "CRTI 06-0186 RD, Brain Storming Meeting: Summary Results," Ottawa, Ontario, February 2009.
50. G.A. Diaz-Quijada, R. Peytavi, A. Nantel, E. Roy, M.G. Bergeron, M.M. Dumoulin, T. Veres. Surface Modification of Thermoplastics – Towards the Plastic Biochip for High Throughput Screening Devices. *Lab on a Chip*. 7, 856-862 (2007)
51. B.J. Lewis, K. McDermott, T. Wood, E. Corcoran, L. Bennett, K. Avarmaa, J-F. Gravel, D. Boudreau, C. Drolet, L. Prud'homme-Lalonde, A. Jones, D. Wilkinson, E. Redmond, C. Gravel E.J. Lemieux, M. Leclerc, I. Charlebois, M. Boissinot, M.G. Bergeron, R. Blagoeva, M. Pierre, T. Veres, E. Roy and C. Vachon, "Final Project Report for CRTI 06-0186RD," CRTI Project Report for DNA Dosimeter project, National Research Council - Industrial Materials Institute, September 2010.
52. I. Charlebois. Novel DNA-Basd Radiological Dosimetry Technology. CRTI Summer Symposium Presentation. (2009)
53. D.B. Rorabacher. Statistical Treatment for Rejection of Deviant Values: Critical Values of Dixon's "Q" Parameter and Related Subrange Ratios at the 95% Confidence Level. *American Chemical Society*. 63, 139-146 (1991)

Appendix A: Calculations

This appendix discusses the conversion between the spectrometer fluorescence values and the number of signaling fluors (Section A1), the development of a scaling conversion factor for the BHQ absorbance per volume (Section A2), the calculation of the contribution of chromophore damage to overall signal in response to radiation (Section A3), and the calculation of the background strength relative to the total signal strength (Section A4).

A1: Fluorescence to Fluors Conversion Factors (see Section 4.2.1 and 5.3)

	BioTek Synergy HT Spectrometer		Custom COPL Fluorimeter
	PMT Sensitivity 75	PMT Sensitivity 85	
A. Fluorescence from slope of standard curve of FAM-dT(10)	23593.5 RFU*/M	16800 RFU/M	1×10^{14} CPS**/M
B. mol in solution (Volume*Concentration)	1.6×10^{-10} mol	1.6×10^{-10} mol	2.3×10^{-13}
C. molecules in solution (B*Na***)	9.6×10^{13}	9.6×10^{13}	1.5×10^{11}
D. Conversion Factor (C/A) (in molecules·RFU ⁻¹ ·M ⁻¹)	4.1×10^9	5.7×10^9	1.5×10^{-3}
The conversion factor is multiplied by RFU values to determine number of signalling fluors, and is in units of molecules/signal.			

* RFU = Relative Fluorescent Units

** CPS = Counts Per Second

*** Na = Avogadro's Number (6.022×10^{23})

A2: Scaling Conversion Factor (see Section 5.2.5)

Solutions being analyzed are composed of 200 μ L of 1.0 μ M of BHQ-1.

$$200 \text{ uL} \times 1.0 \text{ uM} = 2.0 \times 10^{-10} \text{ mol}$$

$$2.0 \times 10^{-10} \text{ mol} \times 2.066 \times 10^{23} \text{ unit/mol} = 1.20 \times 10^{14} \text{ molecules}$$

$$1.20 \times 10^{14} \div 0.018 \text{ (absorbance value pre-irradiation)} = 6.69 \times 10^{15} \text{ Conversion factor at } 200 \mu\text{L}.$$

A3: Fluor and Quencher Contributions (see Section 5.2.5)

	FAM Fluor	BHQ Quencher
A. 0 Gy	8.64×10^{13} Functioning Fluors	9.2×10^{13} Functioning Quenchers
B. 100 Gy	6.81×10^{13} Functioning Fluors	1.34×10^{13} Functioning Quenchers
C. Damage in 100 Gy (A-B)	1.83×10^{13} Fluors	7.86×10^{13} Fluors
D. Damage /Gy (C/100)	1.83×10^{11} Fluors/Gy	7.86×10^{11} Fluors/Gy
E. Damage /Gy /molecule (D/A)	8.55×10^{-03} Fluors/Gy/molecule	2.12×10^{-03} Fluors/Gy/molecule
F. Net effect (quencher – fluor)	6.43×10^{-03} SSB per Gy per molecule	
G. Expressed in terms of breaks (/10):	6.43×10^{-04} SSB/Gy/bp	

A4: Background Signal (see Section 5.2.6)

Unirradiated signal in 50 uL 0.5 uM: 1.5×10^5 CPS

Converted to signal per M: 3×10^{11} CPS

Slope of calibration curve of 50 uL fluor (in CPS/M): 1×10^{14}

Ratio of background signal to full signal: $3 \times 10^{11} / 1 \times 10^{14} = 0.3\%$

Appendix B: Raw Experimental Data for the Unirradiated and Irradiated Samples

The raw data are presented in terms of fluorescent units in counts per second (cps). This analysis provides the mean and standard deviation for the signalling data in terms of: fluorescent units (FU), relative fluorescent units (RFU), and in number of fluors. Outliers are highlighted in red and have been omitted in the analysis (see Appendix C for outlier determination). These omissions have been maintained in post-irradiation data.

B1: Unirradiated Samples

Calibration Standard		0	0.02	0.04	0.06	0.08	0.1
Pre-Irradiation							
Plate 3	A	4183	4723	5183	5702	6183	6305
	B	4110	4622	5027	5505	5973	6150
	C	4140	4535	4974	5414	5889	6054
Plate 7	A	4035	4752	5200	5811	6441	6826
	B	4133	4598	5089	5802	6307	6785
	C	4111	4600	5042	5595	6128	6740
Plate 8	A	4554	4853	5393	5821	6275	6985
	B	4602	4891	5423	5807	6331	6799
	C	4446	4876	5374	5831	6364	6832
Plate 9	A	4210	4863	5245	5889	6423	6877
	B	4286	4762	5386	5802	6291	6911
	C	4268	4757	5310	5772	6197	6739
Plate 10	A	4284	4793	5195	5708	6199	6828
	B	4370	4776	5250	5797	6050	6695
	C	4244	4725	5231	5402	6046	6584
Plate 2	A	4971	5355	5873	6468	6856	7431
	B	5002	5270	5753	6187	6702	7290
	C	4988	5241	5717	6165	8234	7218
Plate 4	A	5027	4910	5389	5986	6417	7434
	B	4468	4825	5364	5926	6390	6689
	C	4523	4806	5340	5919	6231	6594
Plate 5	A	5046	5429	5849	6280	6528	7085
	B	4889	5336	5753	6115	6701	7050
	C	5204	5241	5494	5989	6440	6887
Plate 6	A	4765	5190	5760	6291	6723	7148
	B	4746	5165	5651	6093	6566	6833
	C	4617	5109	5646	6036	6594	6859
FU	MEAN	4526.740741	4926.037037	5404.111111	5893.074074	6355.576923	6838.074074
	STDEV	354.9062273	262.1516709	263.1751878	261.1174104	244.3979007	331.1839979
RFU	MEAN	0	399.2962963	877.3703704	1366.333333	1828.836182	2311.333333
	STDEV	501.9132001	441.2277516	441.8366324	440.6140399	430.9161914	485.4289553
FLUORS	MEAN	0	1.6307E+12	3.58312E+12	5.58001E+12	7.46884E+12	9.43933E+12
	STDEV	2.04978E+12	1.80194E+12	1.80443E+12	1.79944E+12	1.75983E+12	1.98246E+12

FAM-dT(10)-BHQ

Pre-irradiation

		0	0.2	0.4	0.6	0.8	1
Plate 3	E	4180	4179	4205	4258	4257	4301
	F	4149	4197	4207	4319	4333	4346
	G	4090	4199	4299	4350	4375	4459
Plate 7	E	4177	4138	4241	4421	4356	4143
	F	3994	3993	4165	4236	4146	4252
	G	3987	4031	4077	6712	4085	4157
Plate 8	E	4318	4418	4459	4503	4545	4474
	F	4260	4336	4446	4440	4496	4526
	G	4145	4338	4393	4398	4517	4466
Plate 9	E	4447	4336	4444	4480	4444	4365
	F	4190	4293	4389	4392	4403	4415
	G	4132	4233	4372	4387	4378	4433
Plate 10	E	4289	4294	4279	4339	4327	4140
	F	4257	4304	4386	4361	4325	4345
	G	4191	4262	4360	4422	4409	4384
Plate 2	E	4961	5129	4980	5048	4812	4718
	F	4880	5035	4860	4970	4793	4910
	G	4858	4891	4960	4787	4603	4798
Plate 4	E	4971	4419	4456	4474	4456	4419
	F	4856	4429	4396	4585	4408	4704
	G	4669	4336	4379	4518	4557	4378
Plate 5	E	4848	4851	4998	4799	4632	4707
	F	4912	4821	4815	4781	4686	4574
	G	4658	4745	4784	4748	4650	4718
Plate 6	E	4683	4802	4804	4892	4886	4837
	F	4670	4774	4802	4848	4879	4874
	G	4605	4738	4720	4748	4778	4794
FU	MEAN	4458.407407	4463.740741	4506.518519	4557.846154	4501.333333	4505.074074
	STDEV	332.3638251	314.9381615	274.4634444	234.168263	212.2478595	229.8537873
RFU	MEAN	0	5.333333333	48.11111111	99.43874644	42.92592593	46.66666667
	STDEV	470.0334291	457.8774485	431.0404791	406.5716267	394.3537322	404.1020611
FLUORS	MEAN	0	21780975721	1.96483E+11	4.06101E+11	1.75307E+11	1.90584E+11
	STDEV	1.91959E+12	1.86994E+12	1.76034E+12	1.66041E+12	1.61051E+12	1.65033E+12

FAM-dT(20)-BHQ

Pre-Irradiation		0	0.2	0.4	0.6	0.8	1
Plate 3	A	4307	4761	5483	6456	6861	6303
	B	4210	4637	5364	5931	6718	6724
	C	4206	4611	5257	6091	6780	7680
Plate 7	A	4406	7704	5862	6744	7422	10587
	B	4300	4977	5665	6522	7618	6649
	C	4334	4855	5651	6313	7144	7810
Plate 8	A	4426	5070	6041	6820	7685	8590
	B	4451	5042	5820	6670	7552	8189
	C	4416	5099	5846	6620	7663	8381
Plate 9	A	4399	4991	5907	6650	7617	8234
	B	4473	4985	5847	6610	7377	8276
	C	4444	4878	5813	6532	7664	9216
Plate 10	A	4287	4810	6821	6435	7649	8273
	B	4184	4882	5500	6368	7393	8240
	C	4263	4789	5527	6192	7262	8602
Plate 2	A	4862	5351	6332	6857	7457	8565
	B	4691	5328	5968	6688	8480	8503
	C	4784	5204	5909	6503	7752	8498
Plate 4	A	4827	5112	6107	6960	7749	7676
	B	4357	4936	5823	6478	7158	7324
	C	4331	4866	5665	6548	7183	8070
Plate 5	A	4865	5042	6118	6689	7665	8541
	B	4716	5108	5731	6560	7676	8425
	C	4725	5071	5769	6437	7432	8173
Plate 6	A	4969	5546	6277	6917	7818	7911
	B	4915	5434	6118	6679	7578	7252
	C	4933	5332	6029	6691	7660	7691
FU	MEAN	4521.518519	5027.576923	5861.111111	6554.111111	7443.576923	7992.153846
	STDEV	256.9322524	235.8265758	324.2943029	237.7489518	306.7352178	682.8299755
RFU	MEAN	0	506.0584046	1339.592593	2032.592593	2922.058405	3470.635328
	STDEV	363.357076	348.7525716	413.7402291	350.0553477	400.1258254	729.5690219
FLUORS	MEAN	0	2.06671E+12	5.47081E+12	8.30097E+12	1.19335E+13	1.41738E+13
	STDEV	1.48393E+12	1.42428E+12	1.68969E+12	1.4296E+12	1.63409E+12	2.97951E+12

FAM-dT(30)-BHQ

Pre-Irradiation		0	0.2	0.4	0.6	0.8	1
Plate 3	E	4171	5159	6007	7108	7647	8712
	F	4239	5138	6175	6812	7927	9306
	G	4255	5279	6144	7096	8224	9493
Plate 7	E	4182	4624	6104	7344	8245	9067
	F	4063	5182	6054	7722	8142	9644
	G	4071	5155	6212	6915	7923	9753
Plate 8	E	4338	5466	6566	7458	8744	9549
	F	4302	5435	6523	7512	8372	10109
	G	4231	5551	6507	7513	8799	9634
Plate 9	E	4246	5468	6294	7274	8339	9622
	F	4301	5464	6395	7322	8188	9573
	G	4233	5363	6463	7209	8197	9397
Plate 10	E	4137	4973	6078	7056	8118	9385
	F	4165	5160	6247	7228	8765	9349
	G	4336	5250	6251	7258	8452	9861
Plate 2	E	4569	5590	6716	7704	8797	9909
	F	4723	5701	6946	7549	8756	9738
	G	4773	5753	6673	7494	8493	9863
Plate 4	E	4141	5342	6694	7302	8600	9693
	F	4189	5315	6563	7460	8488	10033
	G	4068	5363	6616	7376	8684	9990
Plate 5	E	4418	5658	6451	7365	8835	9928
	F	4496	5564	6368	7347	8370	10208
	G	4510	5634	6588	7391	8096	9365
Plate 6	E	4658	5703	6620	7442	8585	9331
	F	4679	5814	6547	7457	8497	9331
	G	4593	5657	6549	7327	8212	9697
FU	MEAN	4336.555556	5428.346154	6420.407407	7334.851852	8388.703704	9647.230769
	STDEV	213.8551511	225.3585485	238.9110326	211.0199961	310.2695869	286.3887299
RFU	MEAN	0	1091.790598	2083.851852	2998.296296	4052.148148	5310.675214
	STDEV	213.8551511	225.3585485	238.9110326	211.0199961	310.2695869	286.3887299
FLUORS	MEAN	0	4.4588E+12	8.51031E+12	1.22448E+13	1.65487E+13	2.16884E+13
	STDEV	8.7337E+11	9.20349E+11	9.75697E+11	8.61792E+11	1.26712E+12	1.16959E+12

B2: Irradiated Samples

Calibration Standard (Reporter)

Irradiated

DAY 1		0	0.02	0.04	0.06	0.08	0.1
Plate 3	A	3959	4452	4959	5505	6034	6297
	B	4013	4480	5005	5579	6141	6408
0.1 Gy	C	4097	4467	5021	5516	6084	6271
FU	MEAN	4023	4466.333333	4995	5533.333333	6086.333333	6325.333333
	STDEV	69.5413546	14.0118997	32.18695388	39.92910384	53.53814839	72.76216966
RFU	MEAN	0	443.3333333	972	1510.333333	2063.333333	2302.333333
	STDEV	69.5413546	14.0118997	32.18695388	39.92910384	53.53814839	72.76216966
Fluors	MEAN	0	1.81054E+12	3.96958E+12	6.1681E+12	8.42651E+12	9.40257E+12
	STDEV	2.84002E+11	57223658863	1.31449E+11	1.63068E+11	2.18646E+11	2.97156E+11

Plate 7	A	4100	4629	5108	5684	6318	6742
	B	4074	4548	5058	5716	6232	6700
0.5 Gy	C	4100	4578	5048	5495	6092	6720
FU	MEAN	4091.333333	4585	5071.333333	5631.666667	6214	6720.666667
	STDEV	15.011107	40.95119046	32.14550254	119.4333845	114.0701539	21.00793501
RFU	MEAN	0	493.6666667	980	1540.333333	2122.666667	2629.333333
	STDEV	15.011107	40.95119046	32.14550254	119.4333845	114.0701539	21.00793501
Fluors	MEAN	0	2.0161E+12	4.00225E+12	6.29062E+12	8.66883E+12	1.0738E+13
	STDEV	61304354453	1.67242E+11	1.3128E+11	4.87758E+11	4.65855E+11	85794997944

Plate 8	A	4427	4757	5248	5718	6218	6811
	B	4465	4654	5109	5738	6254	6708
1 Gy	C	4450	4584	5038	5510	6036	6432
FU	MEAN	4447.333333	4665	5131.666667	5655.333333	6169.333333	6650.333333
	STDEV	19.13983629	87.02298547	106.8191618	126.2589931	116.864594	195.9702358
RFU	MEAN	0	217.6666667	684.3333333	1208	1722	2203
	STDEV	19.13983629	87.02298547	106.8191618	126.2589931	116.864594	195.9702358
Fluors	MEAN	0	8.88936E+11	2.79477E+12	4.93339E+12	7.03253E+12	8.9969E+12
	STDEV	78165808050	3.55396E+11	4.36242E+11	5.15633E+11	4.77267E+11	8.00329E+11

Plate 9	A	3954	4560	4949	5534	6102	6578
	B	4065	4501	4987	5503	5977	6787
5 Gy	C	3847	4455	5011	5413	5836	6400
FU	MEAN	3955.333333	4505.333333	4982.333333	5483.333333	5971.666667	6588.333333
	STDEV	109.006116	52.63395609	31.2623309	62.85167725	133.0801763	193.7068231
RFU	MEAN	0	550	1027	1528	2016.333333	2633
	STDEV	109.006116	52.63395609	31.2623309	62.85167725	133.0801763	193.7068231

Fluors	MEAN	0	2.24616E+12	4.1942E+12	6.24025E+12	8.23457E+12	1.0753E+13
	STDEV	4.45174E+11	2.14954E+11	1.27673E+11	2.56682E+11	5.43491E+11	7.91086E+11

Plate 10	A	4455	4755	5150	5561	6077	6612
	B	4505	4777	5124	5694	5961	6554
10 Gy	C	4352	4719	5247	5381	5956	6474
FU	MEAN	4437.333333	4750.333333	5173.666667	5545.333333	5998	6546.666667
	STDEV	78.01495583	29.28025501	64.82540654	157.0870247	68.46166811	69.29165414
RFU	MEAN	0	313	736.3333333	1108	1560.666667	2109.333333
	STDEV	78.01495583	29.28025501	64.82540654	157.0870247	68.46166811	69.29165414
Fluors	MEAN	0	1.27827E+12	3.00714E+12	4.525E+12	6.37366E+12	8.61438E+12
	STDEV	3.18608E+11	1.19579E+11	2.64743E+11	6.41533E+11	2.79593E+11	2.82982E+11

DAY 2

Plate 2	A	4557	5007	5421	5920	6354	6995
	B	4539	4903	5473	5900	6236	6880
0.5	C	4285	4719	5407	5763	7835	6667
FU	MEAN	4460.333333	4876.333333	5433.666667	5861	6295	6847.333333
	STDEV	152.1096096	145.8400951	34.77547028	85.45759182	83.43860018	166.422154
RFU	MEAN	0	416	973.3333333	1400.666667	1834.666667	2387
	STDEV	152.1096096	145.8400951	34.77547028	85.45759182	83.43860018	166.422154
Fluors	MEAN	0	1.69892E+12	3.97503E+12	5.72023E+12	7.49266E+12	9.74835E+12
	STDEV	6.21205E+11	5.95601E+11	1.42021E+11	3.49003E+11	3.40758E+11	6.79657E+11

Plate 4	A	4607	4687	5143	5606	5988	6881
	B	4425	4591	5063	5512	5873	6341
1	C	4426	4562	5058	5484	5880	6152
1 Gy	MEAN	4486	4613.333333	5088	5534	5913.666667	6458
	STDEV	104.7902667	65.42425646	47.69696007	63.90618123	64.46963109	378.321292
FU	MEAN	0	127.3333333	602	1048	1427.666667	1972
	STDEV	104.7902667	65.42425646	47.69696007	63.90618123	64.46963109	378.321292
RFU	MEAN	0	127.3333333	602	1048	1427.666667	1972
	STDEV	104.7902667	65.42425646	47.69696007	63.90618123	64.46963109	378.321292
Fluors	MEAN	0	5.20021E+11	2.45853E+12	4.27996E+12	5.83049E+12	8.05352E+12
	STDEV	4.27956E+11	2.67188E+11	1.94791E+11	2.60989E+11	2.6329E+11	1.54504E+12

Plate 5	A	4411	4798	5126	5558	5986	5997
	B	4420	4739	5128	5608	5890	6307
2.5	C	4551	4714	5119	5434	5873	6148
2.5 Gy	MEAN	4460.666667	4750.333333	5124.333333	5533.333333	5916.333333	6150.666667
	STDEV	78.36027905	43.13158162	4.725815627	89.5842248	60.92892034	155.0172033
FU	MEAN	0	289.6666667	663.6666667	1072.666667	1455.666667	1690
	STDEV	78.36027905	43.13158162	4.725815627	89.5842248	60.92892034	155.0172033
RFU	MEAN	0	289.6666667	663.6666667	1072.666667	1455.666667	1690
	STDEV	78.36027905	43.13158162	4.725815627	89.5842248	60.92892034	155.0172033

Fluors	STDEV	78.36027905	43.13158162	4.725815627	89.5842248	60.92892034	155.0172033
	MEAN	0	1.18298E+12	2.71037E+12	4.3807E+12	5.94485E+12	6.90185E+12
	STDEV	3.20018E+11	1.76146E+11	19299914142	3.65856E+11	2.4883E+11	6.3308E+11

Plate 6	A	4321	4648	5071	5458	5757	6029
5	B	4338	4634	4965	5361	5656	5849
5 Gy	C	4259	4529	5039	5323	5728	5911
FU	MEAN	4306	4603.666667	5025	5380.666667	5713.666667	5929.666667
	STDEV	41.58124577	65.0410127	54.36910888	69.61561128	52.00320503	91.44032663
RFU	MEAN	0	297.6666667	719	1074.666667	1407.666667	1623.666667
	STDEV	41.58124577	65.0410127	54.36910888	69.61561128	52.00320503	91.44032663
Fluors	MEAN	0	1.21565E+12	2.93635E+12	4.38887E+12	5.74882E+12	6.63095E+12
	STDEV	1.69815E+11	2.65623E+11	2.2204E+11	2.84305E+11	2.12378E+11	3.73436E+11

FAM-dT(10)-BHQ

Irradiated

DAY 1		1	2	3	4	5	6
Plate 3	E	4163	4226	4265	4336	4351	4340
0.1 Gy	F	4157	4220	4246	4310	4325	4390
	G	4124	4219	4285	4302	4355	4394
FU	MEAN	4148	4221.666667	4265.333333	4316	4343.666667	4374.666667
	STDEV	21	3.785938897	19.50213664	17.77638883	16.28905563	30.08875759
RFU	MEAN	0	73.66666667	117.3333333	168	195.6666667	226.6666667
	STDEV	21	3.785938897	19.50213664	17.77638883	16.28905563	30.08875759
FLUORS	MEAN	0	3.0085E+11	4.79181E+11	6.86101E+11	7.9909E+11	9.25691E+11
	STDEV	85762591900	15461520599	79645418353	72597580052	66523410975	1.2288E+11

Plate 7	E	3967	4115	4152	4289	4236	4125
0.5 Gy	F	3964	4057	4182	4134	4116	4227
	G	3996	4089	4111	4160	4182	4174
FU	MEAN	3975.666667	4087	4148.333333	4211.5	4178	4175.333333
	STDEV	17.67295486	29.05167809	35.64173584	109.6015511	60.09991681	51.01307022
RFU	MEAN	0	111.3333333	172.6666667	235.8333333	202.3333333	199.6666667
	STDEV	17.67295486	29.05167809	35.64173584	109.6015511	60.09991681	51.01307022
Fluors	MEAN	0	4.54678E+11	7.05159E+11	9.63128E+11	8.26316E+11	8.15425E+11
	STDEV	72175162617	1.18645E+11	1.45558E+11	4.47605E+11	2.45444E+11	2.08334E+11

Plate 8	E	4356	4323	4377	4397	4344	4339
1 Gy	F	4393	4290	4325	4344	4365	4341
	G	4179	4270	4395	4400	4474	4514
FU	MEAN	4309.333333	4294.333333	4365.666667	4380.333333	4394.333333	4398
	STDEV	114.3780282	26.76440422	36.35014901	31.50132272	69.78777352	100.4639239
RFU	MEAN	0	-15	56.33333333	71	85	88.66666667
	STDEV	114.3780282	26.76440422	36.35014901	31.50132272	69.78777352	100.4639239
Fluors	MEAN	0	-6.1259E+10	2.30062E+11	2.89959E+11	3.47134E+11	3.62109E+11
	STDEV	4.67112E+11	1.09304E+11	1.48452E+11	1.28649E+11	2.85009E+11	4.10288E+11

Plate 9	E	4099	4064	4267	4485	4363	4369
5 Gy	F	3993	4191	4231	4388	4423	4409
	G	3958	4016	4120	4233	4425	4445
FU	MEAN	4016.666667	4090.333333	4206	4368.666667	4403.666667	4407.666667
	STDEV	73.41888949	90.42307965	76.62245102	127.107566	35.2325607	38.01753981
RFU	MEAN	0	73.66666667	189.3333333	352	387	391
	STDEV	73.41888949	90.42307965	76.62245102	127.107566	35.2325607	38.01753981

Fluors	MEAN	0	3.0085E+11	7.73225E+11	1.43754E+12	1.58048E+12	1.59682E+12
	STDEV	2.99838E+11	3.69282E+11	3.12921E+11	5.19099E+11	1.43887E+11	1.55261E+11

Plate 10 10 Gy	E	4377	4384	4541	4840	5007	4693
	F	4291	4415	4521	4837	4963	5077
	G	4191	4453	4577	4774	4956	5231
FU	MEAN	4286.333333	4417.333333	4546.333333	4817	4975.333333	5000.333333
	STDEV	93.0877722	34.55912808	28.37839554	37.26929031	27.64657905	277.0727943
RFU	MEAN	0	131	260	530.6666667	689	714
	STDEV	93.0877722	34.55912808	28.37839554	37.26929031	27.64657905	277.0727943
Fluors	MEAN	0	5.34995E+11	1.06182E+12	2.16721E+12	2.81383E+12	2.91593E+12
	STDEV	3.80164E+11	1.41137E+11	1.15895E+11	1.52205E+11	1.12907E+11	1.13155E+12

DAY 2

Plate 2 0.5 Gy	E	4329	4396	4612	4668	4310	4442
	F	4408	4338	4524	4464	4383	4394
	G	4374	4279	4308	4401	4337	4482
FU	MEAN	4370.333333	4337.666667	4481.333333	4511	4343.333333	4439.333333
	STDEV	39.62743158	58.50071225	156.4267667	139.5671881	36.90979996	44.06056438
RFU	MEAN	0	-32.6666667	111	140.6666667	-27	69
	STDEV	56.04165118	70.65880459	161.3681092	145.0838838	54.15410111	59.25931713
Fluors	MEAN	0	-1.3341E+11	4.53317E+11	5.74473E+11	-1.1027E+11	2.81791E+11
	STDEV	2.2887E+11	2.88566E+11	6.59017E+11	5.92513E+11	2.21162E+11	2.42011E+11

Plate 4 1.0 Gy	E	4518	4281	4285	4408	4462	4423
	F	4432	4213	4307	4295	4376	4607
	G	4358	4205	4208	4317	4451	4354
FU	MEAN	4436	4233	4266.666667	4340	4429.666667	4461.333333
	STDEV	80.07496488	41.76122604	51.98397189	59.9082632	46.80099714	130.7835362
RFU	MEAN	0	-203	-169.3333333	-96	-6.333333333	25.33333333
	STDEV	113.2431013	90.31057524	95.46901766	100.0049999	92.74876459	153.3503614
Fluors	MEAN	0	-8.2904E+11	-6.9155E+11	-3.9206E+11	-2.5865E+10	1.0346E+11
	STDEV	4.62477E+11	3.68822E+11	3.89889E+11	4.08414E+11	3.7878E+11	6.26273E+11

Plate 5 2.5 Gy	E	4600	4498	4601	4515	4524	4500
	F	4483	4411	4401	4431	4365	4221
	G	4238	4352	4347	4383	4400	4296
FU	MEAN	4440.333333	4420.333333	4449.666667	4443	4429.666667	4339
	STDEV	184.7331409	73.44612538	133.8108117	66.81317235	83.54838917	144.3849023
RFU	MEAN	0	-20	9.333333333	2.666666667	-10.6666667	-101.3333333
	STDEV	261.2521132	198.798055	228.1045082	196.4442245	202.7477908	234.4639276

Fluors	MEAN	0	-8.1679E+10	38116707511	10890487860	-4.3562E+10	-4.1384E+11
	STDEV	1.06694E+12	8.11878E+11	9.31564E+11	8.02265E+11	8.28008E+11	9.57535E+11

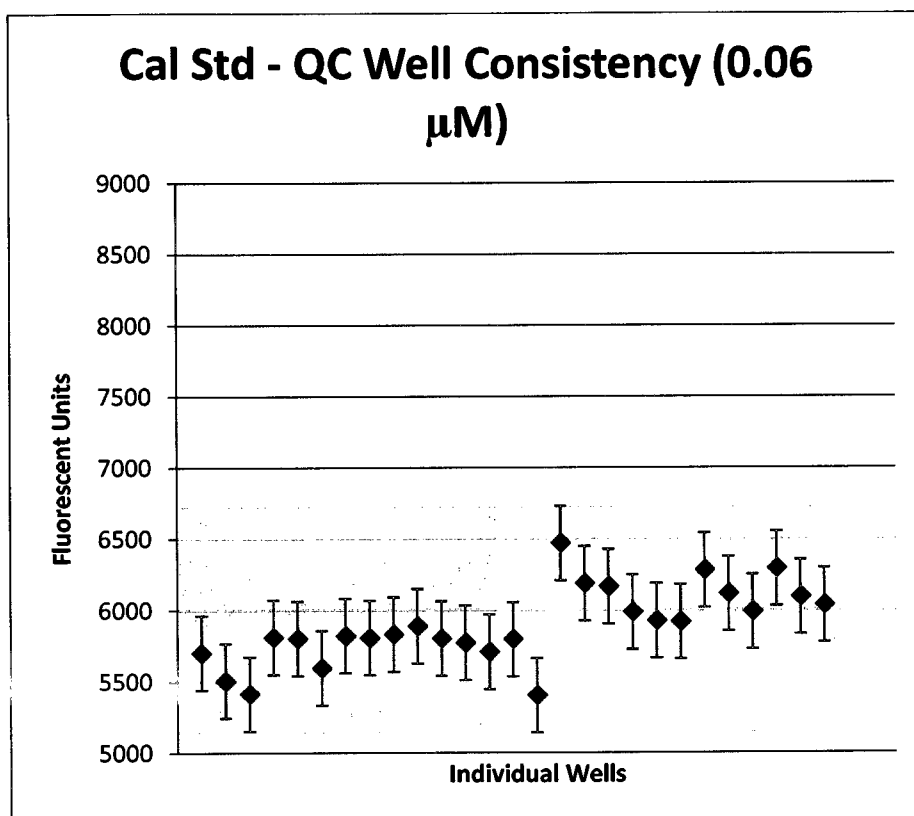
Plate 6 5.0 Gy	E	4229	4337	4370	4596	4621	4599
	F	4182	4232	4431	4489	4604	4496
	G	4198	4285	4304	4426	4574	4512
FU	MEAN	4203	4284.666667	4368.333333	4503.666667	4599.666667	4535.666667
	STDEV	23.89560629	52.50079364	63.51640208	85.94378007	23.797759	55.42863279
RFU	MEAN	0	81.66666667	165.3333333	300.6666667	396.6666667	332.6666667
	STDEV	33.7934905	57.68304199	67.8626063	89.20388631	33.72437299	60.36003093
Fluors	MEAN	0	3.33521E+11	6.7521E+11	1.2279E+12	1.61996E+12	1.35859E+12
	STDEV	1.3801E+11	2.35574E+11	2.77146E+11	3.64303E+11	1.37728E+11	2.46506E+11

Appendix C: Quality Control

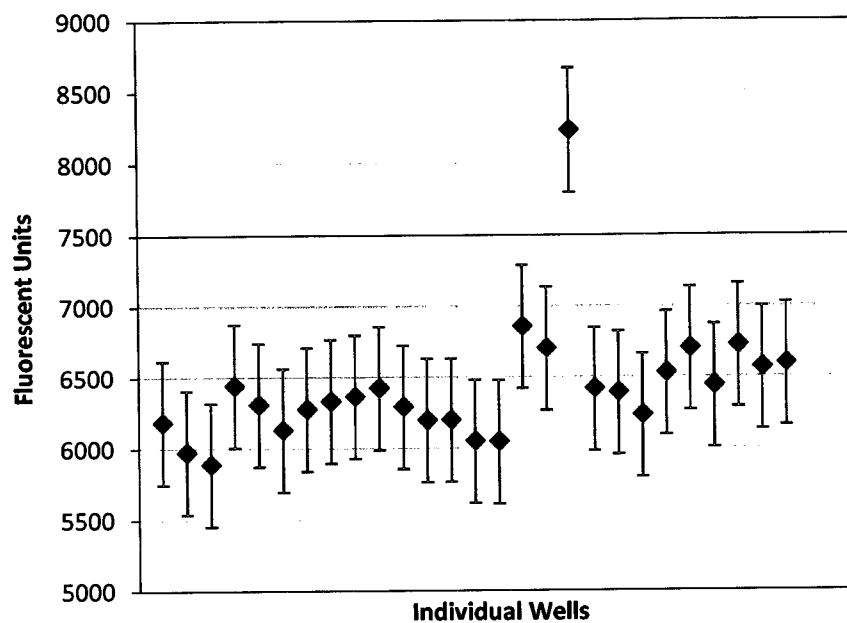
Two methods were employed for quality control in experiments with the dual-labelled oligonucleotides. First, inspection of the data was performed for any possible outliers. A statistical analysis was further considered with the use of Dixon's Q parameter, for $n \geq 14$, using the r_{22} form of the test.^[53]

C1: Visual Analysis for Outliers in Pre-Irradiation Calibration Standard and FAM-dt(10)-BHQ

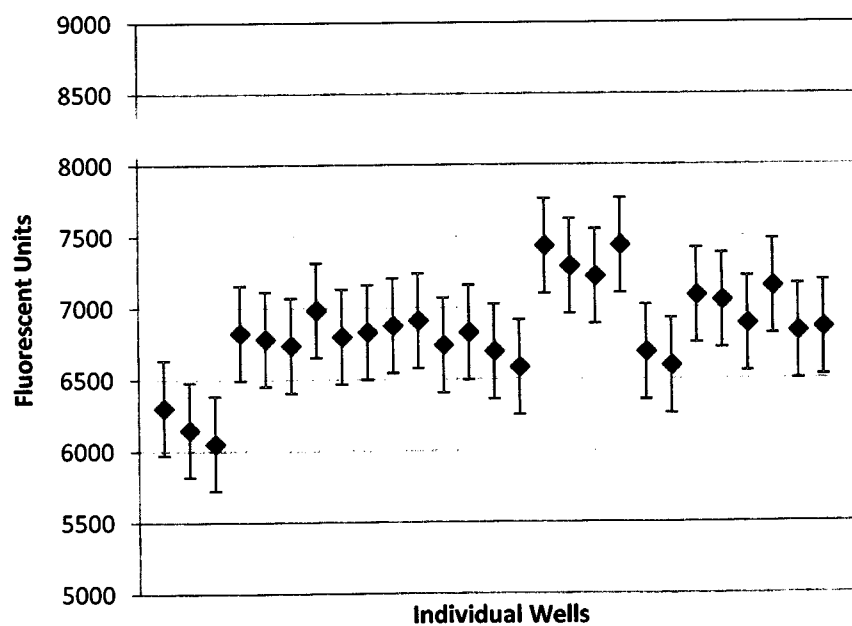
Values have not been converted to the quantity of fluors.



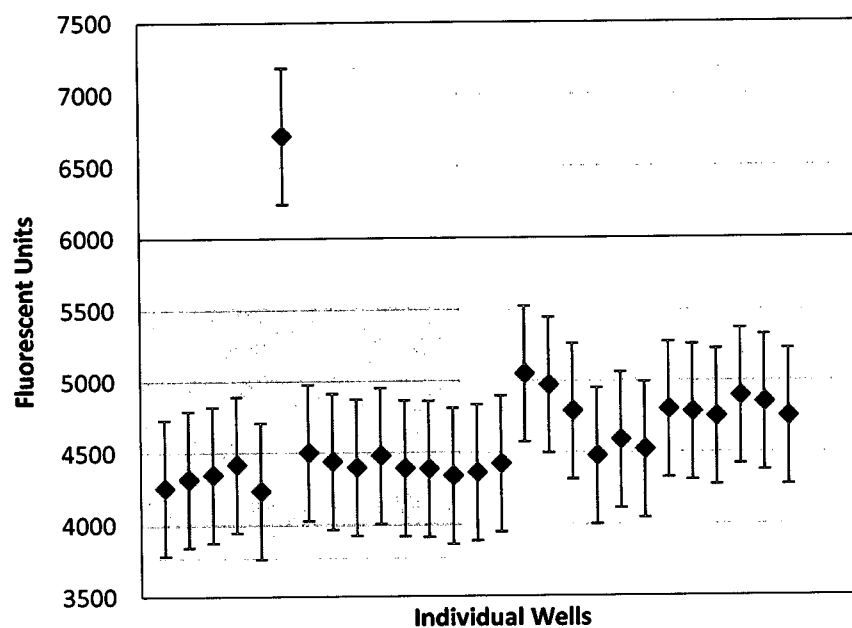
Cal Std - QC Well Consistency (0.08 μM)



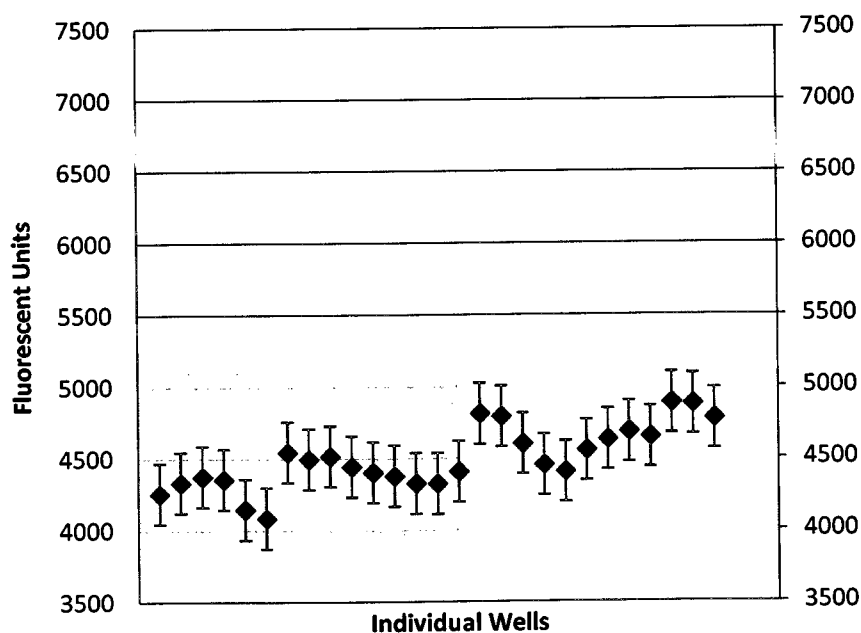
Cal Std - QC Well Consistency (0.1 μM)



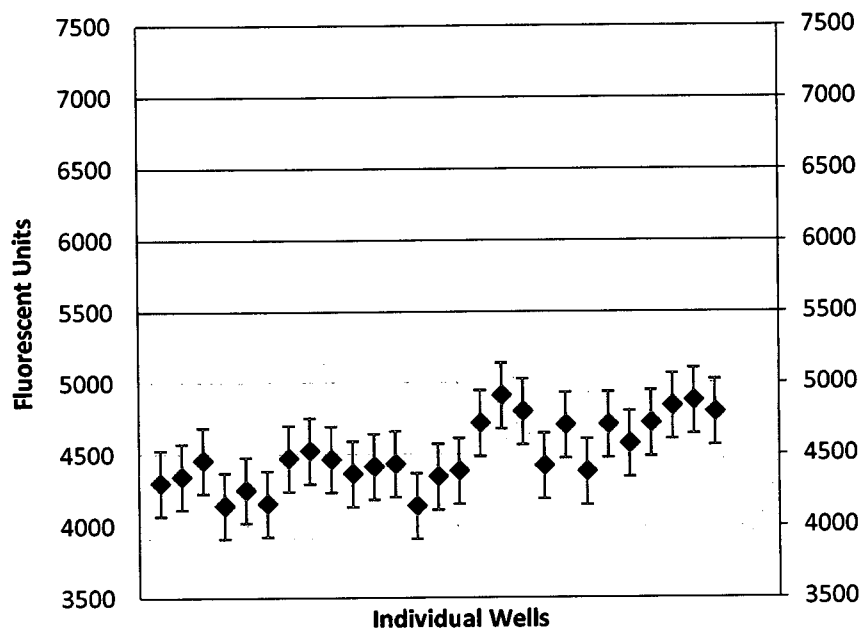
FAM-dT(10)-BHQ - QC Well Consistency (0.6 μM)



FAM-dT(10)-BHQ - QC Well Consistency (0.8 μM)



FAM-dT(10)-BHQ - QC Well Consistency (1.0 μ M)



C2: Statistical Analysis for Outliers in Pre-Irradiation Calibration Standard and FAM-dT(10)-BHQ Using Dixon's Q Test

Calculation

r_{22} Low Outlier Test:

$$r_{22} = \frac{x_3 - x_1}{x_{n-2} - x_1}$$

In Excel (sample):

$$=(\text{SMALL}(\text{H34:H60},3)-\text{SMALL}(\text{H34:H60},1))/(\text{LARGE}(\text{H34:H60},3)-\text{SMALL}(\text{H34:H60},1))$$

r_{22} High Outlier Test:

$$r_{22} = \frac{x_n - x_{n-2}}{x_n - x_3}$$

In Excel (sample):

$$=(\text{LARGE}(\text{H34:H60},1)-\text{LARGE}(\text{H34:H60},3))/(\text{LARGE}(\text{H34:H60},1)-\text{SMALL}(\text{H34:H60},3))$$

For sample size of 27 (as in both tables below), a value can be said to contain an outlier with 95% confidence if $r_{22} > 0.432$.^[53] Those results are highlighted below.

Calibration Standard

Pre-irradiation		1	2	3	4	5	6
Plate 3	A	4183	4723	5183	5702	6183	6305
	B	4110	4622	5027	5505	5973	6150
	C	4140	4535	4974	5414	5889	6054
Plate 7	A	4035	4752	5200	5811	6441	6826
	B	4133	4598	5089	5802	6307	6785
	C	4111	4600	5042	5595	6128	6740
Plate 8	A	4554	4853	5393	5821	6275	6985
	B	4602	4891	5423	5807	6331	6799
	C	4446	4876	5374	5831	6364	6832
Plate 9	A	4210	4863	5245	5889	6423	6877
	B	4286	4762	5386	5802	6291	6911
	C	4268	4757	5310	5772	6197	6739
Plate 10	A	4284	4793	5195	5708	6199	6828
	B	4370	4776	5250	5797	6050	6695
	C	4244	4725	5231	5402	6046	6584
Plate 2	A	4971	5355	5873	6468	6856	7431
	B	5002	5270	5753	6187	6702	7290
	C	4988	5241	5717	6165	8234	7218
Plate 4	A	5027	4910	5389	5986	6417	7434
	B	4468	4825	5364	5926	6390	6689
	C	4523	4806	5340	5919	6231	6594
Plate 5	A	5046	5429	5849	6280	6528	7085
	B	4889	5336	5753	6115	6701	7050
	C	5204	5241	5494	5989	6440	6887
Plate 6	A	4765	5190	5760	6291	6723	7148
	B	4746	5165	5651	6093	6566	6833
	C	4617	5109	5646	6036	6594	6859
Q-Test Results	LOW	0.076613	0.081149	0.086514	0.117312	0.188249	0.203074
	HIGH	0.16194	0.112183	0.135981	0.195223	0.690585	0.127547

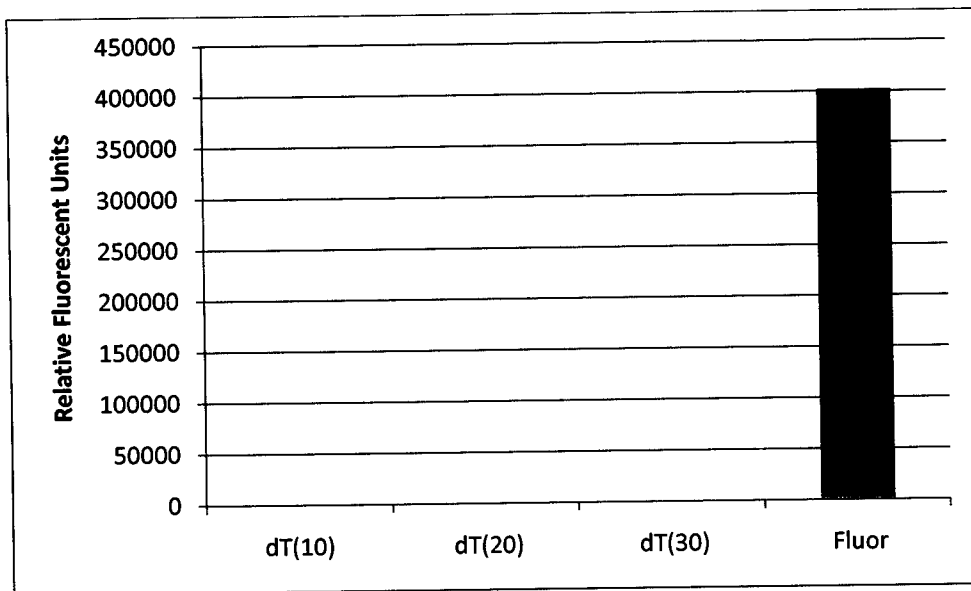
FAM-dT(10)-BHQ

Pre-irradiation

		1	2	3	4	5	6
Plate 3	E	4180	4179	4205	4258	4257	4301
	F	4149	4197	4207	4319	4333	4346
	G	4090	4199	4299	4350	4375	4459
Plate 7	E	4177	4138	4241	4421	4356	4143
	F	3994	3993	4165	4236	4146	4252
	G	3987	4031	4077	6712	4085	4157
Plate 8	E	4318	4418	4459	4503	4545	4474
	F	4260	4336	4446	4440	4496	4526
	G	4145	4338	4393	4398	4517	4466
Plate 9	E	4447	4336	4444	4480	4444	4365
	F	4190	4293	4389	4392	4403	4415
	G	4132	4233	4372	4387	4378	4433
Plate 10	E	4289	4294	4279	4339	4327	4140
	F	4257	4304	4386	4361	4325	4345
	G	4191	4262	4360	4422	4409	4384
Plate 2	E	4961	5129	4980	5048	4812	4718
	F	4880	5035	4860	4970	4793	4910
	G	4858	4891	4960	4787	4603	4798
Plate 4	E	4971	4419	4456	4474	4456	4419
	F	4856	4429	4396	4585	4408	4704
	G	4669	4336	4379	4518	4557	4378
Plate 5	E	4848	4851	4998	4799	4632	4707
	F	4912	4821	4815	4781	4686	4574
	G	4658	4745	4784	4748	4650	4718
Plate 6	E	4683	4802	4804	4892	4886	4837
	F	4670	4774	4802	4848	4879	4874
	G	4605	4738	4720	4748	4778	4794
Q-Test Results	LOW	0.111351	0.16147	0.14496	0.113079	0.236589	0.02439
	HIGH	0.066969	0.240161	0.047919	0.727957	0.117647	0.096946

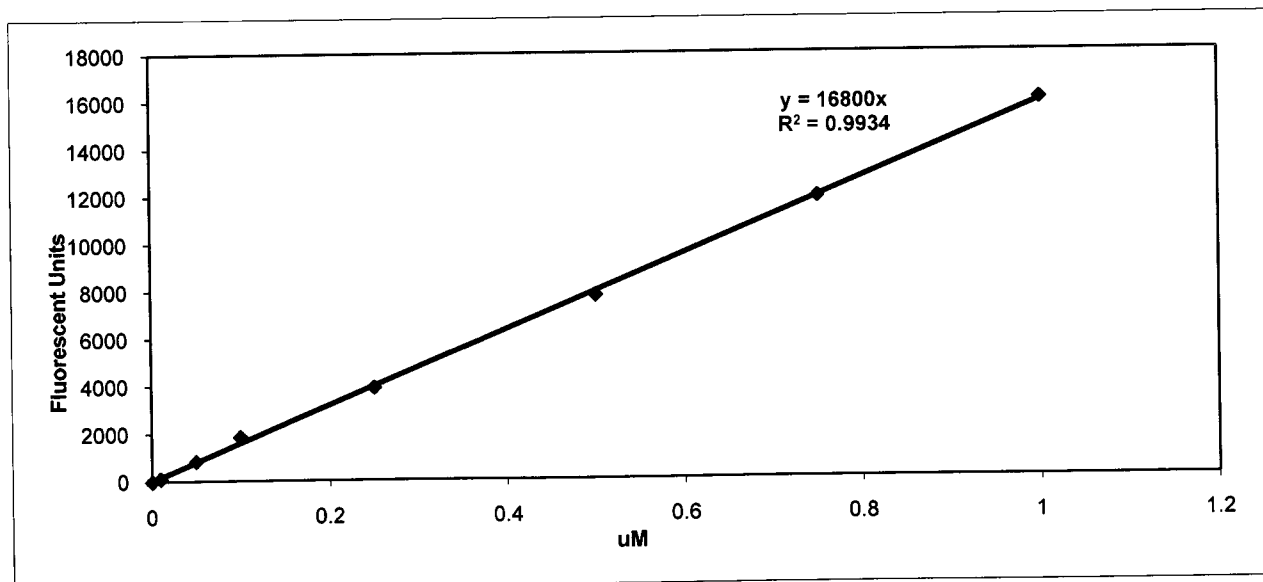
Appendix D: Supporting Data

D1: DNA Fluorescence



DNA contribution to fluorescence. At 66.67 μM , the relative fluorescence of dT(10) reads at 39.3 RFU, dT(20) at 6.3 RFU and dT(30) at 23.3 RFU. Meanwhile, 1.0 μM reads of the FAM standard at 6019.7 RFU, which, multiplied by 66.67 to compare with the DNA contribution yields a value of 401331 RFU, a difference of 4 orders of magnitude.

D2: Calibration curve for Biotek Synergy HT at PMT sensitivity 85. (provided courtesy of Aimee Jones of DRDC-O)

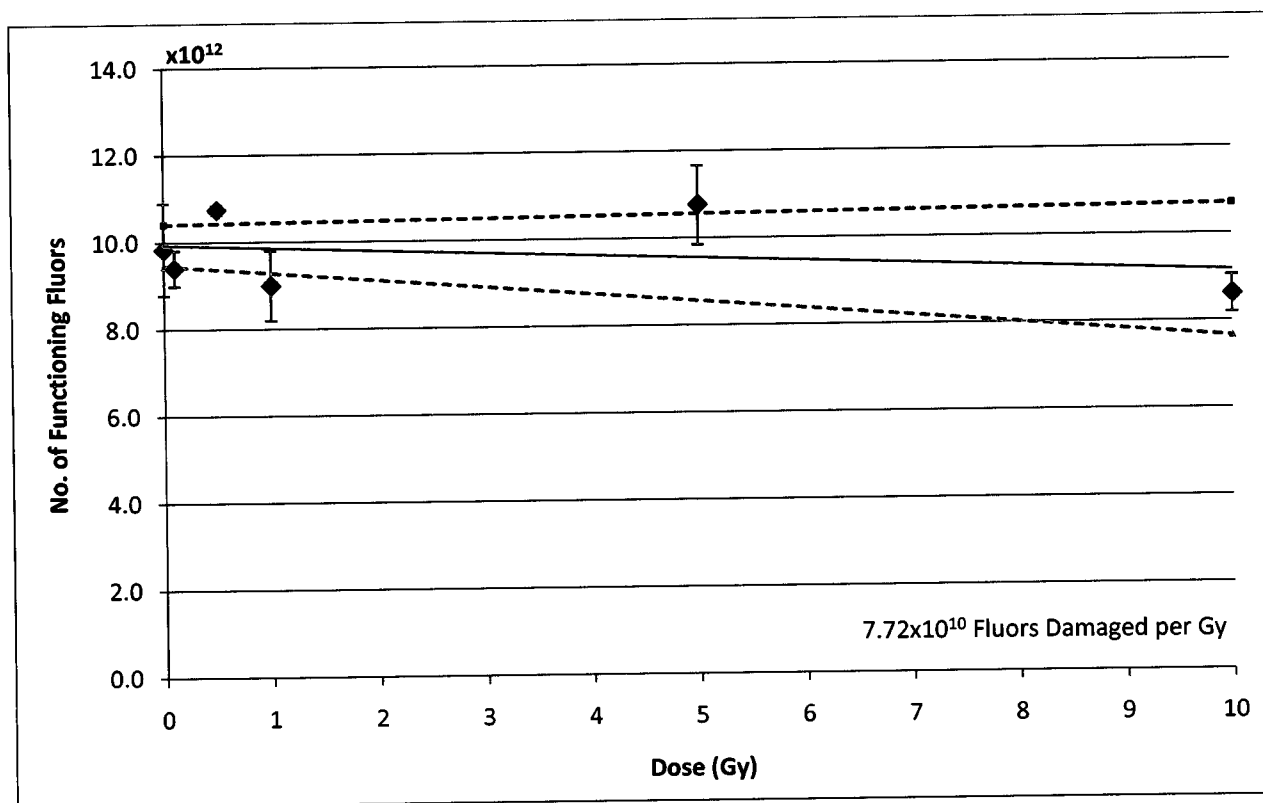


D3. Regression Analyses

Regression analyses were performed for plots that generated a slope, to determine the significance of the apparent slope. These plots are the fluorophore radiosensitivity and photosensitivity, and dosimetric performance of the FAM-dT(10)-BHQ construct.

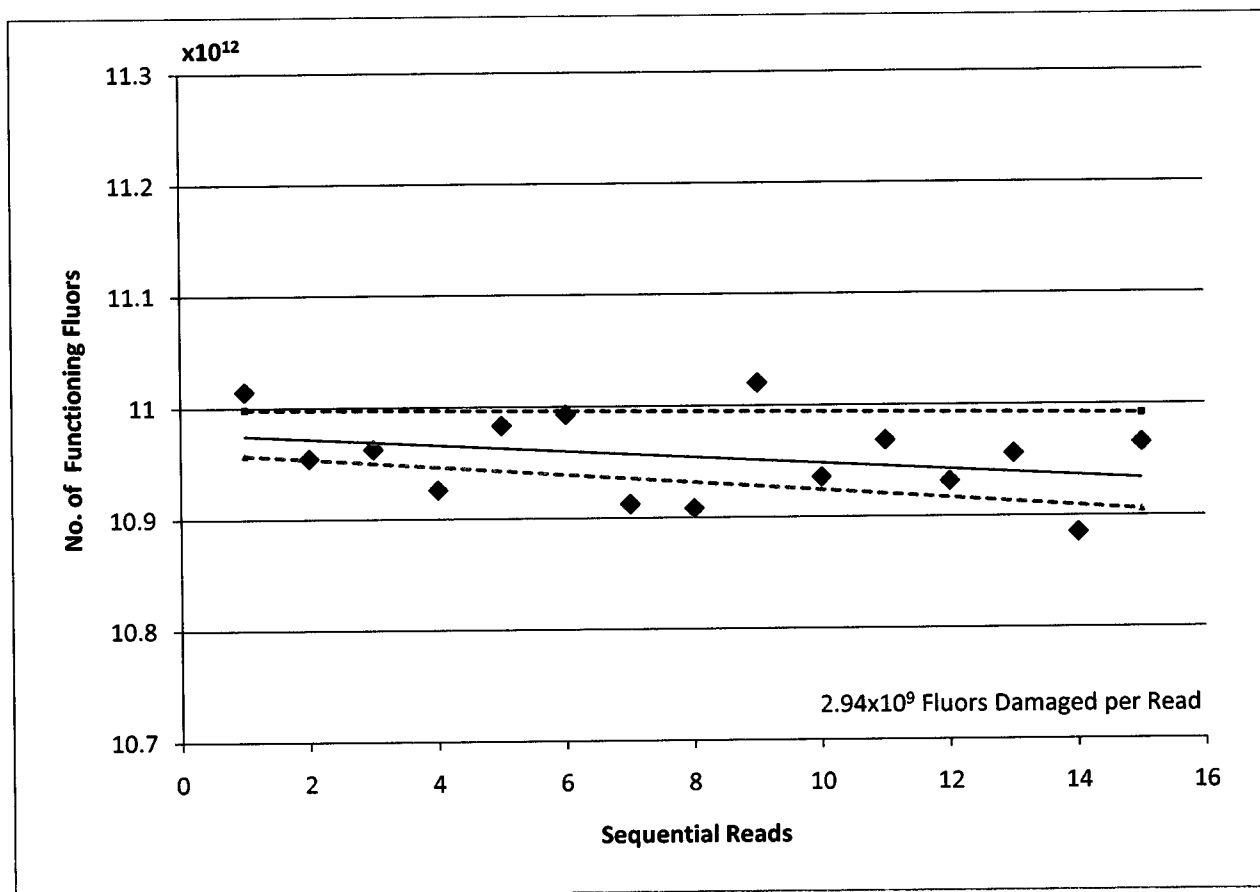
FAM Radiosensitivity

Over 10 Gy, a decrease of 7.72×10^{10} fluors per gray is not significantly different from a slope of zero.



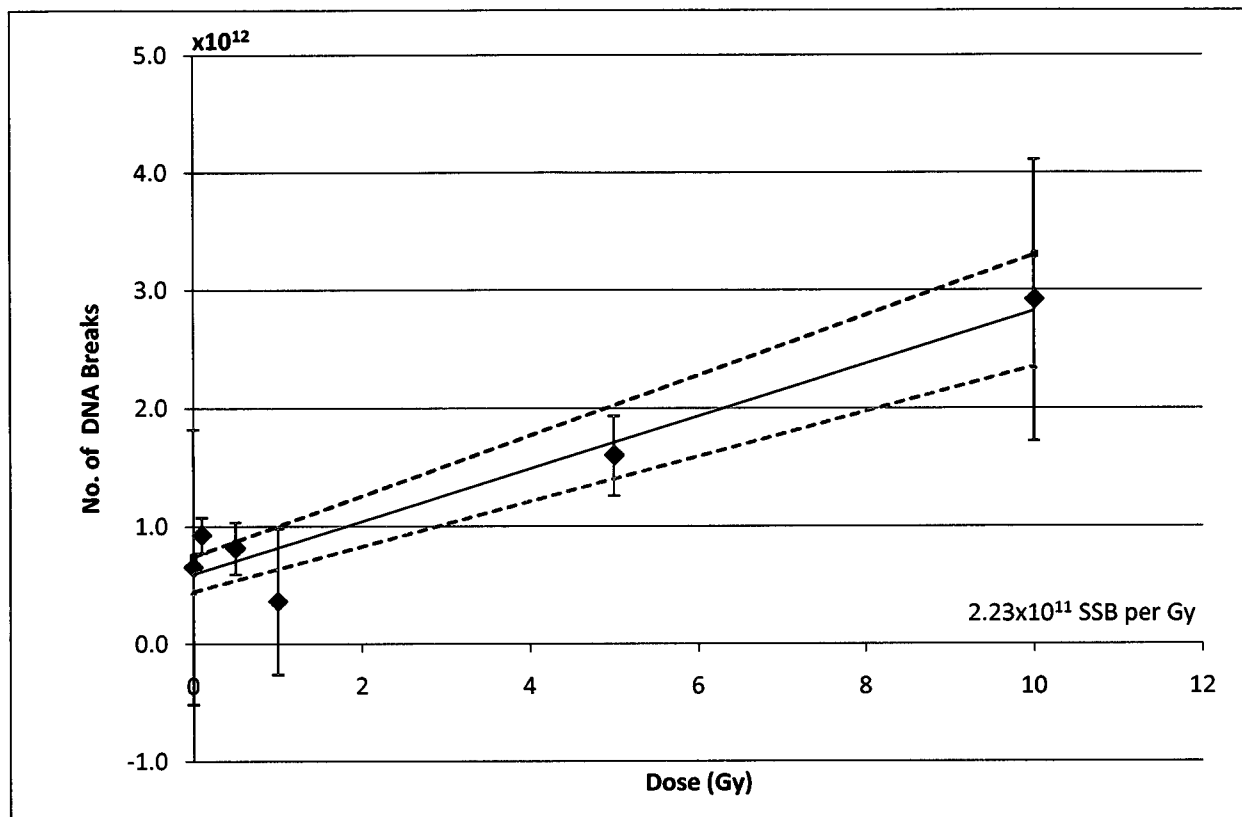
FAM Photosensitivity

In the 15 reads performed on Day 1, submitting FAM fluorophores to analytical light, a decrease of 2.94×10^9 fluors damaged per read was observed. Regression analysis shows that this value is significantly different from a slope of zero, so it is necessary to include this damage rate when analyzing dosimetric performance.



Dual-Labelled Oligonucleotide Dosimeter Performance

The linear response of the dual-labeled oligonucleotide, at 2.23×10^{11} SSB/Gy is reinforced by a simple regression analysis – values tend to fall within the upper and lower bounds, and the slope is significantly different from 0.



CURRICULUM VITAE

CURRICULUM VITAE

Kirsten A. Avarmaa

Education:

September 2001 - April 2007

McMaster University (Hamilton, Ontario)

B.Sc. in Biology, Genetics specialization

January 2008 – November 2010

Royal Military College of Canada (Kingston, Ontario)

Graduate studies in Nuclear Engineering

Publications:

T. Wood, B. Lewis, K. McDermott, L. Bennett, K. Avarmaa, E. Corcoran, D. Wilkinson, A. Jones, T. Jones, E. Kennedy, L. Prud'homme-Lalonde, D. Boudreau, J.-F. Gravel, C. Drolet, A. Kerr, J. Schreiner, M. Pierre, R. Blagoeva, T. Veres. Use of a Dual-Labelled Oligonucleotide as a DNA Dosimeter for Radiological Exposure Detection. Submitted to *Radiation Protection Dosimetry*. (2010)